A COUPLING-OF-MODES ANALYSIS OF SAW GRATING STRUCTURES

by

Peter Vickers Wright

University of Cambridge, England
B.A. (1972), M.A. (1976)

Massachusetts Institute of Technology
S.M. (1980)

SUBMITTED IN PARTIAL FULFILLMENT
OF THE REQUIREMENTS FOR THE
DEGREE OF

DOCTOR OF PHILOSOPHY

at the

MASSACHUSETTS INSTITUTE OF TECHNOLOGY

April 1981

Signature of Author _____
Department of Electrical Engineering
and Computer Science, April 1981

Certified by _____
Hermann A. Haus
Thesis Supervisor

Accepted by _____
Arthur C. Smith, Chairman
Departmental Graduate Committee

A COUPLING-OF-MODES ANALYSIS OF SAW GRATING STRUCTURES

by

PETER VICKERS WRIGHT

Submitted to the Department of Electrical Engineering and Computer Science on April 17, 1981 in partial fulfillment of the requirements for the degree of Doctor of Philosophy

ABSTRACT

Grating structures are currently used in surface-acoustic-wave (SAW) devices to perform a variety of signal processing functions. With the development of single-mode optical transmission systems, it is also likely that they will find increasing application in integrated optics for performing similar functions. We demonstrate here the power and simplicity of coupling-of-modes theory in analyzing the behavior of such gratings. The major part of this thesis is concerned specifically with the analysis of SAW gratings. However, most of the theoretical methods developed, and the general solutions obtained for several complex grating problems, are equally valid for integrated optics, holographic or other grating structures.

The first step in the analysis is the derivation of a variational principle for SAW's. From this the coupled-wave equations, to first order in the grating perturbation, are derived for a grating resonator. The coefficients of these equations are evaluated to obtain in a relatively simple manner, the reflection coefficient of a normal-incidence groove, to first order in the groove depth. A second method for obtaining the reflection coefficient by matching boundary conditions, and interpreting the results via coupling-of-modes theory is also presented. The results of both analyses are in agreement with existing theory. The analysis of a normal-incidence grooved grating is then extended to second order in the groove depth. Theoretical closed-form expressions are obtained for both the

reflection coefficient and the center of the stop-band at all the grating harmonics. A detailed analysis of these second-order effects is presented at Bragg and the second-harmonic frequency of the grating. The strong influence of the groove profile in determining these effects is investigated. Oblique-incidence gratings are also analyzed.

In the second half of the thesis, coupled-wave theory is used to obtain, in exact closed form, the responses of both normal- and oblique-incidence (45°) gratings with a linear spatial chirp. Using these solutions the filter characteristics of constant-period oblique-incidence gratings are studied. In addition the exact response of a reflective-array-compressor (RAC) is determined. The exact solutions for the RAC are then approximated to a form much simpler to evaluate, yet more accurate than those currently used in RAC analysis. These approximate solutions are applied to a detailed analysis of a low-loss RAC.

Thesis Supervisor: Hermann A. Haus

Title: Elihu Thomson Professor of Electrical Engineering

ACKNOWLEDGEMENTS

I wish to thank Professor H. A. Haus for his constant guidance and encouragement during the course of this work. His enthusiasm, and his great physical insight, served as a constant inspiration. I am also grateful to J. Melngailis and Professor R. L. Kyhl for their help during the course of this thesis. J. Melngailis, in particular, helped direct my attention to problems of practical concern, whilst Professor Khyl was instrumental in developing my analytic skills.

I alsc wish to acknowledge the many years of help and encouragement given to me by my parents. Without their love nothing would have been possible. In addition,I wish to thank my wife for all she sacrificed during my years of graduate study.

Thanks go to Cindy Kopf for doing such an excellent job in typing this thesis. The support of the National Science Foundation Grant ENG 7909980 is gratefully acknowledged.

LABOR OMNIA VINCIT

For my parents

TABLE OF CONTENTS

PART II

LIST OF FIGURES

Figure | Page

CHAPTER 1

INTRODUCTION

1.1. Motivation for Grating Study

Grating structures are capable of performing many complex signal processing functions, and are currently employed extensively in surface-acoustic-wave (SAW) technology.[1,2] Such SAW grating devices usually operate in the VHF-UHF range (typically below 1 GHz). Important applications are in oscillators, filters, pulse compression, and chirp Fourier transform systems.[1-13] In general, such devices offer considerable advantages in terms of size, power requirements, and speed over alternative digital processing systems, if they are even available. SAW grating devices operate in real time and over very large bandwidths. Pulse compression devices have been fabricated to date with time bandwidth products as high as 16,200.[14]

Analogue signal processing with gratings, however, is not restricted to acoustics. The current development of magneto-static wave devices shows promise for extending the SAW grating technology well into the microwave regime (up to 10 GHz)[15,16]. In addition, grating structures are also important in optics.[17-24] Holograms have been used for some

time for recording information and the shaping of optical beams. Furthermore, as grating technology is advanced it is expected that most current SAW grating functions will also become feasible for the processing of optical guided waves. In this respect, the development of single-mode optical transmission systems can be expected to stimulate the development of such integrated-optics devices.

The growing importance of grating devices for signal processing has created a new need for a deeper understanding of the behavior of such structures. The exacting responses required of modern acoustic and optical signal processing devices demand the inclusion of previously ignored effects into grating design and analysis. Of particular importance among the latter are the effects of stored energy and multiple reflections, within a grating, on the device performance.

Stored-energy effects are associated with the generation of local evanescent bulk waves within a grating. These cause a small additional phase shift at each reflecting discontinuity. The most important consequence is a reduction of the surface-wave velocity in the grating, compared with that on the free surface.[3,5,25] The latter results in a lowering of the Bragg frequency, i.e. the frequency of maximum grating reflection. This effect is particularly important in filter design as it often necessitates empirical adjustments in design.[25]

The reduction of the grating surface-wave velocity has also been observed in the grating transmission phase response.[26] In addition, stored-energy effects within a grating have been shown to cause strong spurious harmonic responses of the grating.[27-29] No theoretical method of analyzing these effects in closed-form currently exists. Moreover, the dependence on the various grating parameters is not well understood.

Modern grating devices frequently employ complex grating structures, with spatial chirps and/or operation of oblique incidence. Most current analyses of such structures neglect the effects of depletion and multiple reflections within the grating. However, these effects may have important consequences for the device response. An important case of interest is the reflective array compressor (RAC). This oblique-incidence structure uses spatially-chirped gratings to achieve pulse compression. It finds widespread application in modern sophisticated radar and signal processing devices. A disadvantage of current designs, however, is that they suffer from high insertion loss. To achieve lower-loss performance the gratings must be designed for stronger reflection and the effects of multiple reflections and depletion included in the analysis.

The areas mentioned above are the principal areas where it is desired to develop an improved theoretical understanding of grating behavior, for applications in modern SAW, and optical, signal processing devices.

1.2. Existing Theory

Early analyses of grating devices neglected the effects of energy storage within the grating on device performance. Since these effects are "second order", i.e. vary quadratically with the grating perturbation, they were assumed to be too small to have a significant effect on the grating response. More recently, however, many papers have stressed the importance of including second-order effects in SAW grating design.[3,5] In modern high-Q grating designs the second-order reduction in the Bragg frequency is particulary important. Despite the latter, very few theoretical analyses of second-order effects have been attempted. To date, second-order effects have been accounted for in grating designs largely on an empirical basis.

An equivalent transmission-line model was proposed by Li et al. for including second-order effects in the analysis of SAW gratings.[26,27] In this model, the energy storage is accounted for by a periodic loading of equal shunt susceptances across a transmission line [Fig. 1.2.1]. However, they proposed that the appropriate shunt susceptance value be determined experimentally. This approach, while quantitatively predicting the grating behavior, fails to relate the effects of energy storage to the relevant grating parameters. In a later paper, an attempt was made by Shimizu et al. to derive the susceptance

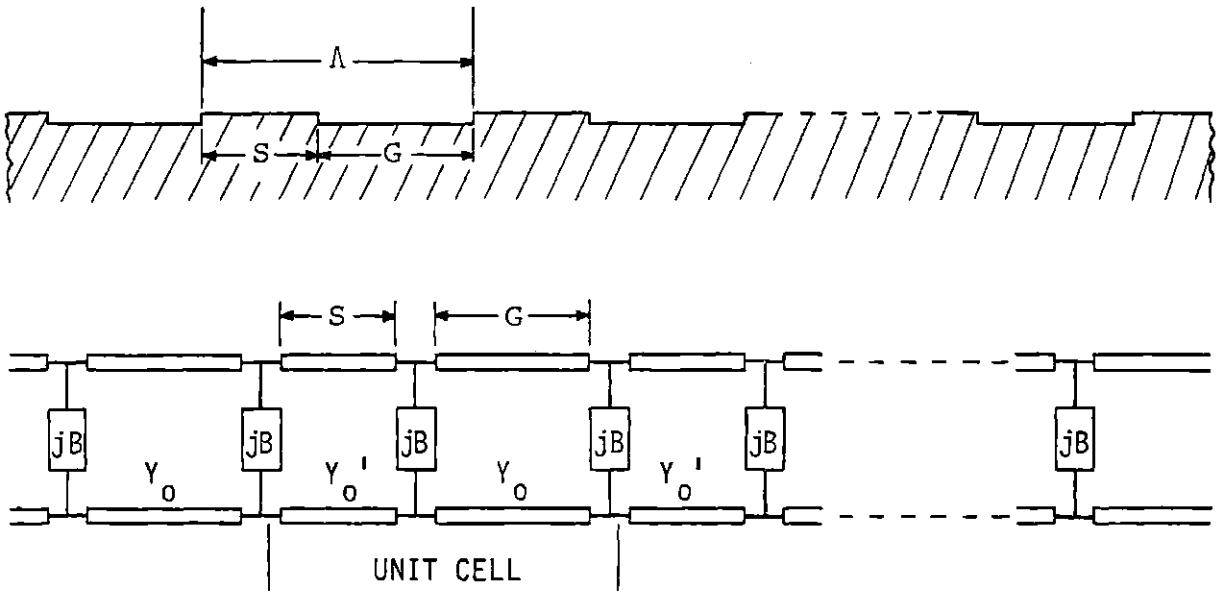

FIG. 1.2.1 EQUIVALENT TRANSMISSION-LINE MODEL FOR INCLUDING STORED-ENERGY EFFECTS.

elements of Li entirely theoretically.[30] However, because of a perturbation technique employed in their solution, the results are in error for steep-sided grooves.

In two recent papers, by Wright et al., a new method for analyzing second-order effects in closed form was described.[31,32] That analysis will be given in detail in this thesis. The results are in good agreement with experimental data and reveal the critical importance of groove profile in determining second-order effects.

The analysis of second-order effects, and the other grating analyses considered in this thesis, are based on coupled-wave theory. Coupled-wave theory was first introduced into grating analysis by Kogelnik, for the analysis of thick hologram gratings.[33] Later Kogelnik and Shank successfully applied it to the analysis of distributed-feedback lasers.[34] They demonstrated that such an approach could greatly simplify the analysis of grating structures. Subsequently, coupled-wave theory was successfully applied by several authors to the analysis of SAW transducers and gratings.[35-37]

Modern SAW grating devices such as the RAC, rely on oblique-incidence grating structures for their operation. However, the coupled-wave theory developed by Kogelnik applied only to one-dimensional structures. Thus only gratings at

normal incidence could be analyzed. Coupled-wave theory was extended to two dimensions by L. Solymar et al., for the analysis of large-volume holograms.[38] Solymar et al. solved the problem of uniform illumination of a large-volume hologram at Bragg incidence. They showed that the output waveforms from a holographic grating could be expressed in terms of Bessel functions. Bloch et al., by analogy, applied these solutions to the analysis of oblique-incidence SAW gratings.[39] Since the solutions were only valid at Bragg, however, they were not able to predict the frequency behavior of the gratings. In addition they could not analyze the transmission through a "U" or "Z" -path unchirped grating structure [Fig. 1.2.2]. In the latter structures the illumination of the second grating is non-uniform, thus the solutions of Solymar did not apply.

In a recent paper, Russell and Solymar extended the analysis of large-volume overlap-holograms to the case of non-uniform illumination and non-Bragg incidence.[40] However, these solutions have not yet been applied to the analysis of SAW grating structures. In addition, the solutions are valid only for gratings with a constant spatial-period. They thus cannot be applied to the RAC, which is a chirped grating structure.

Gerard et al. performed an analysis of the RAC in the limit of small coupling between the incident and reflected grating waves.[41] This analysis is currently used to design

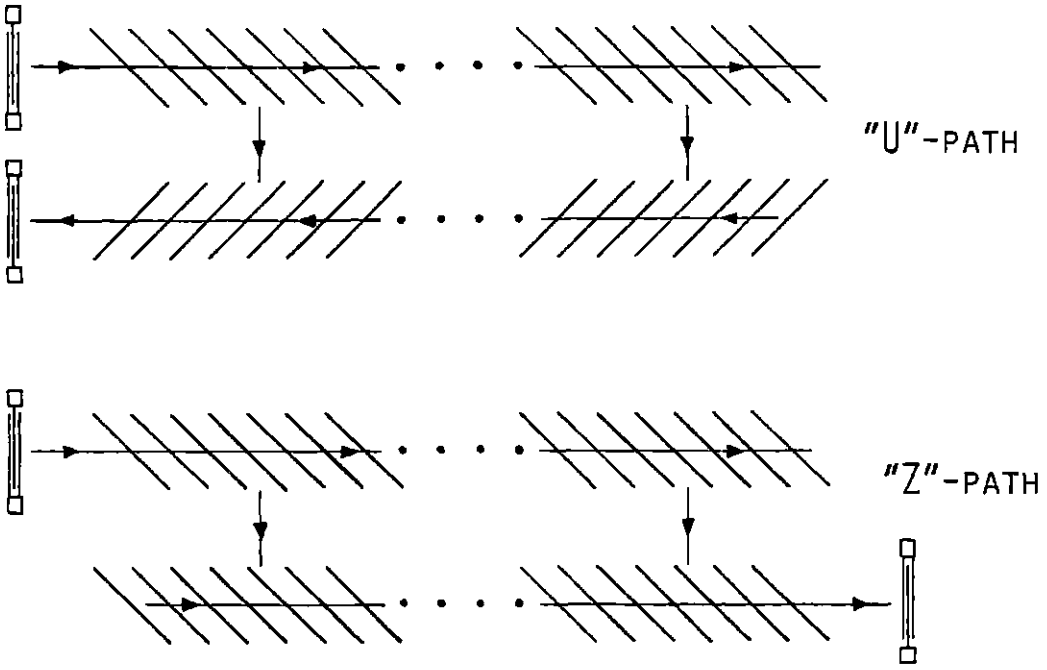

FIG. 1.2.2 "U" AND "Z"-PATH GRATING CONFIGURATIONS.

RAC devices. However, under the small coupling assumption the effects of energy depletion and multiple reflections within the gratings are completely neglected. This analysis is therefore unsuitable for the design of low-loss RAC devices, where the coupling in the gratings must be strong.

In a separate paper, Otto attempted to examine the effects of multiple reflections on grating performance and also to estimate when they become important.[42] He chose to analyze an unchirped U-path grating by dividing both gratings into small unit-cells, each with identical scattering parameters [Fig. 1.2.3]. By employing a computer to multiply together each of the individual scattering matrices, he was then able to investigate the role of multiple reflections on the performance of the device. The analysis, however, was only performed for unchirped gratings. Moreover, closed-form solutions were not obtained and the complexities of the numerical analysis failed to make clear the role of the design parameters in determining these effects.

In a recent paper, Bloch et al. suggested an extension of the unit-cell scattering approach of Otto to the analysis of a RAC (i.e. to include a chirped grating).[39] The method, however, is not as well suited to this structure. In addition, the complex numerical analysis required, again obscures a clear understanding of how these effects might be included for improved

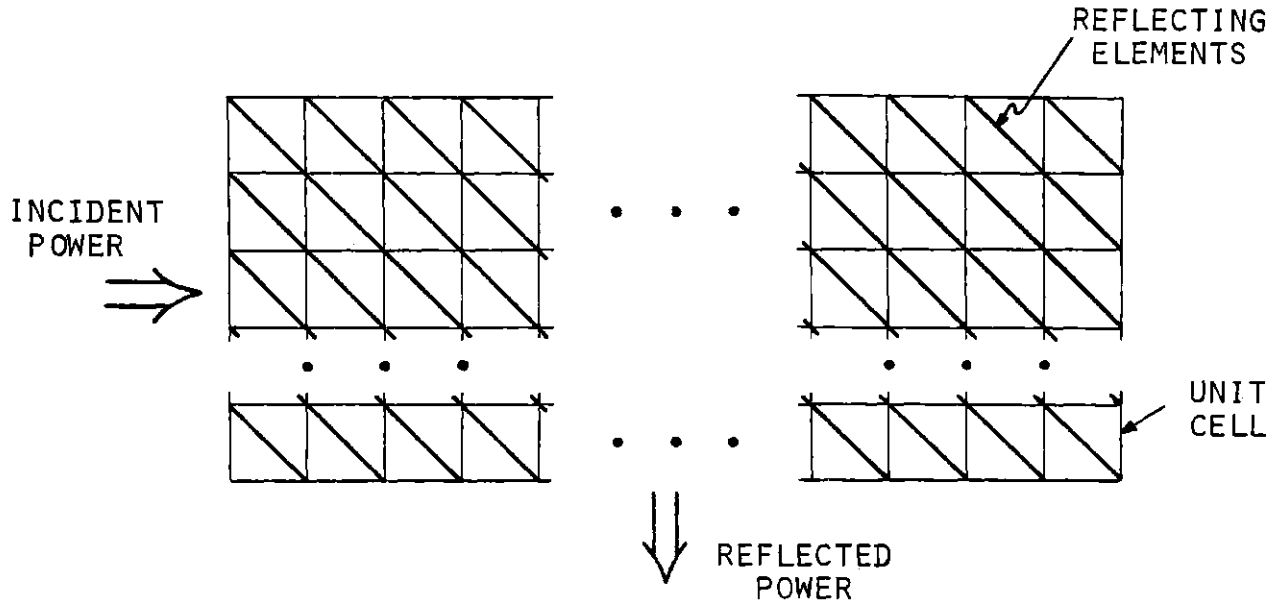

(A) SUBDIVISION OF GRATING INTO UNIT CELLS

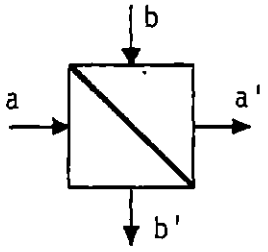

(B) UNIT CELL 4-PORT REPRESENTATION

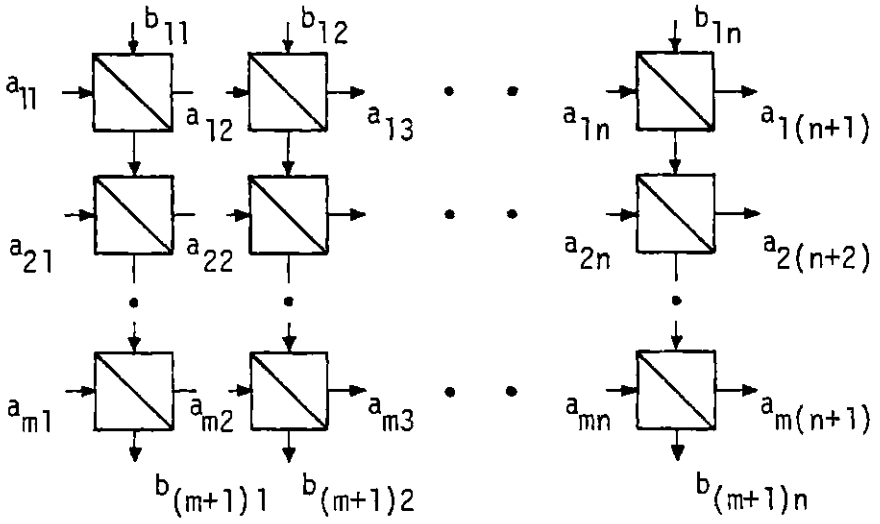

(C) UNIT CELL MATRIX ANALYSIS OF GRATING

FIG. 1.2.3 UNIT-CELL APPROACH

RAC design.

More recently, a closed-form analysis of reflective-array gratings was reported by Wright et al.[43] That analysis will be described in detail in this thesis. The new analysis, for the first time, permits closed-form solutions to be obtained for the RAC. The solutions incorporate all orders of multiple reflections and wave depletion within the gratings. They have important application to the design of low-loss RAC's.

1.3. Objectives

A main objective of this thesis will be to demonstrate that, in many cases, coupled-wave theory provides the most convenient approach to the solution of complex grating problems. In particular, we shall show that a coupled-wave analysis frequently permits solutions to be obtained in closed form. Alternate methods, by contrast, are invariably more complicated, frequently involve infinite matrices, and rarely permit closed-form solutions to be obtained. Furthermore, grating analyses of general validity can be performed, using coupling-of-modes theory, without regard to the specific nature of the waves, i.e. acoustic, optical, etc. We shall show that a coupled-wave analysis is valid for most grating structures of practical importance.

A new, relatively straightforward method for obtaining second-order effects in grooved gratings will be presented. The analysis will be performed assuming propagation in an isotropic material. However, by invoking an equivalent Poisson ratio, the results of the analysis will be extended to include typical anisotropic materials, such as Quartz and $LiNbO_3$. The solutions will be obtained in closed form. Analyses that involve numerical integration, and/or truncation

of infinite matrices, are particularly to be avoided as they may lead to incorrect results as will be shown.

All the stop-bands of a grating will be determined correct to second order in the groove depth. From this analysis the response of a grating at Bragg and the second harmonic will be examined in detail. Both normal- and oblique-incidence gratings will be considered. The second-order reduction in the free-surface wave velocity within a grating, usually attributed to so-called stored-energy effects, will be determined theoretically and in closed form. The sensitivity of the resulting downward shift in the frequency of maximum reflection of the grating (i.e. Bragg) to the groove profile will be investigated. It has been reported in the literature that this frequency shift is not a simple quadratic function of groove depth, as might be expected.[25] We shall show that the new theory explains this behavior. We shall also determine the transmission phase response of a grating, using the corrected wave velocity as determined by the analysis. Whenever possible, all theoretical analyses will be compared with existing experimental data.

From the second-order analysis, the reflection coefficient of a grating will also be determined to second order (in groove depth). Stored-energy effects have been shown to cause a strong grating reflection near the second-harmonic frequency, where

to first order none would be expected. This reflection, and the associated bulk radiation within the grating, will be determined theoretically by the new analysis. The sensitivity of the reflection coefficient to the groove/strip ratio of the grating will be examined. We shall show that a second-order analysis reveals that a groove/strip ratio of 1:1 may not always be the ideal choice.

As a further example of the usefulness of coupling-of-modes theory in grating analysis, we shall derive exact, closed-form solutions for gratings with a linear spatial chirp. Both normal- and oblique-incidence (45°) gratings will be considered. All the grating waves will be obtained in closed form, and the response at arbitrary detuning, to an arbitrary input profile, will be determined. Constant-period, or unchirped gratings, will be considered as limiting cases. The design of constant-period oblique-incidence gratings as bandpass and bandstop filters will be described.

U-path grating devices will also be studied. In particular, a detailed analysis of the RAC will be performed. The emphasis will be directed towards understanding the effects of multiple reflections, within each grating, on the overall amplitude and phase response of the device. The implications of the new analysis for low-loss RAC design will be examined in detail, and distortions of the device response, caused by the previously ignored effects, will be elucidated.

PART I

Analysis of Constant-Period SAW Grooved Gratings to First and Second-Order

I(a): Normal Incidence

CHAPTER 2

FIRST-ORDER REFLECTION COEFFICIENT FROM A VARIATIONAL PRINCIPLE

2.1. Variational Principle for SAW's

Variational principles are extremely useful in that they yield the values of parameters to an accuracy greater than that of the solutions used in deriving them. If a system undergoes a small perturbation, such principles permit the new perturbed solutions of the system to be determined from the unperturbed solutions. They are thus frequently used in resonator problems to determine the change in resonant frequency of the system, resulting from a small perturbing influence.

In this section a variational principle for SAW's is developed. The analysis ignores the effects of piezo-electricity and assumes propagation in an isotropic material. In the following sections, the variational principle is used to derive the coupled-wave equations for a normal-incidence grooved grating. From these equations the reflection coefficient of a single groove is determined, in a simple manner, from the free-surface wave solutions.

Consider a SAW of angular frequency ω, propagating on an isotropic acoustic material of mass density ρ. From Newton's second law, the equation of motion is

$$\nabla \cdot \bar{\bar{\sigma}} = \rho \frac{\partial^2}{\partial t^2} \bar{u} = - \rho\omega^2 \bar{u}$$

which in Einstein summation notation becomes

$$\frac{\partial}{\partial x_j} \sigma_{ij} = - \rho\omega^2 u_i . \tag{2.1.1}$$

Multiplying by u_i^* gives

$$- \rho\omega^2 |u_i|^2 = u_i^* \frac{\partial}{\partial x_j} \sigma_{ij} . \tag{2.1.2}$$

Here $\bar{\bar{\sigma}}$ is the associated stress tensor of the wave and $\bar{u}$ is the displacement tensor. We now integrate (2.1.2) over the volume of one cell of the structure. The latter extends from the surface to $z = +\infty$ (z into the bulk) and if the surface is periodic occupies one full period of the structure. We obtain

$$- \rho\omega^2 \int dv |u_i|^2 = \int ds_j u_i^* \sigma_{ij} - \int dv \left(\frac{\partial}{\partial x_j} u_i^* \right) \sigma_{ij}$$

$$= - \int dv \left(\frac{\partial}{\partial x_j} u_i^* \right) \sigma_{ij}$$

since the integration is over one full period and the surface is stress free (i.e. has no normal stress). Thus

$$\omega^2 = \frac{\int dv \left(\frac{\partial}{\partial x_j} u_i^*\right) \sigma_{ij}}{\rho \int dv |u_i|^2}$$

or, introducing the stiffness tensor $c_{ijk\ell}$

$$\omega^2 = \frac{\int dv \left(\frac{\partial}{\partial x_j} u_i^*\right) c_{ijk\ell} \left(\frac{\partial}{\partial x_k} u_\ell\right)}{\rho \int dv |u_i|^2} . \qquad (2.1.3)$$

This is the desired variational principle for SAW's. In this form, the value determined for ω^2 is stationary, when the correct solutions for the resonator are used to evaluate the expression. Any error in a trial function used to evaluate (2.1.3), thus introduces only a second-order error in ω^2. The variational nature of (2.1.3) is easily established.

Let ω_o be the exact resonant frequency of a SAW grating resonator. Let the stress and displacement of the exact solutions in the resonator be σ_{ij}^o and u_i^o respectively. Then

$$\sigma_{ij}^o = c_{ijk\ell} \frac{\partial}{\partial x_k} u_\ell^o \qquad (2.1.4)$$

from (2.1.1)

$$\frac{\partial}{\partial x_j}\,\sigma_{ij}^{o} = -\,\rho\omega_o^{2}\,u_i^{o} \tag{2.1.5}$$

and, from (2.1.3)

$$\omega_o^{2} = \frac{\int dv \left[\frac{\partial}{\partial x_j}\,u_i^{o*}\right] c_{ijk\ell} \left[\frac{\partial}{\partial x_k}\,u_\ell^{o}\right]}{\rho \int dv |u_i^{o}|^2}\,. \tag{2.1.6}$$

Assume a trial solution for the resonator in the form $u_i = u_i^{o} + \delta u_i$. The trial solution does not satisfy the stress-free boundary condition on the surface of the resonator, i.e., $\bar{\bar{\sigma}}_{ij} \cdot \hat{z}' = 0$, where $\hat{z}'$ is the surface-normal unit-vector. Using the trial solution to evaluate ω^2 from (2.1.3), we shall ignore all terms of second, or higher, order in the error term δu_i. Thus

$$\omega^2 = \frac{\int dv \left[\frac{\partial}{\partial x_j}\,(u_i^{o*} + \delta u_i^{*})\, c_{ijk\ell}\, \frac{\partial}{\partial x_k}\,(u_\ell^{o} + \delta u_\ell)\right]}{\rho \int dv (u_i^{o} + \delta u_i)(u_i^{o*} + \delta u_i^{*})}$$

$$= \left\{\int dv \left[\frac{\partial}{\partial x_j}\,u_i^{o*}\, c_{ijk\ell}\, \frac{\partial}{\partial x_k}\,u_\ell^{o} + \frac{\partial}{\partial x_j}\,(\delta u_i^{*})\, c_{ijk\ell}\, \frac{\partial}{\partial x_k}\,u_\ell^{o}\right.\right.$$

$$+ \frac{\partial}{\partial x_j} u_i^{o*} c_{ijk\ell} \frac{\partial}{\partial x_k} (\delta u_\ell)\Big]\Big\} \Big/ \Big\{ \rho \int dv[|u_i^o|^2 + u_i^o \delta u_i^*$$

$$+ u_i^{o*} \delta u_i] \Big\} .$$

In any medium, $c_{ijk\ell} = c_{\ell kji}$.[44] Hence, using the binomial theorem, and relations (2.1.4) and (2.1.6)

$$\omega^2 = \omega_o^2 + \frac{\int dv \left[\frac{\partial}{\partial x_j}(\delta u_i^*)\, \sigma_{ij}^o + \frac{\partial}{\partial x_j}(\delta u_i)\, \sigma_{ij}^{o*}\right] - \rho\omega_o^2 \int dv[u_i^o \delta u_i^* + u_i^{o*} \delta u_i]}{\rho \int dv |u_i^o|^2}$$

$$= \omega_o^2 - \frac{\left\{\int dv \left[\delta u_i^* \frac{\partial}{\partial x_j} \sigma_{ij}^o + \delta u_i \frac{\partial}{\partial x_j} \sigma_{ij}^{o*}\right] + \rho\omega_o^2 \int dv[u_i^o \delta u_i^* + u_i^{o*} \delta u_i]\right\}}{\rho \int dv |u_i^o|^2}$$

since the stress σ_{ij}^o, of the exact solution in the grating, satisfies the stress-free boundary condition on the surface of the grating. Introducing (2.1.5) we obtain

$$\omega^2 = \omega_o^2 .$$

Hence, (2.1.3) is a variational formula. The error in ω^2

is of a higher order than that of the trial solution used to evaluate it.

2.2. Derivation of Coupled-Wave Equations

The coupling-of-modes formalism provides an elegant mathematical approach for determining the behavior of two coupled waves. For such a description to apply the local coupling (either in time or in space), between the two waves, must be everywhere very weak. However, the resulting interaction between the two waves may be very strong, and in fact complete power transfer may occur. We shall be concerned here with coupling-of-modes in space.

The advantage of a coupling-of-modes description lies in its generality. The form of the equations is unaffected by the nature of the waves. It does not matter whether the two interacting waves are both electromagnetic, acoustic, or a combination of the two. In addition, the details of the structure and the coupling mechanism are avoided. The structure is simply described by a coupling coefficient K between the two waves. The details of a particular structure, the type of waves involved, and the manner in which they interact, need only be considered when determining K. It is thus advantageous, where possible, in a system containing two weakly coupled waves to cast the governing equations in the form of coupling-of-modes. Once this has been done, much can be immediately ascertained about the behavior of the structure

by drawing on the large body of existing knowledge of coupled-wave equations.

We begin by presenting the coupled-wave equations of a distributed-feedback structure. We then show that the variational principle (2.1.3) leads directly to this formalism for the wave amplitudes in a SAW grooved grating. The variational principle also determines the coupling coefficient K in terms of the physical parameters of the grating.

In a distributed-feedback structure (Fig. 2.2.1), the forward wave $R(x)$ is coupled to a backward wave $S(x)$ via a small periodic perturbation of the medium, along the propagation direction x. In the absence of coupling the waves have dependence

$$R(x) \sim e^{j(\omega t - kx)}$$

$$S(x) \sim e^{j(\omega k + kx)}$$

where $k = \omega/v$ is the propagation constant. The waves are strongly coupled when the period of the perturbation $\Lambda = \lambda/2$, where $\lambda = 2\pi/k$ is the wavelength of the propagating waves. The wave scattered from $R(x)$, by the $\bar{k}$-vector of the perturbation $\bar{k}_p = -(2\pi/\Lambda)\hat{x} = -2k\hat{x}$, then has the propagation constant $(k + k_p) = -k$ and is thus synchronous with $S(x)$. The frequency at which this synchronous scattering occurs, and the coupling

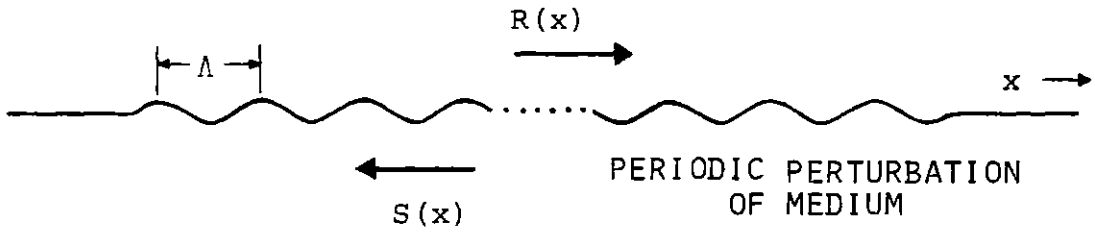

FIG. 2.2.1 DISTRIBUTED-FEEDBACK STRUCTURE

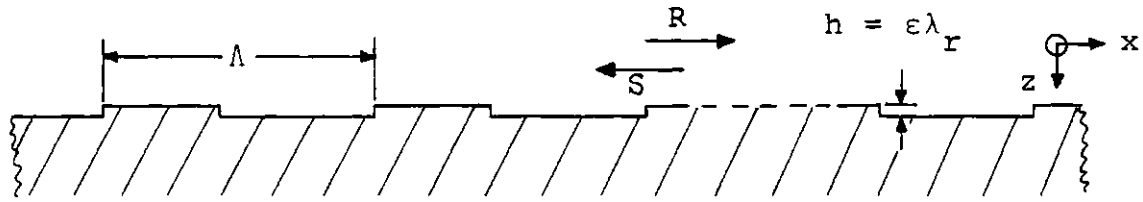

FIG. 2.2.2 SURFACE-WAVE GRATING

between the two counter-propagating is a maximum, is referred to as Bragg.

Before writing the coupled-wave equations, we introduce the slowly varying wave amplitudes $\tilde{R}(x)$ and $\tilde{S}(x)$, where

$$R(x) = \tilde{R}(x)\ e^{j(\omega t - kx)}$$

$$S(x) = \tilde{S}(x)\ e^{j(\omega t + kx)}.$$

The coupled-wave equations for the Bragg condition, are then[45]

$$\begin{aligned} \frac{d}{dx}\tilde{R}(x) &= K\,\tilde{S}(x) \\ \frac{d}{dx}\tilde{S}(x) &= K^*\,\tilde{R}(x). \end{aligned} \qquad (2.2.1)$$

We now use the variational formula (2.1.3) to determine the governing equations for the waves in a SAW grooved grating. We shall show that these equations can be cast in the same form as (2.2.1) and identify the coupling coefficient K.

For an acoustic substrate, extending from $z = 0$ to $z = +\infty$, the solutions for guided waves propagating along the surface in the $x - y$ plane are well known Rayleigh waves. We assign them a propagation constant $k_r = 2\pi/\lambda_r$, where λ_r

is the Rayleigh wavelength. These waves no longer satisfy the stress-free boundary conditions if the surface is perturbed by a grating. However, the Rayleigh wave solutions will be used as zeroth-order trial solutions in the variational principle (2.1.3).

Consider an acoustic substrate with a surface grating of infinite extent in the x direction, and of period Λ (Fig. 2.2.2). The perturbed boundary is at $z = \varepsilon\lambda_r f(x)$, where $\varepsilon(= h/\lambda_r) << 1$, and the normalized surface perturbation $f(x)$ has a peak amplitude of unity. We seek to determine the perturbed wave solutions for forward and reverse guided SAW's along the x direction, and the degree of coupling introduced between them by the grating. Ignoring diffraction, no dependence on y will be assumed. If the grating were not present (i.e. $\varepsilon = 0$) the forward and reverse wave solutions would both be Rayleigh waves. Thus, we take as a trial solution for the variational principle (2.1.3)

$$u_i = Ru_i^+ + Su_i^- \qquad (2.2.2)$$

where $u_i^{\pm}$ are the displacements of the (zeroth order) Rayleigh wave solutions. The wave amplitudes R and S are assumed to be slowly varying functions of x, such that

$$\left|\frac{\Lambda(dR/dx)}{R}\right| << 1 \qquad \text{and} \qquad \left|\frac{\Lambda(dS/dx)}{S}\right| << 1.$$

Introducing the trial solution (2.2.2), into the variational principle (2.1.3), thus gives

$$\omega^2 = \frac{\int dv\left(R^* \frac{\partial}{\partial x_j} u_i^{+*} + S^* \frac{\partial}{\partial x_j} u_i^{-*}\right) c_{ijk\ell}\left(R \frac{\partial}{\partial x_k} u_\ell^{+} + S \frac{\partial}{\partial x_k} u_\ell^{-}\right)}{\rho \int dv(R^* u_i^{+*} + S^* u_i^{-*})(R u_i^{+} + S u_i^{-})} \tag{2.2.3}$$

where the integration in x is taken over one full period Λ.

We now determine the relationships between R and S, necessary for ω to be a minimum. Since the trial solution is correct to zeroth order, the variational principle will yield relationships that are correct to first order (in ε). In the analysis all terms of the order ε^2 ($O(\varepsilon^2)$) and above will thus be neglected. To derive the requirements for ω^2 to be stationary we differentiate (2.2.3) with respect to the wave amplitudes R and S. This may be shown to be equivalent to differentiating with respect to R^* and S^*. The results are

$$\omega^2 \left\{\rho \int dv[R|u_i^{+}|^2 + S u_i^{+*} u_i^{-}]\right\} = \int dv\left[R \frac{\partial}{\partial x_j} u_i^{+*} c_{ijk\ell} \frac{\partial}{\partial x_k} u_\ell^{+}\right.$$

$$+ S \frac{\partial}{\partial x_j} u_i^{+*} c_{ijk\ell} \frac{\partial}{\partial x_k} u_\ell^- \Big]$$

$$\omega^2\{\rho\int dv[S|u_i^-|^2 + Ru_i^{-*}u_i^+]\} = \int dv \Big[S \frac{\partial}{\partial x_j} u_i^{-*} c_{ijk\ell} \frac{\partial}{\partial x_k} u_\ell^-$$

$$+ R \frac{\partial}{\partial x_j} u_i^{-*} c_{ijk\ell} \frac{\partial}{\partial x_k} u_\ell^+ \Big] .$$

Defining

$$K_{+-} = \rho \int dv\ u_i^{+*} u_i^-$$

$$H_{+-} = \int dv \frac{\partial}{\partial x_j} u_i^{+*} c_{ijk\ell} \frac{\partial}{\partial x_k} u_\ell^-$$

the equations become

$$\omega^2 K_{++} R + \omega^2 K_{+-} S = H_{++} R + H_{+-} S$$

$$\omega^2 K_{--} S + \omega^2 K_{-+} R = H_{--} S + H_{-+} R. \qquad (2.2.4)$$

Evaluating H_{++}, we have

$$H_{++} = \int dv \frac{\partial}{\partial x_j} u_i^{+*} c_{ijk\ell} \frac{\partial}{\partial x_k} u_\ell^+ = \int ds_j\ u_i^{+*} c_{ijk\ell} \frac{\partial}{\partial x_k} u_\ell^+$$

$$- \int dv\ u_i^{+*} \frac{\partial}{\partial x_j} \left(c_{ijk\ell} \frac{\partial}{\partial x_k} u_\ell^{+} \right) = - \int dv\ u_i^{+*} \frac{\partial}{\partial x_j} \sigma_{ij}^{+}$$

where the surface integral vanishes because the integration is over one full period of the grating. Denoting the angular frequency of the unperturbed Rayleigh waves by ω_o, and introducing (2.1.1), we obtain

$$H_{++} = \rho\omega_o^2 \int dv\ u_i^{+*}\ u_i^{+} = \omega_o^2\ K_{++}.$$

Similarly,

$$H_{--} = \omega_o^2\ K_{--}.$$

Evaluating H_{+-}, we have

$$H_{+-} = \int dv \frac{\partial}{\partial x_j} u_i^{+*}\ c_{ijk\ell} \frac{\partial}{\partial x_k} u_\ell^{-}$$

$$= \int ds_j\ u_i^{+*}\ c_{ijk\ell} \frac{\partial}{\partial x_k} u_\ell^{-} - \int dv\ u_i^{+*} \frac{\partial}{\partial x_j} \left(c_{ijk\ell} \frac{\partial}{\partial x_k} u_\ell^{-} \right)$$

$$= \int ds_j\ u_i^{+*}\ \sigma_{ij}^{-} - \int dv\ u_i^{+*} \frac{\partial}{\partial x_j} \sigma_{ij}^{-}.$$

Defining

$$C_{+-} = \int dS_j \; u_i^{+*} \; \sigma_{ij}^{-}$$

and again introducing (2.1.1), we obtain

$$H_{+-} = C_{+-} + \rho\omega_o{}^2 \int dv \; u_i^{+*} u_i^{-} = C_{+-} + \omega_o{}^2 K_{+-}.$$

Similarly,

$$H_{-+} = C_{-+} + \omega_o{}^2 K_{-+}.$$

Substituting in (2.2.4) the relations between R and S become

$$\begin{aligned} (\omega^2 - \omega_o{}^2) K_{++} R + (\omega^2 - \omega_o{}^2) K_{+-} S &= C_{+-} S \\ (\omega^2 - \omega_o{}^2) K_{--} S + (\omega^2 - \omega_o{}^2) K_{-+} R &= C_{-+} R. \end{aligned} \qquad (2.2.5)$$

The waves within the grating have propagation constants of $\pm k_r$, but are of frequency ω. The presence of the grating thus perturbs the frequency of the waves from the free surface Rayleigh wave frequency ω_o. We may Taylor expand ω in terms of the perturbation parameter ε

$$\omega = \omega_o + \omega\varepsilon_1 + \ldots$$

Introducing this expansion into (2.2.5), to $O(\varepsilon)$, we obtain

$$2\varepsilon\omega_1\omega_o K_{++} R = C_{+-} S$$

$$2\varepsilon\omega_1\omega_o K_{--} S = C_{-+} R$$

or

$$\varepsilon\omega_1 R = \left(\frac{C_{+-}}{2\omega_o K_{++}}\right) S$$

$$\varepsilon\omega_1 S = \left(\frac{C_{-+}}{2\omega_o K_{--}}\right) R. \qquad (2.2.6)$$

The second terms on the LHS of (2.2.5) do not contribute to these equations, since K_{+-} and K_{-+} are themselves of $O(\varepsilon)$.

The grating waves have time dependence $e^{j\omega t}$. For the slowly varying wave amplitudes R and S we therefore identify the time derivative, $\partial/\partial t = j\varepsilon\omega_1$. Thus equations (2.2.6) take the form

$$\frac{\partial}{\partial t} R = j \left(\frac{C_{+-}}{2\omega_o K_{++}}\right) S$$

$$\frac{\partial}{\partial t} S = j \left(\frac{C_{-+}}{2\omega_o K_{--}} \right) R.$$

By reciprocity $|u_i^-| = |u_i^+|$, and $C_{-+} = C_{+-}^*$. Defining

$$K_t = j \left(\frac{C_{+-}}{2\omega_o K_{++}} \right) \tag{2.2.7}$$

we have

$$\begin{aligned} \frac{\partial}{\partial t} R &= K_t S \\ \frac{\partial}{\partial t} S &= -K_t^* R \end{aligned} \tag{2.2.8}$$

which are of the general form of coupling-of-modes in time. These equations describe the time evolution of the wave amplitudes in the grating. However, we are interested in the spatial evolution of the waves. The corresponding coupling-of-modes equations in space are easily obtained.

A plane wave, of unspecified nature, propagating in the +x direction has the general dependence $e^{j(\omega t - kx)}$. The propagation constant k is given by $k = \omega/v$, where v is the velocity of the wave. Thus

$$\frac{\partial}{\partial t} = j\omega$$

$$\frac{\partial}{\partial x} = -jk = -j\omega/v.$$

Hence, for a wave propagating in the +x direction

$$\frac{\partial}{\partial x} = -\frac{1}{v}\frac{\partial}{\partial t}.$$

Similarly, for a wave propagating in the -x direction

$$\frac{\partial}{\partial x} = \frac{1}{v}\frac{\partial}{\partial t}.$$

From (2.2.8) the coupling-of-modes equations in space are therefore,

$$\frac{\partial}{\partial x} R = KS \qquad (2.2.9)$$

$$\frac{\partial}{\partial x} S = K^*R$$

where from (2.2.7), the spatial coupling coefficient is given by

$$K = -j\left(\frac{C_{+-}}{2v_r\omega_o K_{++}}\right) = -j\,\frac{\int ds_j\, u_i^{+*}\sigma_{ij}^{-}}{2v_r\omega_o\rho\int dv|u_i^{+}|^2}\,. \qquad (2.2.10)$$

In (2.2.10) v_r is the velocity of the zeroth-order Rayleigh waves.

The homogeneous equations (2.2.9), obtained for R and S using the variational principle, are thus identical in form to the resonant coupling-of-modes equations (2.2.1) for a distributed-feedback structure. The specific form of the coupling coefficient K, for a surface-wave grating, has been determined, by the variational analysis, in (2.2.10).

2.3. First-Order Reflection Coefficient

We now evalute the coupling coefficient K, determined in Section 2.2, in terms of the grating parameters and the Rayleigh wave constants. From this evaluation the first-order reflection coefficient of a Rayleigh wave from a single normal-incidence groove is obtained.

The coupling coefficient K, between the forward and reverse waves in a SAW grating, is given by (2.2.10). We consider a grating of period Λ, where the grating boundary is defined by $z = \varepsilon\lambda_r f(x)$ [Fig. 2.2.2]. The surface perturbation $f(x)$ has a peak amplitude of unity. In Appendix A the stress on the surface of a grating $\bar{\sigma}_s$, due to an acoustic wave, is determined. For a Rayleigh wave, from (A.5), we have to $O(\varepsilon)$

$$\bar{\sigma}_s^r = \varepsilon\lambda_r[f(x)\ \sigma_{xz}^{r'}(0) - f'(x)\ \sigma_{xx}^{r}(0)]\hat{x} + \varepsilon\lambda_r\ f(x)\ \sigma_{zz}^{r'}(0)\hat{z}$$

where

$$\sigma_{ij}^{r}(0) = \sigma_{ij}^{r}\Big|_{z=0}$$

and

$$\sigma_{ij}^{r'}(0) = \frac{\partial}{\partial z}\ \sigma_{ij}^{r}\Big|_{z=0}.$$

Hence, to $O(\varepsilon)$

$$\int ds_j \; u_i^{+*} \; \sigma_{ij}^{-} = \varepsilon\lambda_r \int_0^{\Lambda} dx \; \{u_x^{r*}(0)[f(x) \; \sigma_{xz}^{-r'}(0) - f'(x) \; \sigma_{xx}^{-r}(0)]$$

$$+ u_z^{r*} \; f(x) \; \sigma_{zz}^{-r'}(0)\} \qquad (2.3.1)$$

where the superscript $(-r)$ denotes a backward Rayleigh wave (propagating in the direction $-x$), and

$$u_x^r(0) = u_x^r\Big|_{z=0}.$$

In Appendix B the displacements, stress components, and the dispersion relation for Rayleigh waves are derived. Again, let the amplitude of the forward wave be denoted by R, and that of the backward wave by S. Evaluating (2.3.1), using the displacements and stress components given in (B.20), and using the Rayleigh wave dispersion relation (B.18) gives

$$\int ds_j \; u_i^{+*} \; \sigma_{ij}^{-} = 2\mu\varepsilon\lambda_r \; R^*S \; k_2{}^2(r_r - q_r)q_r \int_0^{\Lambda} dx \; f(x) \; e^{2jk_r x}$$

$$(2.3.2)$$

Since $f(x)$ is a periodic function, only the component of $f(x)$

with dependence $e^{-2jk_r x}$ contributes to the integration. The latter result was made use of in obtaining (2.3.2), by identifying $f'(x) = -2jk_r f(x)$.

Considering the denominator of (2.2.10), we have

$$2v_r\omega_o\rho \int dv|u_i^+|^2 = 2v_r\omega_o\rho\Lambda \int_0^\infty dz|u_i^r|^2. \qquad (2.3.3)$$

However, the time average power (per unit width) of a forward propagating Rayleigh wave is

$$P_r = v_r W$$

where W is the time average energy of the wave per unit surface area of the solid. Thus,

$$W = \frac{1}{2}\rho\omega^2 \int_0^\infty dz|u_i{}^r|^2.$$

Hence,

$$P_r = \frac{1}{2} v_r\rho\omega^2 \int_0^\infty dz|u_i{}^r|^2. \qquad (2.3.4)$$

But from (C.3)

$$P_r = 2\omega\mu k_2{}^2 Y_o |R|^2 \qquad (2.3.5)$$

where Y_o is a dimensionless quantity, analogous to a characteristic admittance for the solid. From (C.5)

$$Y_o = k_2^4 \frac{(k_r^2 r_r - k_r^2 q_r + 2q_r^2 r_r)}{32 k_r^3 q_r^3 r_r} . \qquad (2.3.6)$$

A plot of Y_o, as a function of the isotropic Poisson ratio $\nu = \lambda/2(\lambda + \mu)$, is given in Fig. 2.3.1. Substituting in (2.3.3) from (2.3.4) and (2.3.5), we obtain

$$2v_r \omega_o \rho \int dv |u_i^+|^2 = 8\mu k_2^2 \Lambda Y_o |R|^2 . \qquad (2.3.7)$$

The magnitude of the coupling coefficient K, in a SAW grating, is now readily determined. By reciprocity $|R| = |S|$. Introducing (2.3.2) and (2.3.7) into (2.2.10), and noting that for an isotropic material

$$k_2 > k_1$$

and thus

$$r_r > q_r$$

we determine

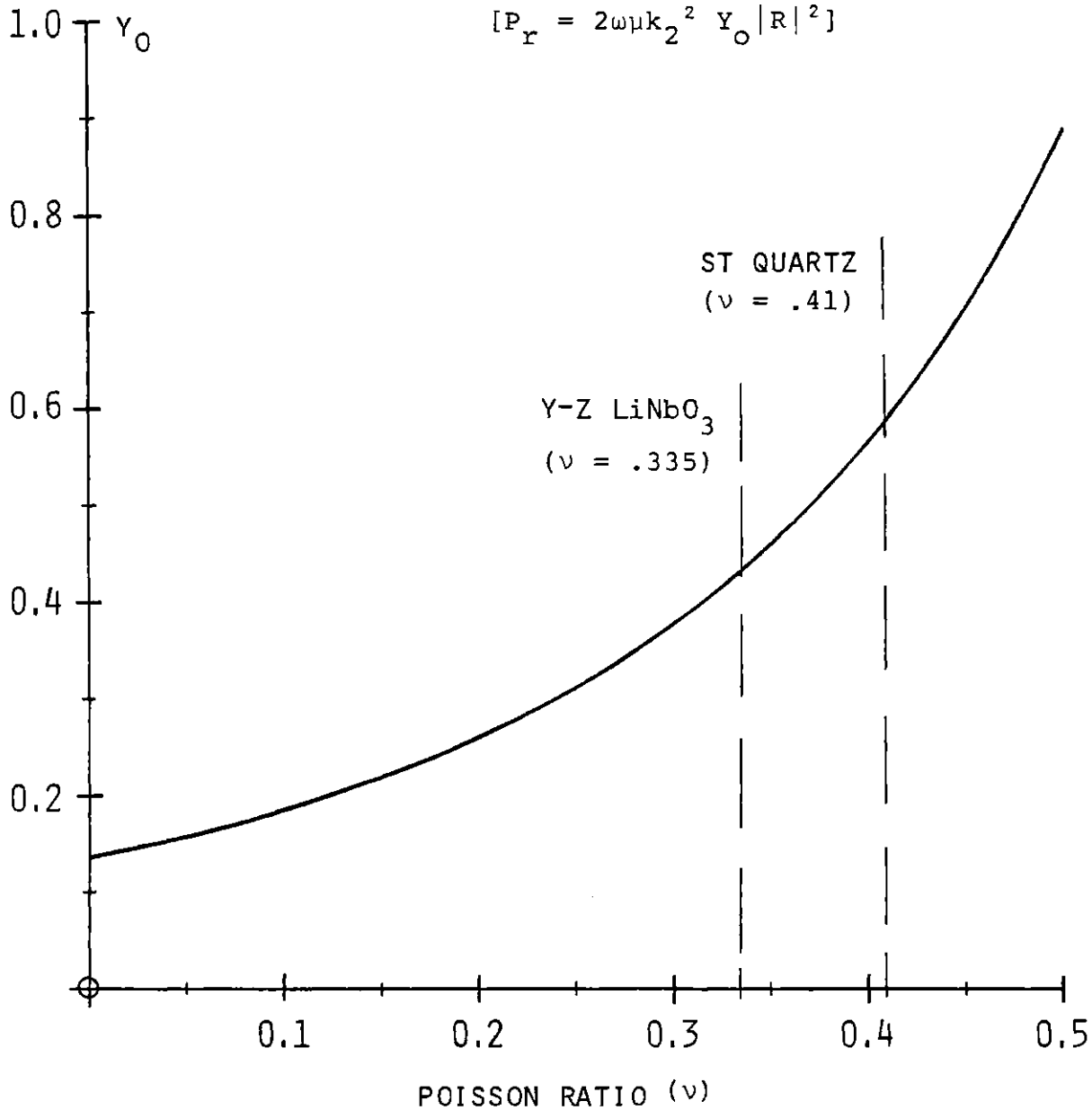

FIG. 2.3.1 ADMITTANCE VS. POISSON RATIO

$$|K| = \varepsilon\lambda_r \frac{(r_r - q_r)q_r}{4\Lambda Y_o} \left| \int_0^{\Lambda} dx\ f(x)\ e^{2jk_r x} \right| . \qquad (2.3.8)$$

If the normalized surface perturbation $f(x)$ is decomposed into a Fourier series

$$f(x) = \sum_{n=1}^{\infty} A_n \cos(n\, k_g x)$$

then at Bragg

$$k_g = 2k_r$$

and, at p × Bragg,

$$k_g = 2k_r/p.$$

Hence,

$$\int_0^{\Lambda} dx\ f(x)\ e^{2jk_r x} = \begin{cases} \frac{\Lambda}{2} A_1, & \text{at Bragg} \\ \frac{\Lambda}{2} A_p, & \text{at } p\text{-th harmonic.} \end{cases}$$

From (2.3.8) the magnitude of the first-order coupling coefficient in a normal-incidence SAW grating is thus, at Bragg

$$|K| = \varepsilon\lambda_r \frac{(r_r - q_r)q_r}{8Y_o} A_1 \tag{2.3.9}$$

and in general, at the p-th harmonic

$$|K| = \varepsilon\lambda_r \frac{(r_r - q_r)q_r}{8Y_o} A_p. \tag{2.3.10}$$

Finally, we determine the first-order Rayleigh wave reflection coefficient of a single normal-incidence (two-sided) groove. To be consistent with previous work we define the reflection coefficient to be $2r$.[46] Since $2r = |K|\Lambda$, we have

$$2r = \begin{cases} |K|(\lambda_r/2), & \text{at Bragg} \\ |K|(\lambda_r/2)p, & \text{at p-th harmonic} \end{cases} \tag{2.3.11}$$

Thus from (2.3.9)-(2.3.11), and replacing $\lambda_r = (2\pi/k_r)$, at Bragg

$$2r = \frac{\varepsilon\pi^2(r_r - q_r)q_r}{4k_r^2 Y_o} A_1 \tag{2.3.12}$$

and in general, at the p-th harmonic

$$2r = \frac{\varepsilon\pi^2(r_r - q_r)q_r}{4k_r^2 Y_o} pA_p. \tag{2.3.13}$$

For the special case of an "idealized" grating, with a square-wave profile, $A_n = 2/n\pi$ for n odd, $A_n = 0$ for n even. Thus, at Bragg and the odd harmonics,

$$2r\Big|_{\substack{\text{square}\\\text{wave}}} = \frac{\varepsilon\pi(r_r - q_r)q_r}{2k_r{}^2 Y_o} \tag{2.3.14}$$

and, at the even harmonics,

$$2r\Big|_{\substack{\text{square}\\\text{wave}}} = 0$$

to $O(\varepsilon)$. The reflection coefficient of an idealized grating at the odd harmonics (2.3.14) is plotted in Fig. 2.3.2, as a function of the isotropic Poisson ratio ν. Throughout this thesis to apply the results of the analyses to typical anisotropic substrate materials, we shall use the concept of an "equivalent isotropic Poisson ratio".[47] In particular, we shall use the theoretically derived values of $\nu = .335$ for Y - Z $LiNbO_3$, and $\nu = .41$ for ST Quartz.[30] Thus, from Fig. 2.3.2 we find that for Y - Z $LiNbO_3$ $2r \simeq 0.69\varepsilon$, and for ST Quartz $2r \simeq 0.53\varepsilon$.

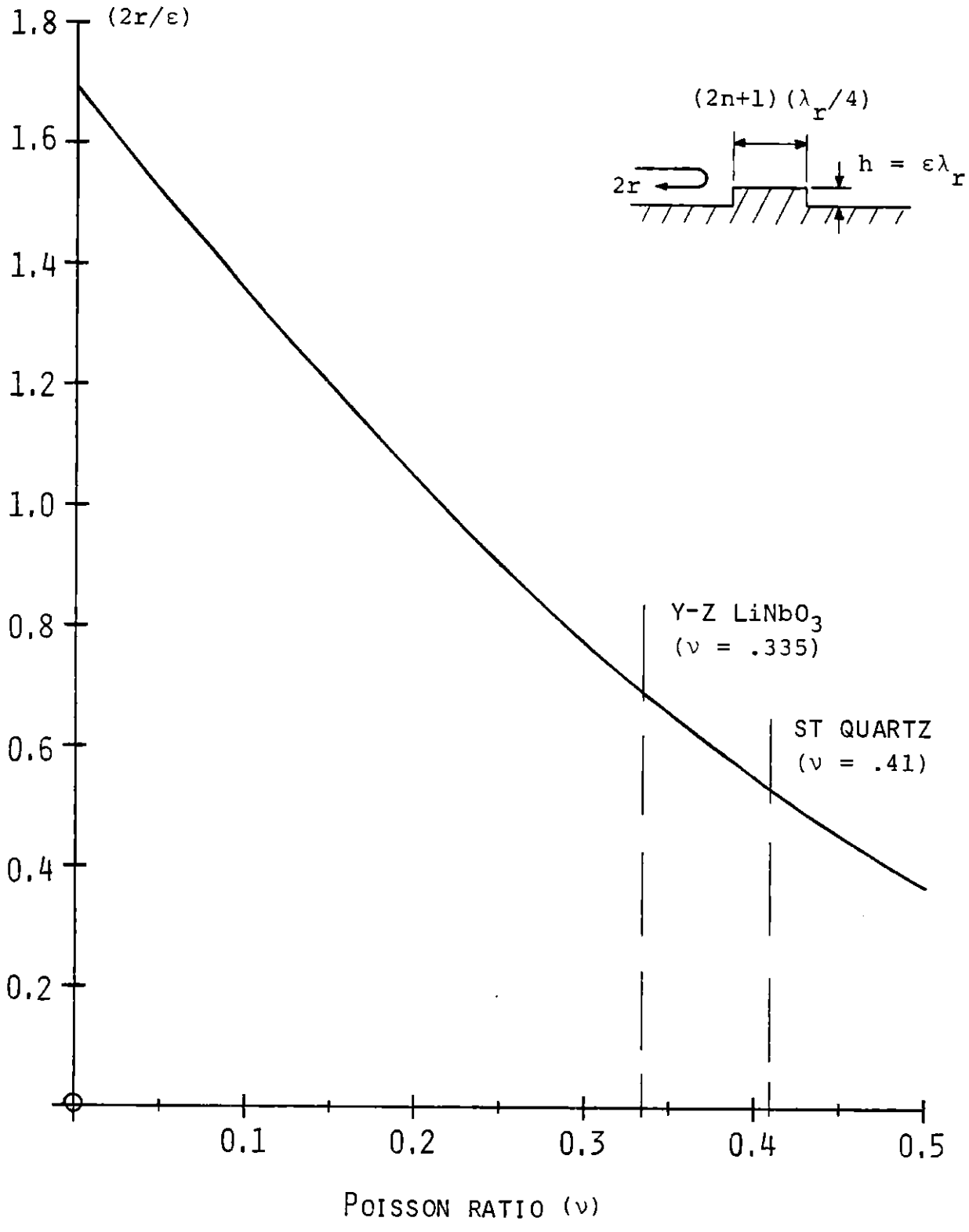

FIG. 2.3.2 NORMALIZED FIRST-ORDER GROOVE REFLECTION COEFFICIENT (AT ODD HARMONICS) VS. POISSON RATIO.

CHAPTER 3

FIRST-ORDER REFLECTION COEFFICIENT FROM BOUNDARY CONDITIONS

3.1. Coupling-of-Modes Approach

In Chapter 2 the first-order reflection coefficient of a normal-incidence groove was obtained from a variational principle. An alternative approach is now presented.

The method to be described is based on determining the width of the grating stop-band, by considering the boundary conditions on the surface of the grating. By means of coupling-of-modes theory the reflection coefficient of a single groove of the grating is then determined. The approach is "quasi-variational", in that the reflection coefficient, and the width of the stop-band, are obtained to one higher order (in ε) than the stresses used in the analysis.

The coupled-wave equations for a normal-incidence grating are

$$\begin{aligned} \frac{\partial}{\partial x}\tilde{R}(x) &= K\, e^{-2j\Delta x}\,\tilde{S}(x) \\ \frac{\partial}{\partial x}\tilde{S}(x) &= K^{*}\, e^{2j\Delta x}\,\tilde{R}(x) \end{aligned} \qquad (3.1.1)$$

where $\tilde{R}(x)$ and $\tilde{S}(x)$ are again the slowly varying amplitudes

of the two counter-propagating waves, i.e.

$$R(x) = \tilde{R}(x)\, e^{j(\omega t - k_r x)}$$
$$S(x) = \tilde{S}(x)\, e^{j(\omega t + k_r x)} . \qquad (3.1.2)$$

The parameter Δ is the amount by which the waves are "detuned" from the synchronous frequency of the grating ω_o.

$$\Delta = \frac{(\omega_o - \omega)}{v_r} \qquad (3.1.3)$$

where $(\omega_o / v_r)\Lambda = p\pi$ ($p = 1$ at Bragg). The dispersion relation for the forward wave $R(x)$, is easily obtained. From (3.1.1)

$$\frac{\partial^2}{\partial x^2} \tilde{R}(x) + 2j\Delta \frac{\partial}{\partial x} \tilde{R}(x) - |K|^2 \tilde{R}(x) = 0.$$

Assuming a solution of the form $e^{-j\alpha x}$ gives

$$\alpha^2 - 2\Delta\alpha + |K|^2 = 0$$

$$\alpha = \Delta \pm \sqrt{\Delta^2 - |K|^2}. \qquad (3.1.4)$$

If the propagation constant of $R(x)$ is denoted by β, then from (3.1.2)-(3.1.4)

$$\beta = k_r + \alpha = (\omega_o/v_r) \pm \sqrt{\Delta^2 - |K|^2}. \tag{3.1.5}$$

This dispersion relation is shown schematically in Fig. 3.1.1. We observe that within the grating stop-band the propagation constant β is complex. The stop-band is symmetric about ω_o and is of width

$$\frac{(\omega_+ - \omega_-)}{v_r} = 2|K|. \tag{3.1.6}$$

At the upper and lower stop-band frequencies, ω_+ and ω_- respectively, the propagation constant is equal to that of a free-surface Rayleigh wave of frequency ω_o, i.e.

$$\beta(\omega_\pm) = k_r = \omega_o/v_r = p\pi/\Lambda. \tag{3.1.7}$$

In the above analysis β was determined for a given ω. However, we may instead choose to define β and determine the resulting ω. This will be the approach used in determining the grating reflection coefficient from boundary conditions.

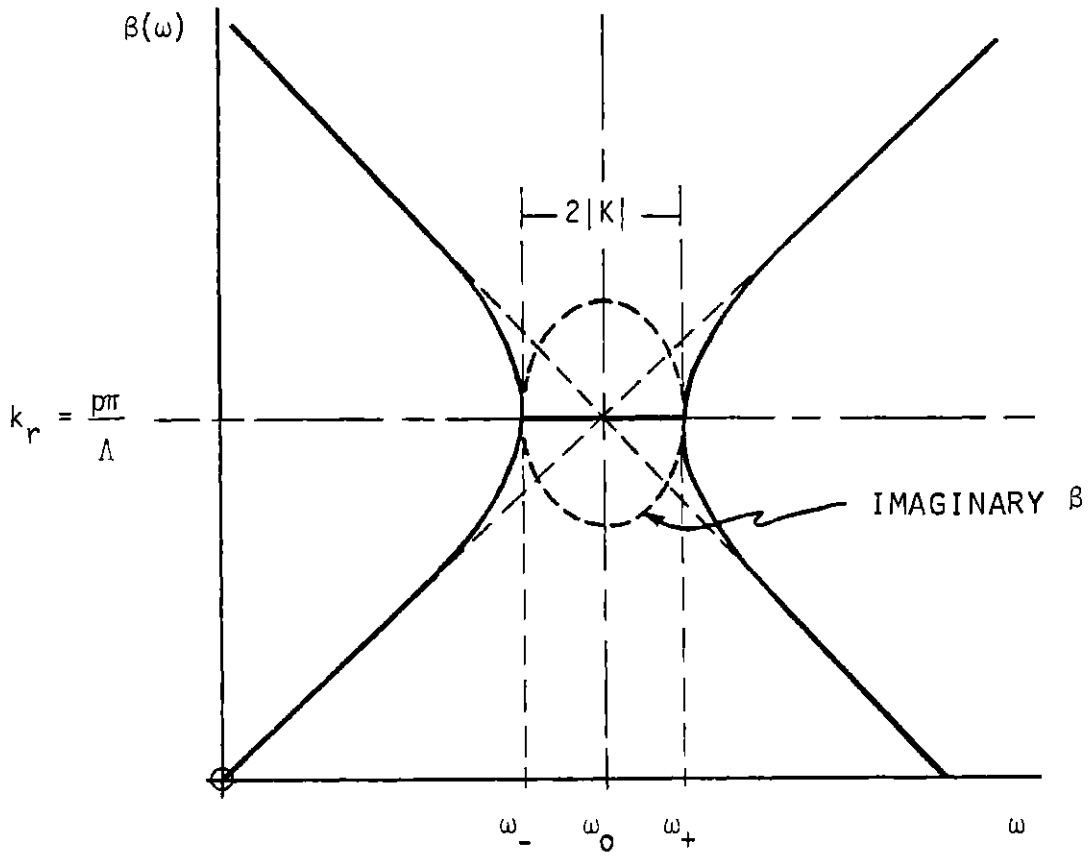

FIG. 3.1.1 FIRST-ORDER GRATING DISPERSION DIAGRAM, β VS. ω.

Interchanging the dependent and independent variables β and ω in Fig. 3.1.1, the dispersion diagram is redrawn in Fig. 3.1.2. The procedure to be followed for determining the reflection coefficient will now be described.

The method is based on determining the upper and lower frequencies of the stop-band, ω_+ and ω_- respectively. At these frequencies the fundamental waves, propagating in the grating, have dependence $e^{\mp jk_r x}$, with k_r given by (3.1.7). From (3.1.7)

$$k_g = 2\pi/\Lambda = \begin{cases} 2kr, & \text{at Bragg} \\ 2k_r/p, & \text{at } p \times \text{Bragg} \end{cases} \tag{3.1.8}$$

Assuming propagating wave solutions in the grating, with dependence $e^{\mp jk_r x}$, the frequency of the waves is determined from the grating boundary conditions. Requiring the surface of the grating to be stress free leads to two determinantal equations that determine ω_+ and ω_-. The coupling coefficient of the grating is then obtained from (3.1.6) and the reflection coefficient of a single groove computed from (2.3.11).

A significant advantage of this method is that in determining the perturbed frequencies (ω_+ and ω_-) to $O(\varepsilon)$, only the fundamental wave components with dependence $e^{\mp jk_r x}$

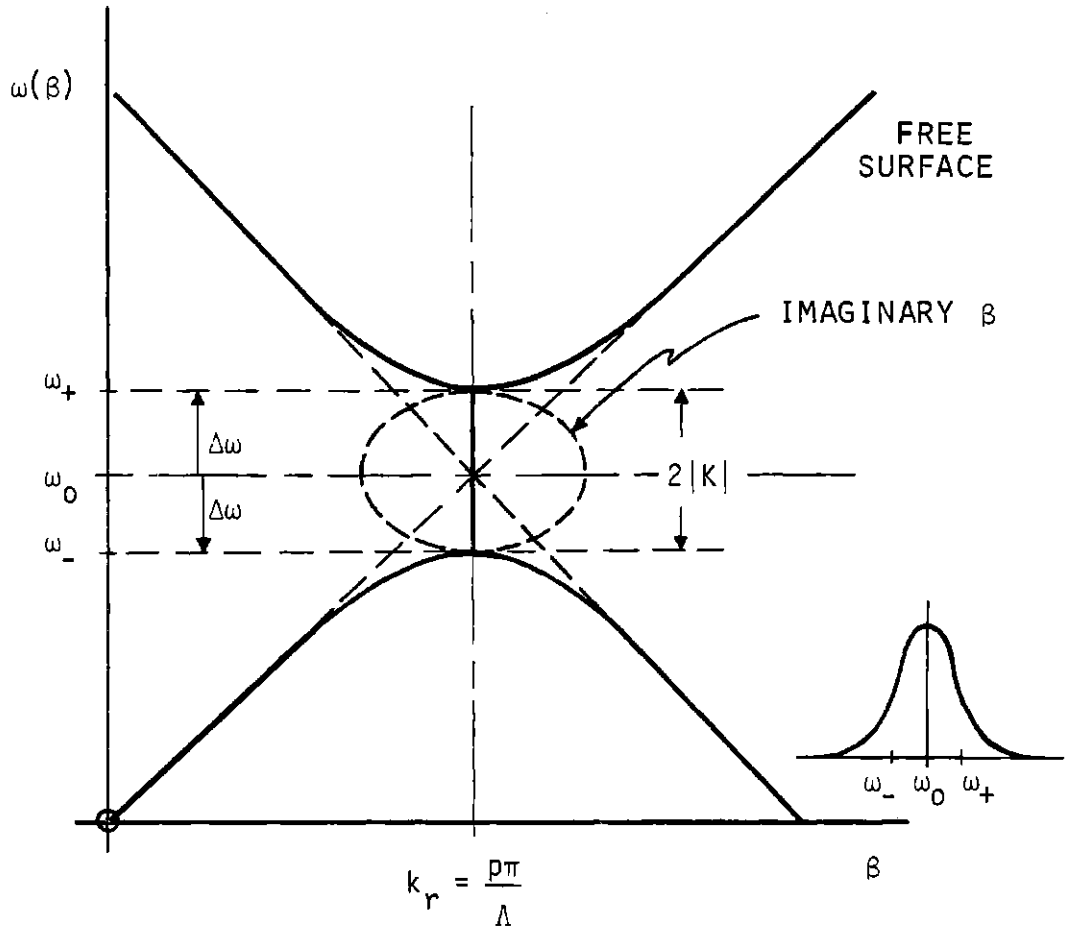

FIG. 3.1.2 FIRST-ORDER GRATING DISPERSION DIAGRAM, ω VS. β.

need be considered. Though components with other spatial dependencies are of finite amplitude to $O(\varepsilon)$, in the grating, they are not required in the analysis. The method is thus computationally very efficient with similar advantages to the variational principle of Chapter 2.

3.2. Determinantal Equations from Boundary Conditions

In this section the first-order determinantal equations are derived, from which the upper and lower stop-band frequencies ω_+ and ω_- respectively (Fig. 3.1.2), are to be determined.

At ω_+, ω_- the fundamental waves in the grating have dependence $e^{\mp jk_r x}$, with k_r given by (3.1.7). To satisfy the boundary conditions on the surface of the grating to $O(\varepsilon)$, we shall assume these waves to comprise a compressional wave and a vertical shear wave propagating in the direction $+x$; also a compressional wave and a vertical shear wave propagating in the direction $-x$. The amplitudes of these waves are zeroth order (and above) in ε, the depth of the grating perturbation, since these solutions continue to exist for $\varepsilon = 0$. In the limit $\varepsilon = 0$, each pair of co-propagating waves combines to form a Rayleigh wave. However, for $\varepsilon \neq 0$ the ratio of the shear/compressional wave amplitudes of each pair is different from that of a Rayleigh wave, by $O(\varepsilon)$. In addition, the waves no longer satisfy the Rayleigh wave dispersion relation (B.18).

To satisfy the boundary conditions on the surface of the grating completely, to $O(\varepsilon)$, additional wave components with other spatial dependencies are required. These waves, however, exist only in the presence of the grating ($\varepsilon \neq 0$) and are thus

of $O(\varepsilon)$ (or above). As discussed in Section 3.1, the amplitudes of these waves are not required to determine the determinantal equations for the upper and lower stop-band frequencies to $O(\varepsilon)$. (We shall see later in this thesis that these waves are responsible for the stored-energy effects in the grating.)

From (A.4) the stress on the surface of the grating is, to $O(\varepsilon)$

$$\bar{\sigma}_s = \{\sigma_{xz}(0) + \varepsilon\lambda_r[f(x)\ \sigma'_{xz}(0) - f'(x)\ \sigma_{xx}(0)]\}\ \hat{x}$$

$$+ \{\sigma_{zz}(0) + \varepsilon\lambda_r[f(x)\ \sigma'_{zz}(0) - f'(x)\ \sigma_{xz}(0)]\}\ \hat{z} \qquad (3.2.1)$$

where

$$\sigma_{ij}(0) = \sigma_{ij}\Big|_{z=0}$$

and

$$\sigma'_{ij}(0) = \frac{\partial}{\partial z}\,\sigma_{ij}\Big|_{z=0}.$$

As in section 2.3 we represent the normalized surface perturbation $f(x)$ by a Fourier series

$$f(x) = \sum_{n=1}^{\infty} A_n \cos(nk_g x) \qquad (3.2.2)$$

thus

$$f'(x) = - \sum_{n=1}^{\infty} nk_g A_n \sin(nk_g x). \qquad (3.2.3)$$

Since the surface of the grating is a free boundary, it must be stress free i.e. $\bar{\sigma}_s = 0$. This condition, from (3.2.1)-(3.2.3), requires

$$\sigma_{xz}(0) + \varepsilon\lambda_r \left\{ \left[\sum_{n=1}^{\infty} A_n \cos(nk_g x) \right] \sigma'_{xz}(0) + \left[\sum_{n=1}^{\infty} nk_g A_n \sin(nk_g x) \right] \sigma_{xx}(0) \right\} = 0 \qquad (3.2.4)$$

$$\sigma_{zz}(0) + \varepsilon\lambda_r \left\{ \left[\sum_{n=1}^{\infty} A_n \cos(nk_g x) \right] \sigma'_{zz}(0) + \left[\sum_{n=1}^{\infty} nk_g A_n \sin(nk_g x) \right] \sigma_{xz}(0) \right\} = 0. \qquad (3.2.5)$$

The only waves in the grating with a finite zeroth-order amplitude (in ε) are the propagating waves with dependence $e^{\mp jk_r x}$. Thus, to $O(\varepsilon)$ only the stress components of these waves are required in the terms $\varepsilon\lambda_r\{\ \}$ of (3.2.4) and (3.2.5). The latter terms thus comprise, in general, an infinite set of

components with the dependence $e^{\mp jk_r x}\, e^{(\mp) jnk_g x}$. From (3.2.4) and (3.2.5) the same wave components are required for $\sigma_{xz}(0)$, $\sigma_{zz}(0)$. Thus, an infinite set of waves with spatial dependence $e^{\mp jk_r x}\, e^{(\mp) jnk_g x}$ is required to satisfy the boundary conditions on the surface of the grating to $O(\varepsilon)$. The wave components with $n \neq 0$ are referred to as Brillouin components and are of $O(\varepsilon)$ (or above).

Equations (3.2.4) and (3.2.5) must be satisfied separately for each of the spatial dependencies of the waves. The determinantal equations, for the upper and lower stop-band frequencies, are obtained by considering only those terms with the spatial dependence of the fundamental waves, $e^{\mp jk_r x}$.

To simplify the analysis the following notation is introduced. The amplitude of the acoustic waves with spatial dependence $e^{\mp jk_r x}$ is denoted by $S_i^{\pm}$, where

$$i = \begin{cases} 1, & \text{for compressional wave} \\ 2, & \text{for shear wave.} \end{cases}$$

Also the x-independent stress components of these waves $\tilde{\sigma}_{ij}^{\pm}$, are defined by

$$\sigma_{ij}^{\pm} = \tilde{\sigma}_{ij}^{\pm}\, e^{\mp jk_r x}.$$

To zeroth order, the co-propagating compressional and

shear waves in each direction are Rayleigh waves (with amplitude $S_1^{\pm}$). In (3.2.4) and (3.2.5) it can be seen that the propagating waves with dependence $e^{\mp jk_r x}$ are coupled together only via the Fourier component of the grating A_n, with $nk_g = 2k_r$. At the p-th harmonic from (3.1.8) $k_g = 2k_r/p$. Thus, for the stop-band at the p-th harmonic, the propagating waves are coupled together only via the Fourier component A_p of the grating. Hence, from (3.2.4) we obtain, to $O(\varepsilon)$

cf. $e^{-jk_r x}$ dep.

$$S_i^+ \tilde{\sigma}_{ixz}^+(0) + \varepsilon\lambda_r[(A_p/2)\, S_1^- \tilde{\sigma}_{xz}^{-r'}(0) + jk_r A_p S_1^- \tilde{\sigma}_{xx}^{-r}(0)] = 0$$

cf. $e^{+jk_r x}$ dep.

$$S_i^- \tilde{\sigma}_{ixz}^-(0) + \varepsilon\lambda_r[(A_p/2)\, S_1^+ \tilde{\sigma}_{xz}^{r'}(0) - jk_r A_p S_1^+ \tilde{\sigma}_{xx}^{r}(0)] = 0$$

where a repeated subscript again implies summation. From (3.2.5) we obtain, to $O(\varepsilon)$

cf. $e^{-jk_r x}$ dep

$$S_i^+ \tilde{\sigma}_{izz}^+(0) + \varepsilon\lambda_r(A_p/2)\, S_1^- \tilde{\sigma}_{zz}^{-r'}(0) = 0$$

cf. $e^{+jk_r x}$ dep.

$$S_i^- \tilde{\sigma}_{izz}^-(0) + \varepsilon\lambda_r(A_p/2)\, S_l^+ \tilde{\sigma}_{zz}^{r'}(0) = 0$$

since $\sigma_{xz}^{\pm r} = 0$. By reciprocity $\sigma_{ij}^r = \sigma_{ij}^{r*}$ and $\sigma_{ij}^- = \sigma_{ij}^{+*}$, with this replacement the equations are

$$S_i^+ \tilde{\sigma}_{ixz}^+(0) + \varepsilon\lambda_r A_p S_l^- \left[\frac{1}{2}\tilde{\sigma}_{xz}^{r*'}(0) + jk_r\, \tilde{\sigma}_{xx}^{r*}(0)\right] = 0 \qquad \text{(i)}$$

$$S_i^- \tilde{\sigma}_{ixz}^{+*}(0) + \varepsilon\lambda_r A_p S_l^+ \left[\frac{1}{2}\tilde{\sigma}_{xz}^{r'}(0) - jk_r\, \tilde{\sigma}_{xx}^{r}(0)\right] = 0 \qquad \text{(ii)}$$

$$S_i^+ \tilde{\sigma}_{izz}^+(0) + \varepsilon\lambda_r(A_p/2) S_l^- \tilde{\sigma}_{zz}^{r*'}(0) = 0 \qquad \text{(iii)}$$

$$S_i^- \tilde{\sigma}_{izz}^{+*}(0) + \varepsilon\lambda_r(A_p/2) S_l^+ \tilde{\sigma}_{zz}^{r'}(0) = 0. \qquad \text{(iv)}$$

(3.2.6)

The form of (3.2.6) now suggests a transformation of variables to reduce the four inter-dependent equations, to two independent pairs of equations. Defining

$$S_i^T = S_i^+ + S_i^{-*}$$

$$S_i^D = S_i^+ - S_i^{-*} \tag{3.2.7}$$

from (3.2.6) (i)+(ii)*, and (iii)+(iv)* respectively,

$$S_i^T \tilde{\sigma}_{ixz}^+(0) + \varepsilon\lambda_r A_p S_1^{T*} \left[\frac{1}{2}\tilde{\sigma}_{xz}^{r*'}(0) + jk_r \tilde{\sigma}_{xx}^{r*}(0)\right] = 0$$

$$S_i^T \tilde{\sigma}_{izz}^+(0) + \varepsilon\lambda_r (A_p/2) S_1^{T*} \tilde{\sigma}_{zz}^{r*'}(0) = 0 \tag{3.2.8}$$

and from (3.2.6) (i)-(ii)*, and (iii)-(iv)* respectively,

$$S_i^D \tilde{\sigma}_{ixz}^+(0) - \varepsilon\lambda_r A_p S_1^{D*} \left[\frac{1}{2}\tilde{\sigma}_{xz}^{r*'}(0) + jk_r \tilde{\sigma}_{xx}^{r*}(0)\right] = 0$$

$$S_i^D \tilde{\sigma}_{izz}^+(0) - \varepsilon\lambda_r (A_p/2) S_1^{D*} \tilde{\sigma}_{zz}^{r*'}(0) = 0. \tag{3.2.9}$$

Equations (3.2.8) and (3.2.9) are independent pairs of equations for the amplitudes S_1^T, S_2^T and S_1^D, S_2^D respectively. For $\varepsilon \neq 0$ the determinantal equations for (3.2.8) and (3.2.9) will be different. Since both cannot be satisfied simultaneously, then either

$$S_i^D = 0 \;\rightarrow\; S_i^+ = S_i^{-*}$$

or

$$S_i^T = 0 \rightarrow S_i^+ = - S_i^{-*}$$

to $O(\varepsilon)$.

Case 1: $S_i^+ = S_i^{-*}$

In this case $S_i^D = 0$ and S_i^T is finite. Thus this solution satisfies the determinantal equation of (3.2.8). Introducing the bulk and Rayleigh wave stress components from (B.8), (B.14) and (B.20) into (3.2.8), and defining S_1^+ to be real, gives

$$[2\mu jk_r r - \varepsilon\lambda_r \mu jk_r A_p(r_r - q_r)(2q_r + r_r)]S_1^+ - \mu(k_r^2 + q^2)S_2^+ = 0$$

$$[\mu(k_r^2 + q^2) - \varepsilon\lambda_r \mu(A_p/2)(r_r - q_r)(k_r^2 + q_r^2)]S_1^+ + 2\mu jk_r q\, S_2^+ = 0$$

(3.2.10)

To $O(\varepsilon)$, the determinantal equation is

$$(k_r^2 + q^2)^2 - 4k_r^2 qr = - \varepsilon\lambda_r A_p(r_r - q_r)[2k_r^2 q_r(2q_r + r_r)$$

$$- \frac{1}{2} (k_r^2 + q_r^2)^2]$$

which simplifies, using the Rayleigh wave determinantal equation (B.18), to

$$(k_r^2 + q^2)^2 - 4k_r^2 qr = - \varepsilon\lambda_r \, 4k_r^2 q_r^2 (r_r - q_r) A_p \qquad (3.2.11)$$

Case 2: $S_i^+ = - S_i^{-*}$

In this case $S_i^T = 0$ and S_i^D is finite. This solution therefore satisfies the determinantal equation of (3.2.9). The determinantal equation of (3.2.9) will be identical with that of (3.2.8), except for the replacement $\varepsilon \to -\varepsilon$. Thus, in this case, the determinantal equation is

$$(k_r^2 + q^2)^2 - 4k_r^2 qr = + \varepsilon\lambda_r \, 4k_r^2 q_r^2 (r_r - q_r) A_p. \qquad (3.2.12)$$

Equations (3.2.11) and (3.2.12) are the required determinantal equations for determination of the upper and lower stop-band frequencies, ω_+ and ω_- respectively.

3.3. Determination of Stop-Band and First-Order Reflection Coefficient

At the edges of the stop-band ω_+, ω_- [Fig. 3.1.2] the surface waves in the grating have propagation constant k_r, where k_r is the propagation constant of a Rayleigh wave at frequency ω_o (3.1.7). Corresponding to these two frequencies, it was determined in the previous section that, from boundary considerations, the two solutions with propagation constant k_r in the grating, satisfy the alternate determinantal equations (3.2.11) and (3.2.12). Thus at ω_+, ω_-

$$(k_r^2 + q^2)^2 - 4k_r^2 qr = \pm \varepsilon\lambda_r \, 4k_r^2 q_r^2 (r_r - q_r) A_p \qquad (3.3.1)$$

where r and q are the decay constants of the compressional wave and the shear wave respectively. A_p is the Fourier coefficient of the grating, and p is the harmonic of the stop-band.

From (3.3.1) we now determine the width of the stop-band. Defining the perturbed frequencies at the edges of the stop-band by

$$\omega = \omega_o + \Delta\omega$$

then from (D.6) the modified dispersion relation for the waves is, to $O(\Delta\omega)$

$$(k_r^2 + q^2)^2 - 4k_r^2 qr = \frac{4k_r^2}{q_r r_r}(r_r - q_r)(k_r^2 r_r - k_r^2 q_r + 2q_r^2 r_r)$$

$$(\Delta\omega/\omega_o). \qquad (3.3.2)$$

Hence, from (3.3.1) and (3.3.2) we determine

$$\left(\frac{\Delta\omega}{\omega_o}\right) = \pm \varepsilon\lambda_r \frac{q_r^3 r_r}{(k_r^2 r_r - k_r^2 q_r + 2q_r^2 r_r)} A_p. \qquad (3.3.3)$$

The width of the stop-band is $2|\Delta\omega|$ and, as expected from the coupling-of-modes analysis of Section 3.1, the stop-band is symmetric about ω_o.

The reflection coefficient of a normal-incidence groove $2r$, is easily obtained from (3.3.3). We first determine the magnitude of the coupling coefficient K in the grating. From (3.1.6)

$$|K| = \frac{|\Delta\omega|}{v_r} = k_r \left|\frac{\Delta\omega}{\omega_o}\right|$$

Thus from (3.3.3)

$$|K| = \varepsilon\lambda_r \frac{k_r q_r^3 r_r}{(k_r^2 r_r - k_r^2 q_r + 2q_r^2 r_r)} A_p.$$

Introducing the characteristic admittance Y_o, using (C.5), and using the Rayleigh wave dispersion relation (B.18), we obtain

$$|K| = \varepsilon\lambda_r \frac{(r_r - q_r)q_r}{8Y_o} A_p. \qquad (3.3.4)$$

This is in exact agreement with the first-order coupling coefficient obtained using the variational principle (2.3.10). Using (2.3.11) the reflection coefficient of a normal incidence groove is thus again found to be as given by (2.3.13), i.e.

$$2r = \varepsilon \frac{\pi^2 (r_r - q_r)q_r}{4k_r^2 Y_o} pA_p$$

at the p-th harmonic.

CHAPTER 4

SECOND-ORDER STOP-BAND AND FREQUENCY SHIFT

4.1 Introduction

In the majority of applications, SAW gratings are used as reflective arrays and thus required to operate close to the frequency of maximum reflection. If the surface-wave velocity, within a grating, is assumed to be unchanged from the velocity on the free surface v_r, maximum reflection is to be expected at Bragg. At the Bragg frequency $\omega_o/v_r = \pi/\Lambda$, thus

$$\Lambda = \lambda_r/2 \tag{4.1.1}$$

where Λ is the period of the grating. For an "idealized" grating, with a square wave profile, the reflections from the front and back faces of each groove then add exactly in phase and the grating has maximum reflection.

In Chapter 3 we found that to first order (in ε) the stop-band of a grating is symmetric about the synchronous frequency of the grating ω_o. This is as expected from first-order coupling-of-modes theory. A grating designed for maximum reflection at Bragg (ω_o), according to (4.1.1), will thus have maximum reflection at the expected design frequency and a sym-

metric stop-band response, to $O(\varepsilon)$. The surface-wave velocity within a grating may therefore be assumed to be unchanged to $O(\varepsilon)$, from that on the free surface, when designing a grating reflector.

In narrow-band, high Q SAW gratings second-order effects (in ε) can become important for grating design. In particular several authors have reported that the frequency of maximum grating reflection is found experimentally to be lower, by $O(\varepsilon^2)$, than that predicted by (4.1.1).[3,5,25] For design purposes therefore, the effective surface-wave velocity within a grating must be taken to be less than that on the free surface, by $O(\varepsilon^2)$.

Strong second-order effects have also been observed near the second-harmonic frequency (i.e. 2 × Bragg) of a grating.[26-29] The first-order analysis, given in the preceding chapters, predicts no reflection from an idealized grating, with a square-wave profile, at the second-harmonic, since $A_2 = 0$. However, a reflection comparable with that at Bragg has been reported for such a grating.[28] In addition, another important second-order effect that has been observed near the second-harmonic is the coupling of surface energy into bulk modes.[26]

In this chapter, the analysis of Chapter 3 is extended to obtain the grating stop-bands to $O(\varepsilon^2)$. Both the center

frequency and width of the stop-band are determined at each harmonic of the grating. The second-order reduction in the frequency of maximum grating reflection, at the specified harmonic, is determined from the center frequency of the stop-band. In addition, a change in the width of the stop-band can be interpreted as a change in the grating coupling coefficient K. The latter implying a second-order change in the reflection coefficient/groove. Furthermore, at the second and higher harmonics, the analysis also predicts bulk radiation loss.

In the following chapter the second-order effects, predicted by the theory, are examined in detail around Bragg and the second-harmonic frequency of the grating. The effect of the grating profile on second-order effects is studied. Whenever possible the theory is compared with available experimental second-order data such as that referred to above.

4.2 First-Order Wave Amplitudes

Following the approach of Chapter 3, we now seek to determine the upper and lower frequencies of the stop-band, ω_+ and ω_- respectively, to $O(\varepsilon^2)$. To do so we will require the amplitudes of all the stress components in the grating, at ω_+ and ω_-, to $O(\varepsilon)$. The amplitudes of the fundamental waves, with dependence $e^{\mp jk_r x}$, can be determined immediately.

Case 1. $S_i^+ = S_i^{-*}$

This case corresponds to ω_-. From (3.2.10), to $O(\varepsilon)$

$$\frac{S_2^+}{S_1^+} = \frac{2jk_r r}{(k_r^2 + q^2)} - \varepsilon\lambda_r jk_r A_p \frac{(r_r - q_r)(2q_r + r_r)}{(k_r^2 + q_r^2)}$$

$$\equiv j \frac{(k_r^2 + q^2)}{2k_r q} - \varepsilon\lambda_r j A_p \frac{(r_r - q_r)(k_r^2 + q_r^2)}{4k_r q_r} \qquad (4.2.1)$$

where p is the harmonic of the stop-band ($p = 1$ at Bragg).

Case 2. $S_i^+ = -S_i^{-*}$

This case corresponds to ω_+. The relations for the propagating waves are identical with those for Case 1, except for

the replacement $\varepsilon \to -\varepsilon$. Thus, to $O(\varepsilon)$

$$\frac{S_2^+}{S_1^+} = \frac{2jk_r r}{(k_r^2 + q^2)} + \varepsilon\lambda_r jk_r A_p \frac{(r_r - q_r)(2q_r + r_r)}{(k_r^2 + q_r^2)}$$

$$\equiv j \frac{(k_r^2 + q^2)}{2k_r q} + \varepsilon\lambda_r j A_p \frac{(r_r - q_r)(k_r^2 + q_r^2)}{4k_r q_r} . \qquad (4.2.2)$$

In the limit $\varepsilon = 0$, both (4.2.1) and (4.2.2) are in agreement with the ratio of the shear/compressional wave amplitudes determined for a Rayleigh wave (B.19).

The boundary conditions on the surface of the grating cannot be satisfied, to $O(\varepsilon)$, with only the fundamental wave components considered above. It was shown in Section 3.2 that additional "Brillouin" components are required, with the general spatial dependence $e^{\mp jk_r x}\, e^{(\mp)jnk_g x}$. The amplitudes of these waves, which are of $O(\varepsilon)$ or above, can be determined from the boundary conditions. From (3.2.4) and (3.2.5), for the surface of the grating to be stress free ($\bar{\sigma}_s = 0$) to $O(\varepsilon)$, we require

$$\sigma_{xz}(0) + \varepsilon\lambda_r \left\{ \left[\sum_{n=1} A_n \cos(nk_g x) \right] \sigma'_{xz}(0) \right.$$

$$+ \left[\sum_{n=1}^{\infty} nk_g A_n \sin(nk_g x)\right]\sigma_{xx}(0)\Bigg\} = 0 \qquad (4.2.3)$$

$$\sigma_{zz}(0) + \varepsilon\lambda_r \Bigg\{\left[\sum_{n=1}^{\infty} A_n \cos(nk_g x)\right] \sigma'_{zz}(0)$$

$$+ \left[\sum_{n=1}^{\infty} nk_g A_n \sin(nk_g x)\right] \sigma_{xz}(0)\Bigg\} = 0. \qquad (4.2.4)$$

Only the fundamental waves, with spatial dependence $e^{\mp jk_r x}$, have finite zeroth-order amplitude (in ε) in the grating. Thus, as discussed in Section 3.2, to $O(\varepsilon)$ only the stress components of these waves need be included in the terms $\varepsilon\lambda_r\{\ \}$ in (4.2.3) and (4.2.4).

At the edges of the stop-band, for the p-th harmonic of the grating, from (3.1.8) $k_g = 2k_r/p$. Referring to Fig. 4.2.1, the Brillouin components therefore have the general spatial dependence

$$e^{\mp j(k_r + nk_g)x} \qquad n = 1 \to \infty$$

and

$$e^{\mp j(k_r - nk_g)x} \qquad n = 1 \to \bar{p}$$

where

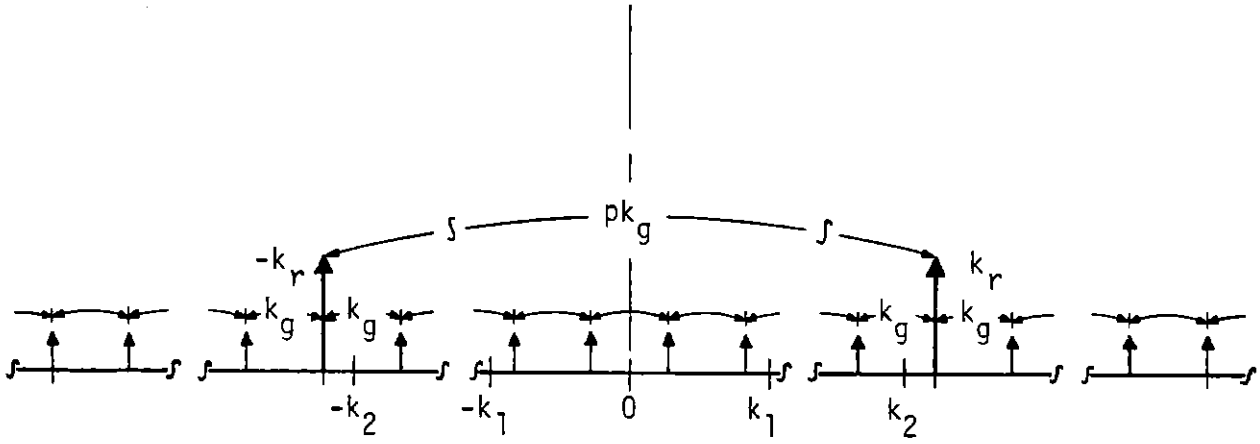

(a) AT ODD HARMONICS (i.e. p_{odd})

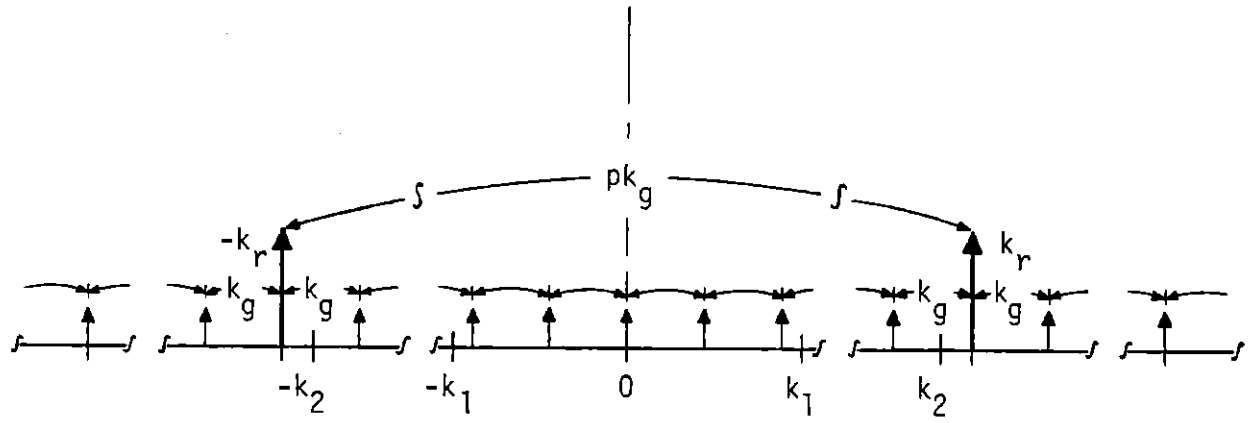

(b) AT EVEN HARMONICS (i.e. p_{even})

FIG. 4.2.1 SPATIAL FREQUENCIES OF GRATING WAVES AT SYNCHRONISM.

$$\bar{p} = \begin{cases} p/2 & \text{for } p \text{ even} \\ (p-1)/2, & \text{for } p \text{ odd} \end{cases} \qquad (4.2.5)$$

We denote the amplitudes of the waves with dependence $e^{\mp j(k_r + nk_g)x}$ by $S_i^{\pm}(n)$. These waves all decay away from the surface and thus radiate no energy into the bulk. The amplitudes of the Brillouin components with dependence $e^{\mp j(k_r - nk_g)x}$ are denoted by $S_i^{\pm}(-n)$. Compressional waves with the latter dependence propagate into the bulk for $(k_r - nk_g) < k_1$; shear waves for $(k_r - nk_g) < k_2$. All the compressional waves, of these Brillouin components, are therefore radiative for $p < 2/(1 - k_1/k_r)$; and the shear waves for $p < 2/(1 - k_2/k_r)$. For an isotropic solid $\sim .87 < k_2/k_r < \sim .95$.[48] All the latter shear waves therefore radiate energy away from the surface, in any isotropic material, for $p \leq 15$. This condition will be the case in almost all problems of practical importance. For $p = 2,3$ the single compressional wave component of these Brillouin waves will radiate for $0 < \nu < .42$, where ν is the Poisson ratio of the solid.

In Appendix E the amplitudes of all the Brillouin components, at the edges of the stop-band, are determined to $O(\varepsilon)$. The amplitudes are determined by considering only terms with the corresponding spatial dependence in (4.2.3) and (4.2.4).

4.3 Determinantal Equations to Second Order

The determinantal equations at the upper and lower frequencies of the stop-bands, ω_+ and ω_- respectively, can be derived to $O(\varepsilon^2)$, using only the first-order wave amplitudes in the grating. The analysis is an extension, to second order, of the approach presented in Section 3.2. It is based on considering the boundary conditions on the surface of the grating to $O(\varepsilon^2)$. From (A.3), the stress on the surface of the grating, for waves with no y-dependence, is to $O(\varepsilon^2)$

$$\begin{aligned}\bar{\sigma}_s = \Big\{ & \sigma_{xz}(0) + \varepsilon\lambda_r [f(x)\ \sigma'_{xz}(0) - f'(x)\ \sigma_{xx}(0)] \\ & - (\varepsilon\lambda_r)^2 [f(x)\ f'(x)\ \sigma'_{xx}(0) + \frac{1}{2}\ (f'(x))^2\ \sigma_{xz}(0) \\ & - \frac{1}{2}\ (f(x))^2\ \sigma''_{xz}(0)] \Big\}\ \hat{x} \\ & + \Big\{ \sigma_{zz}(0) + \varepsilon\lambda_r [f(x)\ \sigma'_{zz}(0) - f'(x)\ \sigma_{xz}(0)] \\ & - (\varepsilon\lambda_r)^2 [f(x)\ f'(x)\ \sigma'_{xz}(0) + \frac{1}{2}\ (f'(x))^2\ \sigma_{zz}(0) \\ & - \frac{1}{2}\ (f(x))^2\ \sigma''_{zz}(0)] \Big\}\ \hat{z} \end{aligned} \qquad (4.3.1)$$

where

$$\sigma_{ij}(0) = \sigma_{ij}\Big|_{z=0}$$

$$\sigma'_{ij}(0) = \frac{\partial}{\partial z}\,\sigma_{ij}\Big|_{z=0}$$

$$\sigma''_{ij}(0) = \frac{\partial^2}{\partial z^2}\,\sigma_{ij}\Big|_{z=0}.$$

Again, we represent the normalized surface perturbation $f(x)$ by the Fourier series (3.2.2). The derivative $f'(x)$ is given by (3.2.3).

The surface of the grating is a free boundary. Thus, it is required to be stress free, i.e. $\bar{\sigma}_s = 0$. To satisfy the boundary conditions, in general, both fundamental ($e^{\mp jk_r x}$ dep.) and Brillouin wave ($e^{\mp jk_r x}\, e^{(\mp)\, jnk_g x}$ dep.) components are required in the grating. These waves consist of both compressional and shear wave components. The fundamental components are the only waves with finite zeroth-order amplitude. All the Brillouin components are of $O(\varepsilon)$ or above. Furthermore, the fundamental wave components, to zeroth order, are counter-propagating Rayleigh waves. Therefore, to $O(\varepsilon^2)$, only the stress components associated with the latter need be included

in the terms $(\varepsilon\lambda_r)^2[\ ]$ in (4.3.1). Hence, to satisfy the boundary conditions to $O(\varepsilon^2)$, from (4.3.1), (3.2.2) and (3.2.3), we require

$$\sigma_{xz}(0) + \varepsilon\lambda_r \left\{ \left[\sum_{n=1}^{\infty} A_n \cos(nk_g x) \right] \sigma'_{xz}(0) + \left[\sum_{n=1}^{\infty} nk_g A_n \sin(nk_g x) \right] \sigma_{xx}(0) \right\} + (\varepsilon\lambda_r)^2 \left\{ \left[\sum_{m=1}^{\infty} \sum_{n=1}^{\infty} A_m A_n nk_g \cos(mk_g x) \sin(nk_g x) \right] \sigma'_{xx}(0) + \frac{1}{2} \left[\sum_{m=1}^{\infty} \sum_{n=1}^{\infty} A_m A_n \cos(mk_g x) \cos(nk_g x) \right] \sigma''_{xz}(0) \right\} = 0 \tag{4.3.2}$$

$$\sigma_{zz}(0) + \varepsilon\lambda_r \left\{ \left[\sum_{n=1}^{\infty} A_n \cos(nk_g x) \right] \sigma'_{zz}(0) + \left[\sum_{n=1}^{\infty} nk_g A_n \sin(nk_g x) \right] \sigma_{xz}(0) \right\} + (\varepsilon\lambda_r)^2 \left\{ \left[\sum_{m=1}^{\infty} \sum_{n=1}^{\infty} A_m A_n nk_g \cos(mk_g x) \sin(nk_g x) \right] \sigma'_{xz}(0) + \frac{1}{2} \left[\sum_{m=1}^{\infty} \sum_{n=1}^{\infty} A_m A_n \cos(mk_g x) \cos(nk_g x) \right] \sigma''_{zz}(0) \right\} = 0 \tag{4.3.3}$$

since $\sigma_{xz}^{\pm r}(0) = \sigma_{zz}^{\pm r}(0) = 0$.

The determinantal equations, at the edges of the stopbands, are obtained by considering only the grating surface stresses in (4.3.2) and (4.3.3) with the spatial dependence $e^{-jk_r x}$. In these equations, to $O(\varepsilon^2)$, the only unknown wave amplitudes are those of the forward propagating compressional and shear wave components with dependence $e^{-jk_r x}$. The other wave components, in the grating, generate surface stress components with dependence $e^{-jk_r x}$, only via their interaction with the spatial components of the surface. Since the surface perturbation is of $O(\varepsilon)$, an error of $O(\varepsilon^2)$, in these wave components, introduces an error of only $O(\varepsilon^3)$ into the equations. Hence, to satisfy the boundary conditions on the surface of the grating, for stress components with dependence $e^{-jk_r x}$, to $O(\varepsilon^2)$, with the exception of the forward propagating fundamental wave components, we only require the amplitudes of the grating waves to $O(\varepsilon)$. All the wave amplitudes were previously determined, to $O(\varepsilon)$, in Section 4.2 and Appendix E.

By considering the surface stress components with dependence $e^{-jk_r x}$, as described above at ω_+ and ω_-, a pair of simultaneous equations for the wave amplitudes S_1^+ and S_2^+, to $O(\varepsilon^2)$, is obtained. For non-trivial solutions, at each frequency, the determinants of the equations must be zero. In

this manner the determinantal equations, at the edges of the stop-bands, are derived. The details of the analysis are given in Appendix E. At the lower edge of the stop-band ω_-, the waves in the grating satisfy the determinantal equation (E.30), to $O(\varepsilon^2)$. At the upper edge ω_+, the waves satisfy the determinantal equation (E.34), to $O(\varepsilon^2)$.

In the determinantal equations (E.30) and (E.34), the compressional and shear wave decay constants, r and q respectively, are as yet undetermined. This is the case because although the grating waves have propagation constant k_r, the frequency of the waves is perturbed by the grating, from ω_o [Fig. 3.1.2], and has yet to be determined to $O(\varepsilon^2)$. In the following section, by Taylor expanding the decay constants in terms of the frequency perturbation at the gap, as in Appendix D, the frequencies of the edges of the stop-bands, ω_+ and ω_-, are determined to $O(\varepsilon^2)$ from the determinantal equations.

4.4 Second-Order Stop-Band and Frequency Shift

At the p-th harmonic (i.e. p × Bragg) the propagation and decay constants of the fundamental waves in the grating satisfy the determinantal equation (E.30), at the lower edge of the stop-band, ω_-; and the determinantal equation (E.34), at the upper edge of the stop-band, ω_+. In this section, we derive, from these equations, the second-order shift of the center of the stop-band and also the width of the stop-band to $O(\varepsilon^2)$.

We begin by determining ω_+ and ω_-, to $O(\varepsilon^2)$.

(1) ω_-:

At the lower edge of the stop-band ω_-, we write

$$\omega_- = \omega_o + \Delta\omega_- \qquad (4.4.1)$$

where ω_o is the unperturbed frequency of a Rayleigh wave with propagation constant k_r (3.1.7). The frequency perturbation $\Delta\omega_-$ may be expanded to $O(\varepsilon^2)$, as

$$\Delta\omega_- = \varepsilon\lambda_r \, \Delta\omega_1^- + (\varepsilon\lambda_r)^2 \, \Delta\omega_2^- .$$

The first-order frequency perturbation $\Delta\omega_1^-$ is already known from the first-order analysis. Replacing $\Delta\omega_1^-$ from (3.3.3), we have

$$\left(\frac{\Delta\omega_-}{\omega_o}\right) = -\varepsilon\lambda_r \frac{A_p\, q_r^3 r_r}{(k_r^2 r_r - k_r^2 q_r + 2q_r^2 r_r)} + (\varepsilon\lambda_r)^2 \left(\frac{\Delta\omega_2^-}{\omega_o}\right). \quad (4.4.2)$$

The modified dispersion relation, for waves in the grating, is given in terms of the frequency perturbation of the waves $\Delta\omega$, by (D.6). Introducing (4.4.2) into (D.6), we have for waves, at frequency ω_-, to $O(\varepsilon^2)$

$$\begin{aligned}(k_r^2 + q^2)^2 - 4k_r^2 qr &= -\varepsilon\lambda_r\, 4k_r^2 q_r^2 (r_r - q_r)\, A_p \\ &+ (\varepsilon\lambda_r)^2 \frac{2k_r^2 q_r^3 (r_r - q_r) A_p^2}{r_r (k_r^2 r_r - k_r^2 q_r + 2q_r^2 r_r)^2} [k_r^4 (r_r - q_r)(r_r + q_r)^2 \\ &+ k_r^2 q_r^2 r_r^2 (r_r - q_r) + 10 q_r^4 r_r^3] \\ &+ (\varepsilon\lambda_r)^2\, 4k_r^2 \frac{(r_r - q_r)}{q_r r_r} (k_r^2 r_r - k_r^2 q_r + 2q_r^2 r_r) \left(\frac{\Delta\omega_2^-}{\omega_o}\right).\end{aligned} \quad (4.4.3)$$

Equating (4.4.3) with the determinantal equation (E.30), and expanding the decay constants q and r, using (D.3)-(D.5) and (4.4.2), we determine

$$\left(\frac{\Delta\omega_2}{\omega_o}\right)^- = -\frac{q_r r_r}{4(k_r^2 r_r - k_r^2 q_r + 2q_r^2 r_r)}\left\{(3k_r^2 q_r + k_r^2 r_r + q_r^2 r_r - q_r^3)A_p^2 - (k_r^2 + q_r^2)(r_r + q_r)\sum_{n=1}^{\infty} A_n A_{n+p} + \sum_{n=1}^{p-1} A_n A_{p-n}[q_r r_r(r_r + q_r) - (n/p)(k_r^2 r_r + k_r^2 q_r + 2q_r r_r^2 + 3q_r^2 r_r + q_r^3)]\right\}$$

$$- \frac{q_r^4 A_p^2 [k_r^4 (r_r - q_r)(5r_r^2 + q_r^2) + q_r^2 r_r^2 (3k_r^2 r_r + k_r^2 q_r - 2q_r^2 r_r)]}{2(k_r^2 r_r - k_r^2 q_r + 2q_r^2 r_r)^3}$$

$$- \frac{q_r r_r [2jk_r q_r T_1 + (k_r^2 + q_r^2) T_2]}{4k_r^2 (r_r - q_r)(k_r^2 r_r - k_r^2 q_r + 2q_r^2 r_r)} \qquad (4.4.4)$$

where T_1 and T_2 are given in (E.28).

(2) ω_+:

At the upper edge of the stop-band ω_+, we write

$$\omega_+ = \omega_o + \Delta\omega_+. \tag{4.4.5}$$

Again $\Delta\omega_+$, the frequency perturbation, may be expanded to $O(\varepsilon^2)$, as

$$\Delta\omega_+ = \varepsilon\lambda_r \Delta\omega_1^+ + (\varepsilon\lambda_r)^2 \Delta\omega_2^+.$$

With the value of $\Delta\omega_1^+$, determined from the first-order analysis (3.3.3), we have

$$\left(\frac{\Delta\omega_+}{\omega_o}\right) = \varepsilon\lambda_r \frac{A_p q_r^3 r_r}{(k_r^2 r_r - k_r^2 q_r + 2q_r^2 r_r)} + (\varepsilon\lambda_r)^2 \left(\frac{\Delta\omega_2^+}{\omega_o}\right). \tag{4.4.6}$$

Introducing (4.4.6) into (D.6) yields the modified dispersion relation, for waves in the grating, at frequency ω_+. Equating this with the determinantal equation (E.34), and expanding the decay constants q and r, using (D.3)-(D.5) and (4.4.6), we determine

$$\left(\frac{\Delta\omega_2^+}{\omega_o}\right) = -\frac{q_r r_r}{4(k_r^2 r_r - k_r^2 q_r + 2q_r^2 r_r)} \left\{(3k_r^2 q_r + k_r^2 r_r\right.$$

$$+ q_r^2 r_r - q_r^3) A_p^2 + (k_r^2 + q_r^2)(r_r + q_r) \sum_{n=1}^{\infty} A_n A_{n+p}$$

$$- \sum_{n=1}^{p-1} A_n A_{p-n} [q_r r_r (r_r + q_r) - (n/p)(k_r^2 r_r + k_r^2 q_r$$

$$+ 2q_r r_r^2 + 3q_r^2 r_r + q_r^3)] \Bigg\}$$

$$- \frac{q_r^4 A_p^2 [k_r^4 (r_r - q_r)(5r_r^2 + q_r^2) + q_r^2 r_r^2 (3k_r^2 r_r + k_r^2 q_r - 2q_r^2 r_r)}{2(k_r^2 r_r - k_r^2 q_r + 2q_r^2 r_r)^3}$$

$$- \frac{q_r r_r [2jk_r q_r T_3 + (k_r^2 + q_r^2) T_4]}{4k_r^2 (r_r - q_r)(k_r^2 r_r - k_r^2 q_r + 2q_r^2 r_r)} \qquad (4.4.7)$$

where T_3 and T_4 are given in (E.33)

The edges of the stop-band, ω_+ and ω_-, are thus completely determined to second order (in ε). If we define the center of the stop-band to be ω', from (4.4.1) and (4.4.5)

$$\omega' = \frac{(\omega_+ + \omega_-)}{2} = \omega_o + \frac{(\Delta\omega_+ + \Delta\omega_-)}{2} .$$

Hence, from (4.4.2) and (4.4.6)

$$(\omega' - \omega_o) = \Delta\Omega = (\varepsilon\lambda_r)^2 \frac{(\Delta\omega_2^+ + \Delta\omega_2^-)}{2} \qquad (4.4.8)$$

where $\Delta\Omega$ is the shift in the center frequency of the stop-band. From (4.4.8), as already determined by the first-order analysis, we observe that $\Delta\Omega$ is of second order (in ε). The width of the stop-band is given, to $O(\varepsilon^2)$ by $(\omega_+ - \omega_-)$.

At Bragg, $\Delta\omega_2^{\pm}$ are both real. Thus, the stop-band center frequency ω' is pure real. However, at the second and higher harmonics ($p \geq 2$) $\Delta\omega_2^{\pm}$ are both complex due to the contributions from the radiating components $T_1 \rightarrow T_4$ in (4.4.4) and (4.4.7). The center frequency ω' is therefore also complex. The amount of radiation into the bulk may be determined from the imaginary part of ω'.

CHAPTER 5

SECOND-ORDER EFFECTS IN NORMAL-INCIDENCE GRATINGS

5.1 Introduction

In Chapter 4, the stop-band of a grating, at an arbitrary harmonic p (i.e. p × Bragg), was determined in general form to second order (in ε). In this chapter, we apply the results of that analysis to examine, in detail, second-order effects in normal-incidence gratings near Bragg and the second-harmonic (i.e. p = 1, 2). These effects are frequently termed "stored-energy" effects. Of particular importance are:

(1) Resonator frequency shift

(2) Transmission phase shift

(3) Strong second-harmonic reflection.

The new theory is used to predict these effects in practical gratings, and the results compared with experimental data. Previous empirical models, for including second-order effects in grating analysis, failed to consider the possible importance of the grating profile. The new theory, by contrast, reveals the critical importance of the latter in these higher-order effects. Previously anomalous second-order behavior can be explained by

by this sensitivity to groove profile.

The second-order analysis, in Chapter 4, was performed only at the grating stop-band. In the following section the variational principle, developed in Section 2.1, is used to determine the broadband grating response outside the stop-band, to $O(\varepsilon^2)$.

5.2 Variational Principle Outside Stop-Band

Using the variational principle (2.1.3), the dispersion relation for a grating may be obtained to one higher order of accuracy (in ε), than that to which the wave components have been determined. At Bragg, at the edges of the stop-band, in order to satisfy boundary conditions to $O(\varepsilon)$, both a forward and a backward zeroth-order wave are required with dependence $e^{\mp jk_r x}$. In addition, first-order Brillouin components are also required, with the dependence $e^{\mp jk_r x}\, e^{(\mp)jnk_g x}$. The frequency perturbation of the waves in the grating $(\omega - \omega_o)$, is of first order (in ε). Away from the stop-band, however, the boundary conditions can be satisfied to $O(\varepsilon)$, with only one zeroth-order wave and its corresponding Brillouin components. If the forward wave, with dependence e^{-jkx} is of zeroth-order, the backward wave with dependence e^{+jkx} is required only to be of first order. In addition, the frequency perturbation of the waves $(\omega - \omega_s)$ is of second order, where ω_s would be the frequency of the waves in the absence of the grating $(\omega_s = kv_r)$. The variational principle may be used to determine this second-order frequency correction to the dispersion diagram, away from the stop-band, from the set of first-order wave solutions.

Let $\sigma_{ij}^{(1)}$ and $u_i^{(1)}$ be the resultant stress and displacement components for one set of first-order wave solutions in the

grating. In general, the latter will comprise an infinite set of spatial components, with dependence $e^{\mp jkx}\, e^{(\mp)jnk_g x}$, where only the component with dependence e^{-jkx}, or the component with dependence e^{+jkx}, is of zeroth order. The remaining components will be of first order, or above. Introducing these first-order solutions into the variational principle (2.1.3), we have

$$\omega^2 = \frac{\int dv\left(\frac{\partial}{\partial x_j} u_i^{(1)*}\right) \sigma_{ij}^{(1)}}{\rho \int dv |u_i^{(1)}|^2} = \frac{\int ds_j\, u_i^{(1)*}\, \sigma_{ij}^{(1)} - \int dv\, u_i^{(1)*} \frac{\partial}{\partial x_j} \sigma_{ij}^{(1)}}{\rho \int dv |u_i^{(1)}|^2} \tag{5.2.1}$$

But, from (2.1.2), we have

$$-\rho\omega_s^2 |u_i^{(1)}|^2 = u_i^{(1)*} \frac{\partial}{\partial x_j} \sigma_{ij}^{(1)} \tag{5.2.2}$$

since to $O(\epsilon)$, away from the stop-band, the frequency of the waves in the grating is unperturbed from that on the free surface ω_s $(= kv_r)$. Thus from (5.2.1) and (5.2.2)

$$\omega^2 - \omega_s^2 = \frac{\int ds_j\, u_i^{(1)*}\, \sigma_{ij}^{(1)}}{\rho \int dv |u_i^{(1)}|^2} . \tag{5.2.3}$$

The surface integral in (5.2.3) is of second order, since $\sigma_{ij}^{(1)}$ satisfies the stress-free boundary requirement, on the surface of the grating, to $O(\varepsilon)$. Therefore, if we define $\omega = \omega_s + \Delta\omega$, from (5.2.3), to $O(\varepsilon^2)$:

$$\left(\frac{\Delta\omega}{\omega_s}\right) = \frac{\int ds_j \; u_i^{(1)*} \; \sigma_{ij}^{(1)}}{2\rho\omega^2 \int dv |u_i^{o}|^2} \qquad (5.2.4)$$

where u_i^{o} is the displacement of the single zeroth-order wave component, and the volume integral is taken over the unperturbed volume (i.e. $z = 0 \rightarrow \infty$). Equation (5.2.4) gives the second-order correction to the dispersion diagram, away from the stop-band, from the first-order wave components.

The variational analysis, described above, is valid away from the stop-band. Unfortunately, close to the grating stop-band the variational frequency perturbation (5.2.4) is no longer valid for determining the grating dispersion relation to $O(\varepsilon^2)$. We assumed, in deriving (5.2.4), that we were far enough away from the stop-band for the frequency perturbation $\Delta\omega$ to be of $O(\varepsilon^2)$. However, from the first-order analysis, earlier in the thesis, we know that in general, at the stop-band, the frequency perturbation $\Delta\omega$ is of $O(\varepsilon)$. At the stop-band the trial solution used to derive (5.2.4) is no longer correct

to $O(\epsilon)$. Only a single fundamental wave was assumed to be of zeroth order in the grating. However, at the edges of the stop-band both the forward and reverse fundamental wave components, with dependence $e^{\mp jk_r x}$, are required to be of zeroth order. Thus, the fundamental wave component which was assumed to be of first order in the trial solution, becomes an eigen solution at the edges of the stop-band. Consequently, the frequency perturbation $\Delta\omega$ predicted by (5.2.4) "blows up" close to the stop-band. The variational analysis cannot therefore be used to directly verify the second-order stop-band analysis of Chapter 4. To smoothly extend the grating dispersion diagram away from the edges of the stop-band, and to check agreement of the second-order analysis with the variational principle, we develop a modified form of coupling-of-modes.

5.3 Modified Coupling-of-Modes Equations

The standard coupling-of-modes equations for a grating, as in Section 3.1, predict a stop-band that is symmetric about the unperturbed frequency ω_o $(= k_r v_r)$, and is of width $(\omega_+ - \omega_-)/v_r = 2|K|$. We have determined, however, that, to $O(\varepsilon^2)$, the center of the stop-band is shifted from $\omega_o \rightarrow \omega'$. Thus

$$(\omega'/\omega_o) = 1 - K_2(h/\lambda_r)^2 \tag{5.3.1}$$

where the coefficient K_2, of the quadratic shift in the grating center frequency, is determined from (4.4.8). In order for the coupled-wave equations to be consistent with this shift in the center frequency, we assume that in the grating the surface wave velocity is perturbed from $v_r \rightarrow v'$, where

$$(v'/v_r) = 1 - K_2(h/\lambda)^2. \tag{5.3.2}$$

The coupling coefficient K, is interpreted as

$$K = j\,\frac{(\omega_+ - \omega_-)}{2v_r} = j\,\frac{k_r}{2}\left[\left[\frac{\Delta\omega_+}{\omega_o}\right] - \left[\frac{\Delta\omega_-}{\omega_o}\right]\right] .$$

Thus, from (4.4.2) and (4.4.6)

$$K = j \left\{ \varepsilon\lambda_r \frac{A_p k_r q_r^3 r_r}{(k_r^2 r_r - k_r^2 q_r + 2q_r^2 r_r)} + (\varepsilon\lambda_r)^2 \frac{k_r}{2} \left[\left[\frac{\Delta\omega_2^+}{\omega_o}\right]\right] - \left[\left[\frac{\Delta\omega_2^-}{\omega_o}\right]\right] \right\} . \qquad (5.3.3)$$

The slowly varying wave amplitudes $\tilde{R}$ and $\tilde{S}$, of the counter-propagating waves R and S respectively, are defined by

$$R = \tilde{R}\, e^{j(\omega t - kx)}$$

$$S = \tilde{S}\, e^{j(\omega t + kx)}$$

where $(\omega/k) = v'$. By symmetry considerations, the coupled-wave equations may then be written in the form

$$\frac{d}{dx}\tilde{R} = K\, e^{-2j\Delta x}\, \tilde{S}$$

$$\frac{d}{dx}\tilde{S} = -K\, e^{2j\Delta x}\, \tilde{R} \qquad (5.3.4)$$

where $\Delta = (\omega' - \omega)/v'$.

At Bragg, the coupling coefficient K determined from (5.3.3) is pure imaginary. The modified coupled-wave equations thus obey power conservation. However, at the higher harmonics the second-order frequency perturbations $\Delta\omega_2^{\pm}$ are, in general, complex due to the radiating Brillouin components in the grating. The coupling coefficient K is therefore also complex and the coupled-wave equations (5.3.4) do not obey power conservation. This is consistent, however, with the power radiated from the surface waves into the bulk at these higher harmonics.

In the following section, we use the modified coupled-wave equations (5.3.4) to extend the grating dispersion relation away from the stop-band. The validity of this approach is checked against the variational analysis of Section 5.2.

5.4 Dispersion Diagram to Second-Order

To first order the stop-band of a grating is symmetric about the unperturbed frequency ω_o [Fig. 3.1.2]. There is thus no change, to $O(\varepsilon)$, in the frequency of maximum grating reflection, i.e. Bragg, from that predicted by a zeroth-order analysis (4.1.1). In addition, at Bragg the width of the stop-band, and hence also the reflection coefficient of the grating, is, to $O(\varepsilon)$, only a function of the lowest Fourier coefficient of the grating A_1 ((2.3.9), (3.1.6)). To first order, the response of the grating is therefore very insensitive to the grating profile.

From (4.4.4) and (4.4.7) it can be seen that, to second order, the upper and lower frequencies of the stop-band, ω_+ and ω_- respectively, are functions of all the grating Fourier coefficients. The second-order corrections to these frequencies $\Delta\omega_2^{\pm}$ contain contributions from all the Brillouin components in the grating, via the terms $T_1 \rightarrow T_4$ ((E.28), (E.33)). It is therefore to be expected that the second-order effects, in a grating, will be much more sensitive to the grating profile than first order effects. Furthermore, since in general $|\Delta\omega_2^{+}| \neq |\Delta\omega_2^{-}|$, both the center and width of the stop-band are changed to second-order.

The profile of a typical SAW grating is shown in Fig. 5.4.1.

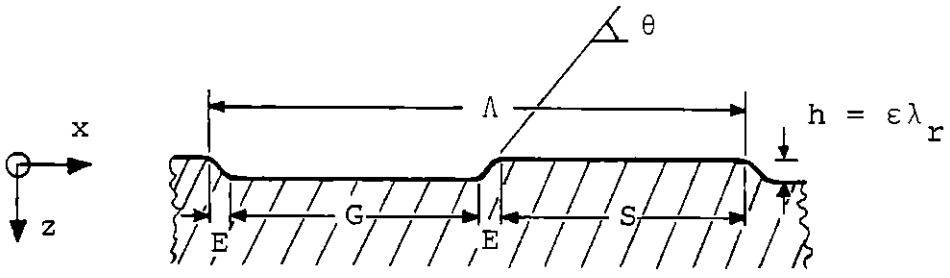

FIG. 5.4.1 TYPICAL SAW GRATING PROFILE
($\Lambda = \lambda_r/2$, $\varepsilon \approx 0.02$, $\theta = 60°$)

It is important to note that we have not assumed the groove walls to be vertical. Instead we have assigned to the edges of the grooves, a finite width E, and a slope θ ($\theta \leq 90°$). The theoretical dispersion diagram for such a grating is presented in Fig. 5.4.2, corrected to $O(\varepsilon^2)$. The edges of the stop-band were determined using (4.4.4) and (4.4.7) and then the modified coupled-wave equations (5.3.4) were used to predict the form of the dispersion relation outside the stop-band. Outside the stop-band the dispersion relation was also determined from the variational solution (5.2.4), as a check on the coupled-wave analysis. The agreement between the two is seen to be good. A major advantage of the coupled-wave analysis, over the variational solution, is that it is considerably simpler to evaluate.

A downward shift in the grating stop-band is clearly predicted by the second-order theory in Fig. 5.4.2. The frequency of maximum reflection from the grating is reduced from ω_o to ω'. The width of the stop-band, however, is not changed, to $O(\varepsilon^2)$, for this grating with a groove/strip ratio of 1:1.

Figure 5.4.2 was determined for an isotropic solid with a Poisson ratio $\nu = .335$. In comparing the theory with experimental data we shall use $\nu = .335$ as the equivalent Poisson ratio for Y - Z $LiNbO_3$. Similarly, we shall use $\nu = .41$ as

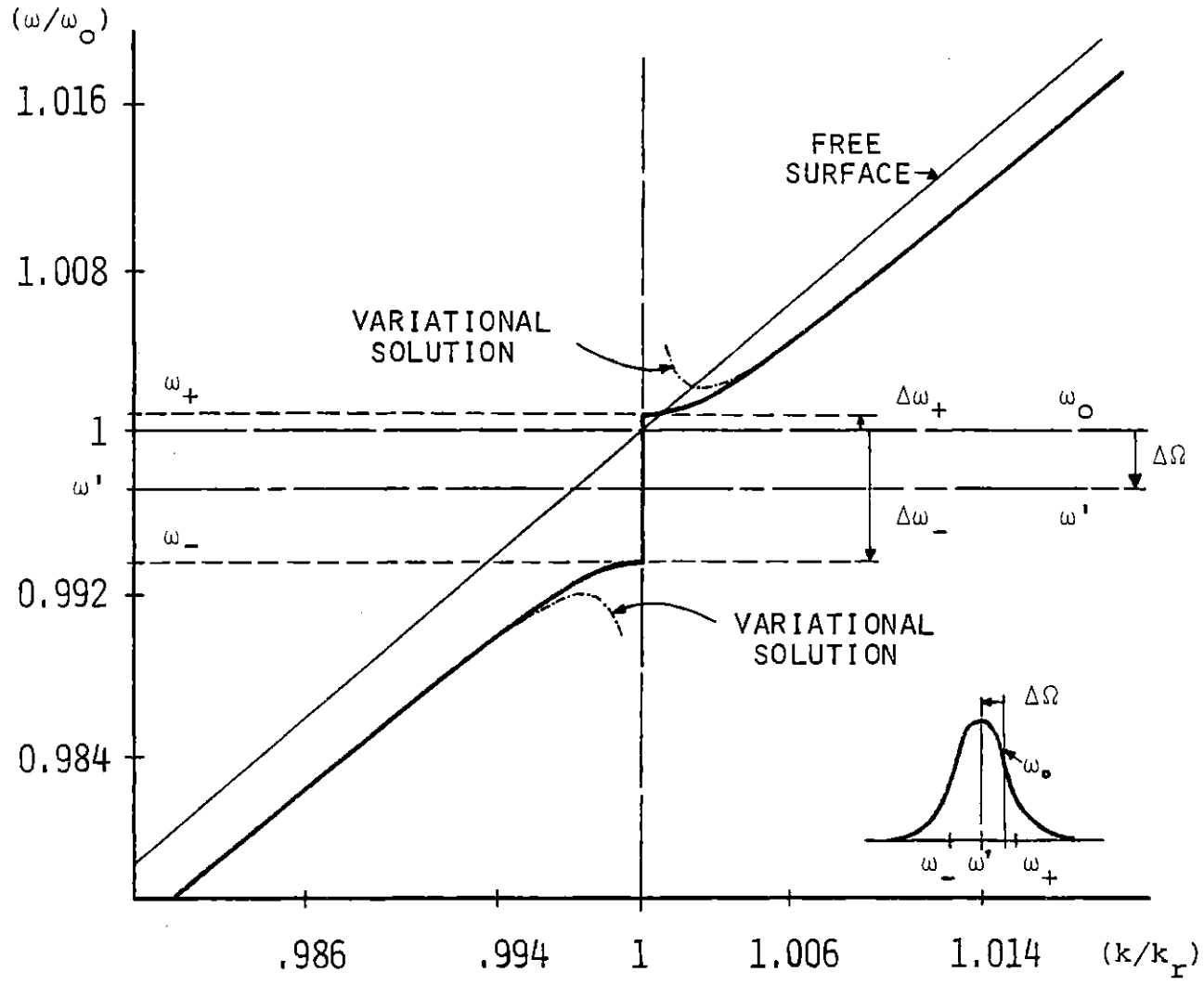

FIG. 5.4.2 THEORETICAL SECOND-ORDER DISPERSION DIAGRAM NEAR BRAGG FOR GRATING ON Y-Z $LiNbO_3$ (ν = .335, (h/λ_r) = .016, θ = 45°).

the equivalent Poisson for ST Quartz. These values were determined from theoretical considerations by Shimuzu et al.[30]

5.5 Second-Order Frequency Shift

It is important, for grating design, to understand how the various parameters of the grating affect the second-order reduction $\Delta\Omega$ in the synchronous response near Bragg. As in (5.3.1), we define the coefficient K_2, of the quadratic shift in the grating center frequency, by

$$(\omega'/\omega_o) = 1 - K_2(h/\lambda_r)^2.$$

In Fig. 5.5.1, K_2 is plotted as a function of the Poisson ratio ν, for a Bragg grating of height $(h/\lambda_r) = .01$, and for various groove slopes θ. As expected, K_2 is seen to be a strong function of the groove profile. It is greatest for steep-sided grooves. In fact, for grooves with vertical edges ($\theta = 90°$), K_2 has a logarithmic singularity. The reason for this behavior is that, to $O(\varepsilon^2)$, in a grating with vertical side-walls the stresses in the region of the corners become infinite. If such corners could be made in practice, of course, the material would flow plastically in the region of the sharp corner to remove the singularity.

The logarithmic singularity of K_2 for a grating with vertical side-walls is very weak, in that it is difficult to detect by direct numerical analysis. The closed-form solutions

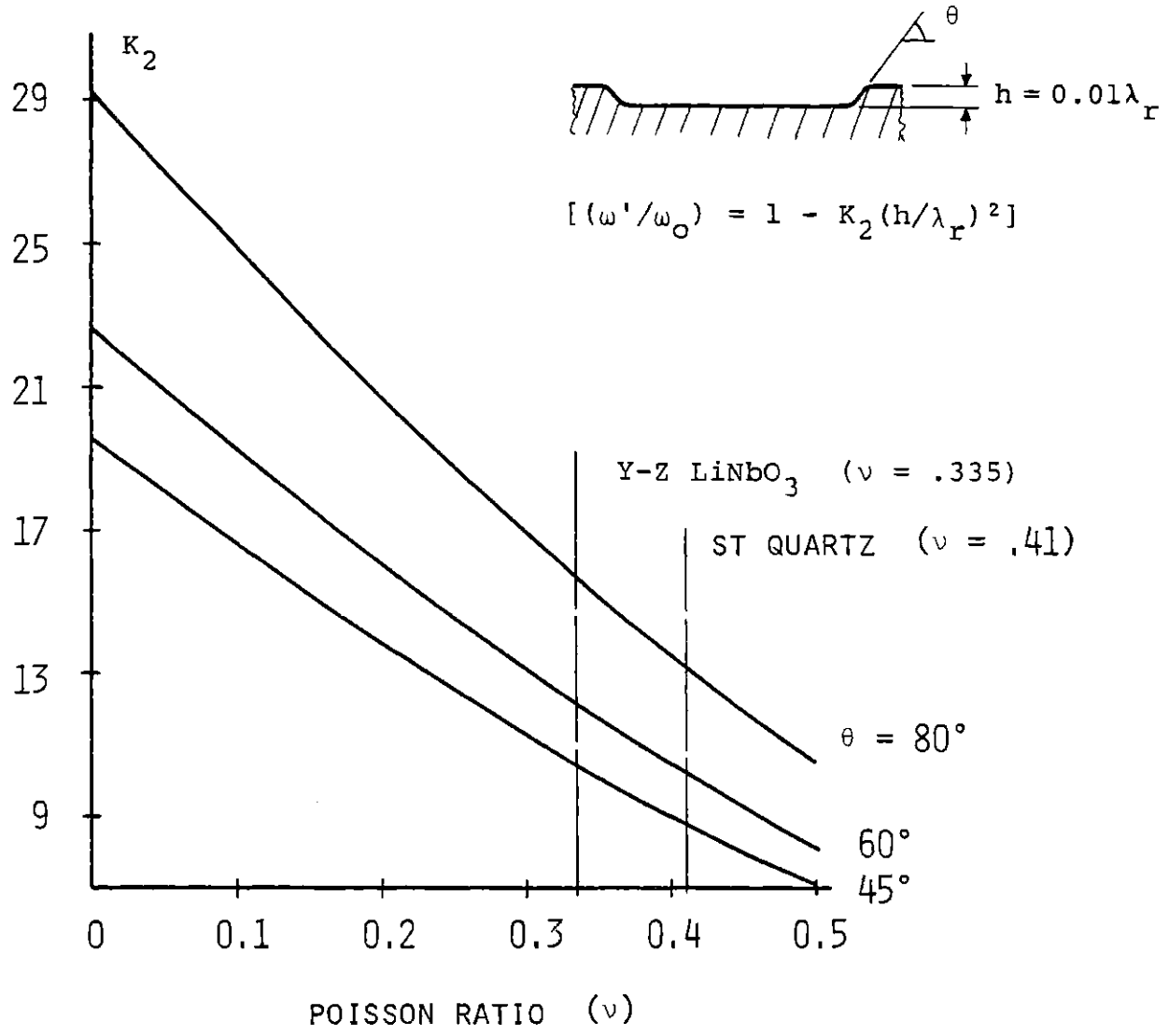

FIG. 5.5.1 THEORETICAL DEPENDENCE OF QUADRATIC FREQUENCY SHIFT COEFFICIENT AT BRAGG ON POISSON RATIO FOR $(h/\lambda_r) = 0.01$.

in Chapter 4, however, clearly reveal this singularity. In such a grating the contributions of the higher-order Brillouin components, to the frequency shift, are found to decrease inversely with the mode order. To correctly identify this singularity, from numerical analysis, would require summing over a near infinite number of ever decreasing terms. It is therefore important, in a theoretical analysis of second-order effects, to avoid using perturbation techniques, truncation, or numerical integration. Such an attempt by Shimizu et al. failed to identify the singularity of K_2, for a grating with a vertical groove profile.[30]

Figure 5.5.2 shows experimental measurements of K_2, for gratings at Bragg, on ST Quartz, made by Tanski.[25] Also shown are theoretical plots of K_2 (assuming an equivalent $\nu = .41$) for various groove slopes. From the experimental data, Tanski inferred an average value for K_2 of approximately 10.3. However, he noted that he found it "very disturbing indeed" that for small groove depths K_2 appeared to increase significantly. The theoretical analysis predicts that such an effect is likely to occur, due to two causes.

(1) For small groove depths, the groove edges are usually steeper because of the fabrication processes involved.

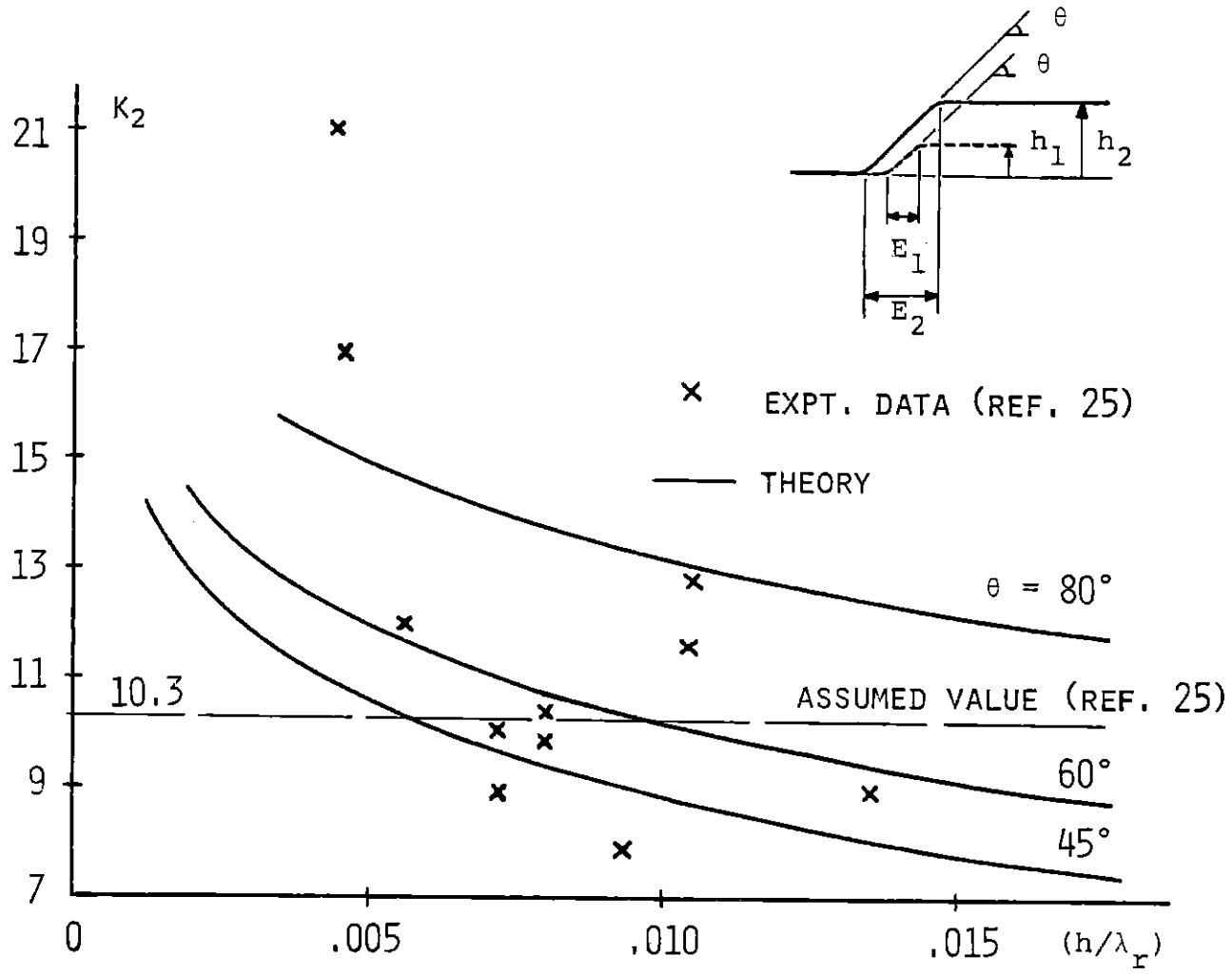

FIG. 5.5.2 DEPENDENCE OF QUADRATIC FREQUENCY SHIFT COEFFICIENT AT BRAGG ON GROOVE DEPTH FOR ST QUARTZ (ν = .41).

(2) Even for grooves with a constant edge slope θ, shallower grooves have a narrower edge width, E. It is the ratio (E/Λ) that determines the Fourier coefficients of the grating, not the groove slope. As E decreases the second-order effects increase, and as $E \to 0$, $K_2 \to \infty$.

For these reasons second-order effects are also expected to be more significant in gratings designed for high-frequency operation. The ratio (h/λ_r) does not vary greatly between gratings, thus $h \simeq \propto (1/f)$.

In Fig. 5.5.3 experimental data is presented, due to Williamson et al., of the resonator frequency shift at Bragg, of gratings on Y - Z $LiNbO_3$.[3,26] The theoretical behavior predicted (for $\nu = .355$), for various groove slopes is plotted. For comparison, the frequency shift of a sinusoidal grating, having the same first-order reflection coefficient as a square-wave grating, is also shown. The second-order resonant frequency shift of the sinusoidal grating, is much lower than that of the other grating profiles. It is important to note that the theoretical curves are not exactly parabolic, due to the dependence of K_2 on (h/λ_r) discussed above. However, the departure from quadratic behavior is very small. The theoretical

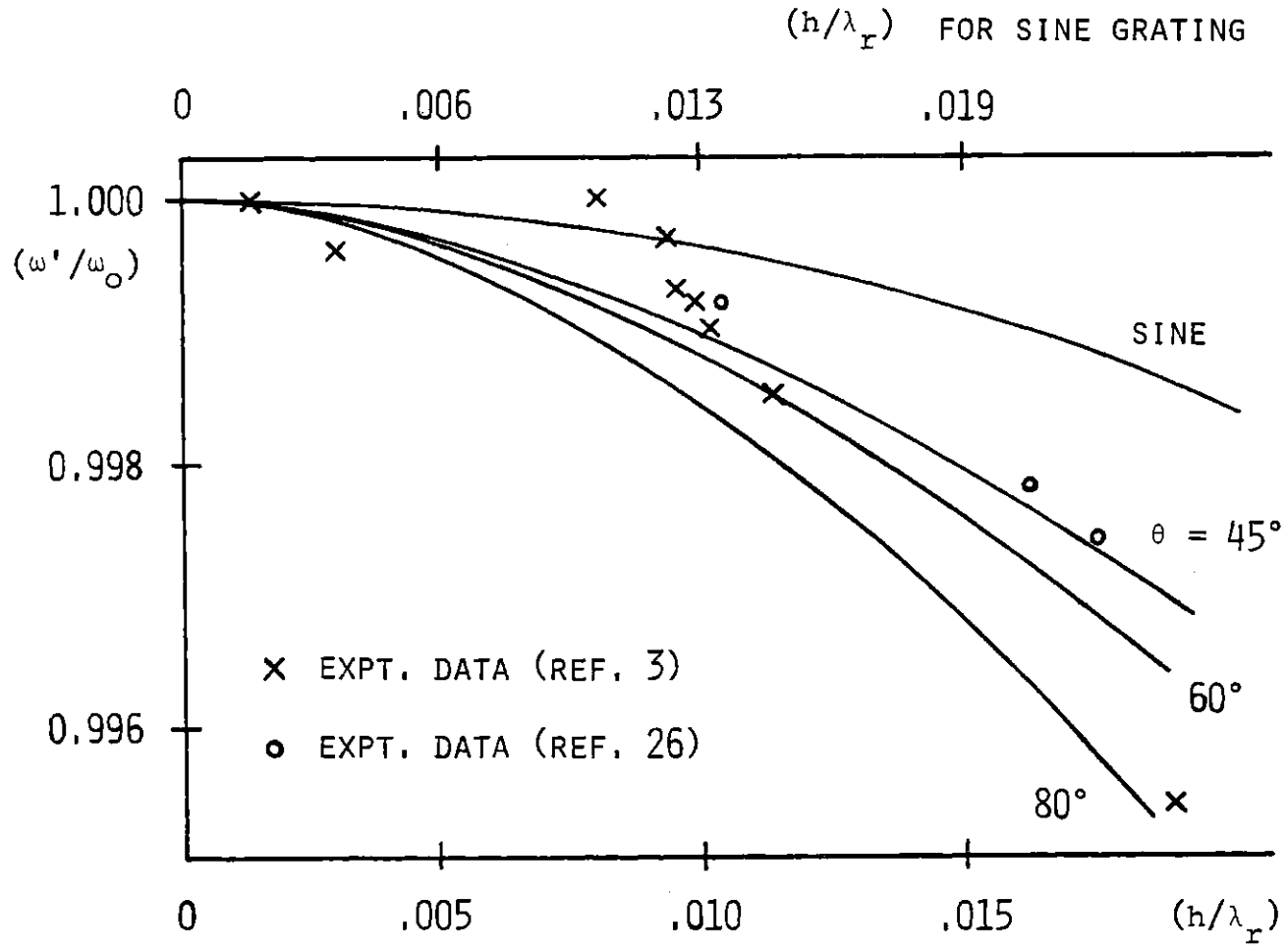

FIG. 5.5.3 DEPENDENCE OF SECOND-ORDER RESONANT FREQUENCY SHIFT ON GROOVE DEPTH FOR A GRATING ON Y-Z $LiNbO_3$ (ν = .335).

curves are well within the experimental uncertainty of the measurements. Finally, observe from Fig. 5.5.3 that although the second-order theory predicts $K_2 \to \infty$ as $(h/\lambda_r) \to 0$, the frequency shift $K_2(h/\lambda_r)^2 \to 0$, as expected, as $(h/\lambda_r) \to 0$, since the logarithmic blow-up of K_2 is so weak.

Figure 5.5.4 shows the theoretical dependence of K_2 on the groove to strip ratio (G/S), for a grating on Y - Z $LiNbO_3$ ($\theta = 45°$). For $G/S > \sim 0.5$ K_2 is not a strong function of this ratio.

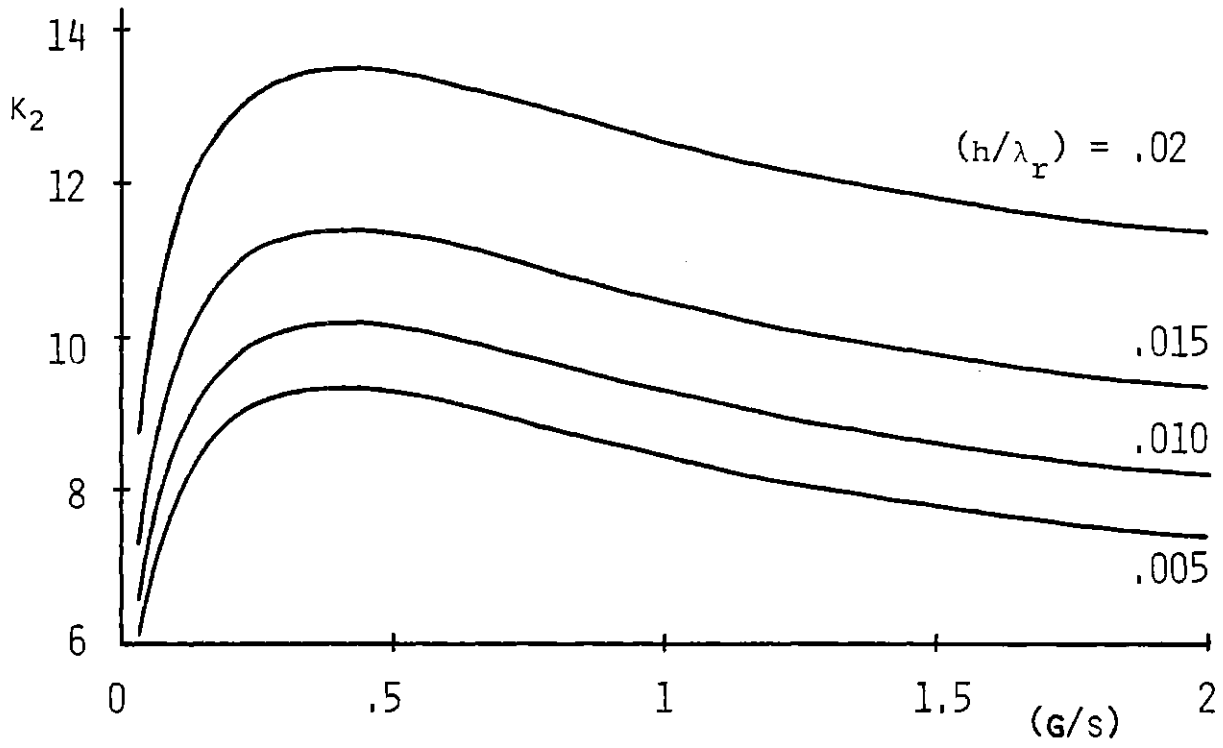

FIG. 5.5.4 THEORETICAL DEPENDENCE OF QUADRATIC FREQUENCY SHIFT COEFFICIENT AT BRAGG ON THE GROOVE/STRIP RATIO FOR Y-Z $LiNbO_3$ (ν = .335, θ = 45°).

5.6 Second-Order Reflection Coefficient

In general, the second-order theory predicts that both the center frequency, and the width of the stop-band will be different to $O(\varepsilon^2)$, than to $O(\varepsilon)$. The second-order change in the width of the stop-band changes the grating coupling coefficient K, to $O(\varepsilon^2)$. This results in second-order contributions to the reflection coefficient/groove 2r, which can result in important effects at both Bragg and the second harmonic.

Figure 5.6.1 shows the first and second-order contributions to the reflection coefficient 2r, as a function of the groove to strip ratio. The curves are plotted for a grating at Bragg with $(h/\lambda_r) = 0.01$, and for various groove slopes. The second-order reflection coefficient is strongly dependent on the groove to strip ratio.

In Fig. 5.6.2 the magnitude of the reflection coefficient Γ is plotted, to $O(\varepsilon^2)$, as a function of the groove to strip ratio, for a grating with 200 grooves ($\theta = 45°$). Note that the reflection coefficient of the grating is skewed about G/S = 1, by the second-order contributions. To first-order we would expect Γ to be a maximum for G/S = 1. However, as G/S is reduced (< 1) the increase in the second-order grating reflection coefficient, at first, more than compensates for the

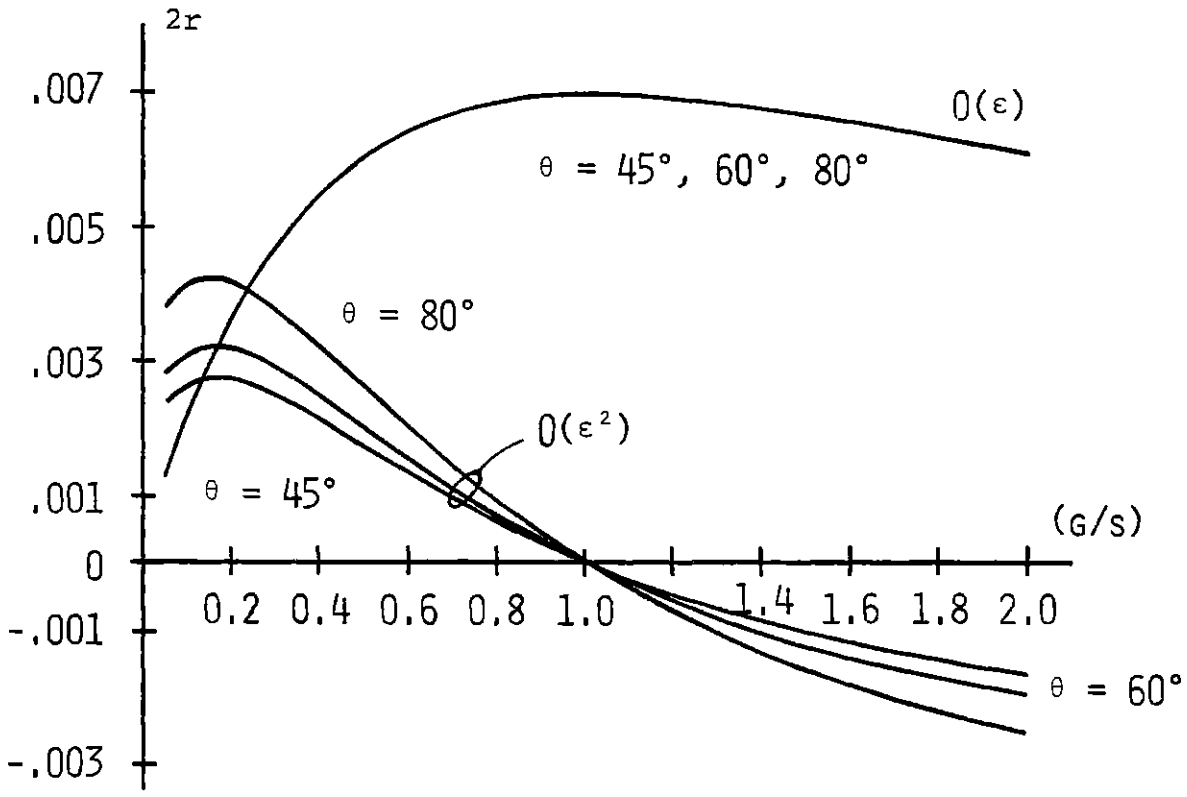

FIG. 5.6.1 FIRST AND SECOND-ORDER CONTRIBUTIONS TO THE GROOVE REFLECTION COEFFICIENT AS A FUNCTION OF THE GROOVE/STRIP RATIO ON Y-Z $LiNbO_3$ (ν = .335, (h/λ_r) = 0.01).

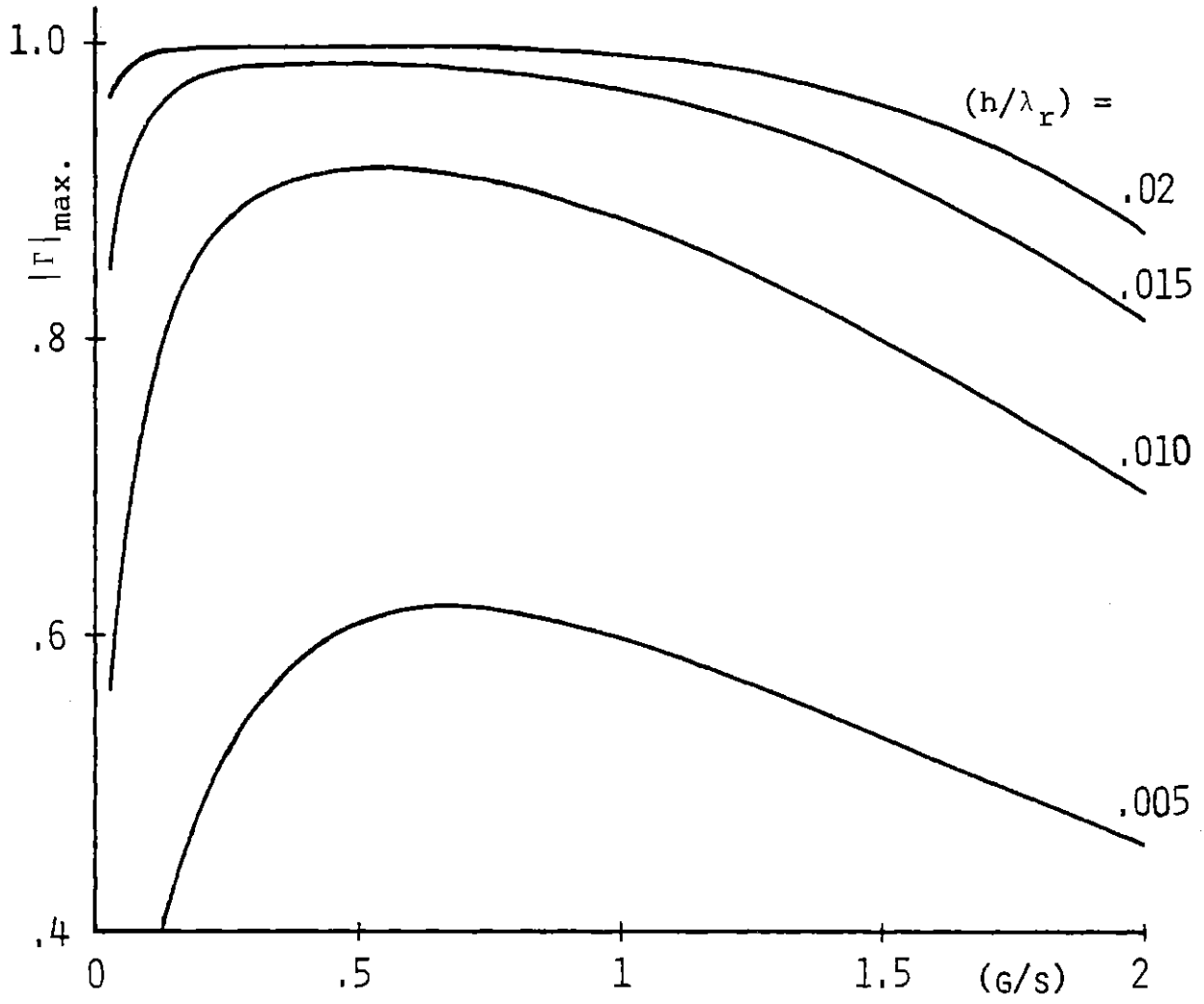

FIG. 5.6.2 THEORETICAL DEPENDENCE OF MAXIMUM REFLECTION COEFFICIENT NEAR BRAGG ON THE GROOVE/STRIP RATIO FOR 200 GROOVES ON Y-Z $LiNbO_3$ (ν = .335, θ = 45°).

decrease in the first-order coefficient. For $G/S > 1$ the first and second-order reflection coefficients partially cancel, and thus Γ decreases more rapidly than expected. To minimize the sensitivity of Γ to fabrication tolerances, Fig. 5.6.2 suggests that a groove to strip < 1 may be desirable.

First-order theory (2.3.13) predicts no reflection from a grating, with $G/S = 1$, in the neighborhood of the second-harmonic frequency (i.e. $2 \times$ Bragg). However, in practical SAW gratings a strong reflection is often observed. Figure 5.6.3 shows experimental measurements of the maximum grating reflection coefficient near second harmonic, taken for gratings on Y - Z $LiNbO_3$ by Li et al.[28] The grating reflection coefficient determined from the second-order theory is also shown for various groove slopes, as a function of (h/λ_r). The theory correctly predicts a strong second-harmonic grating response of the form observed. In addition, the theory also determines the bulk radiation, in the grating, at the second-harmonic frequency.

Figure 5.6.3 shows, for comparison, the theoretical reflection coefficient, near the second harmonic, from a sinusoidal grating having the same first-order reflection coefficient as a square wave grating. The reflection from the sinusoidal grating is much lower than that of any of the trapezoidal

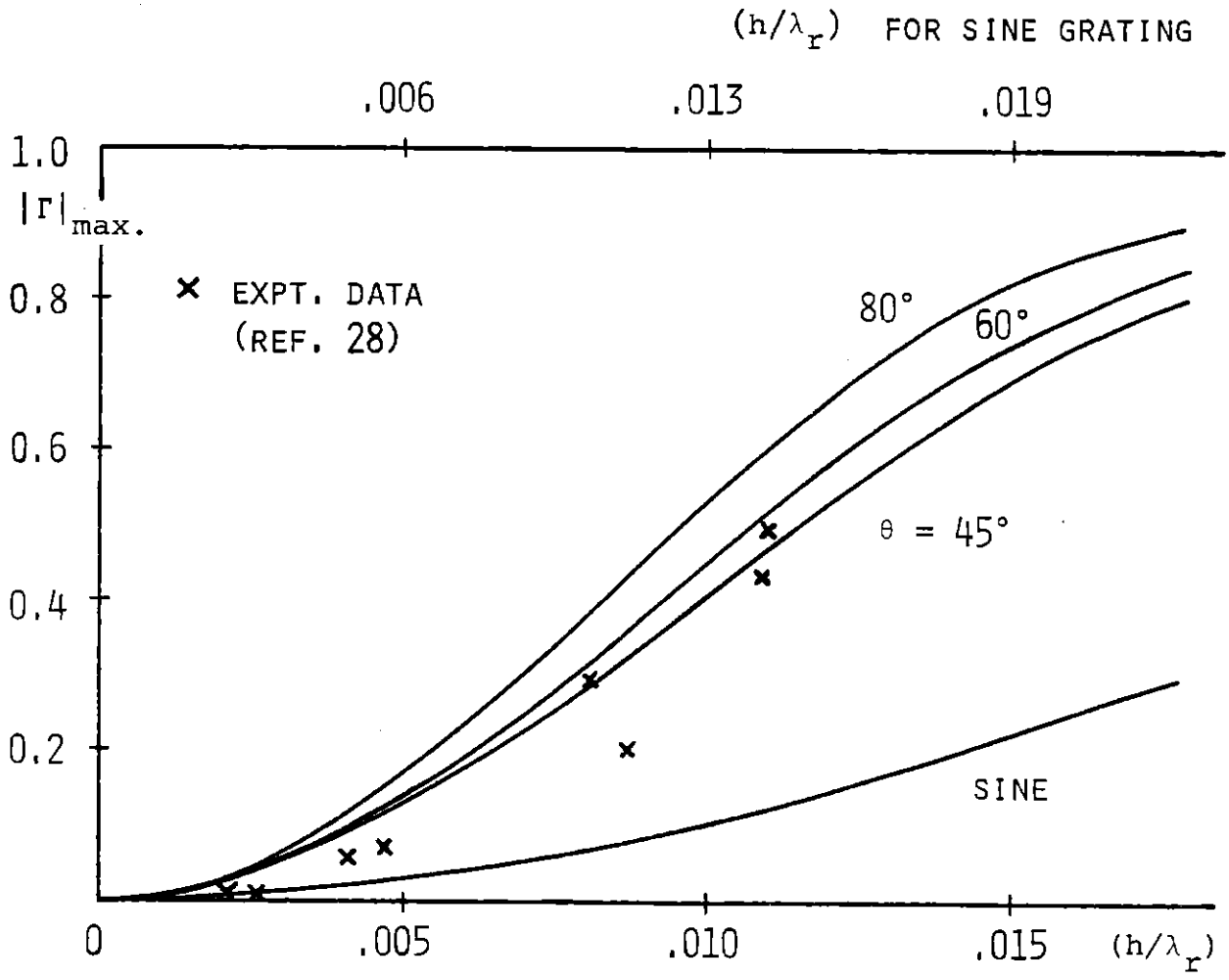

FIG. 5.6.3 DEPENDENCE OF MAXIMUM REFLECTION COEFFICIENT ON GROOVE DEPTH NEAR SECOND HARMONIC FOR 100 GROOVES ON Y-Z $LiNbO_3$ (ν = .335).

gratings. In general, second-order effects in a grating can be considerably reduced by avoiding groove profiles with sharp corners and vertical side-walls. The latter reduces the amplitudes of the Brillouin components, in the grating, that contribute to these effects. A sinusoidal grating, ideally, has the lowest second-order effects.

Finally, in Fig. 5.6.4, experimental measurements by Li et al. are shown of the maximum reflection coefficient near second harmonic, for gratings on Y - Z $LiNbO_3$ with a groove to strip ratio of 1.33. The corresponding theoretical curves, for various groove slopes, are also shown. Note that in this case, since $G/S \neq 1$, the grating reflection coefficient has both first and second-order contributions.

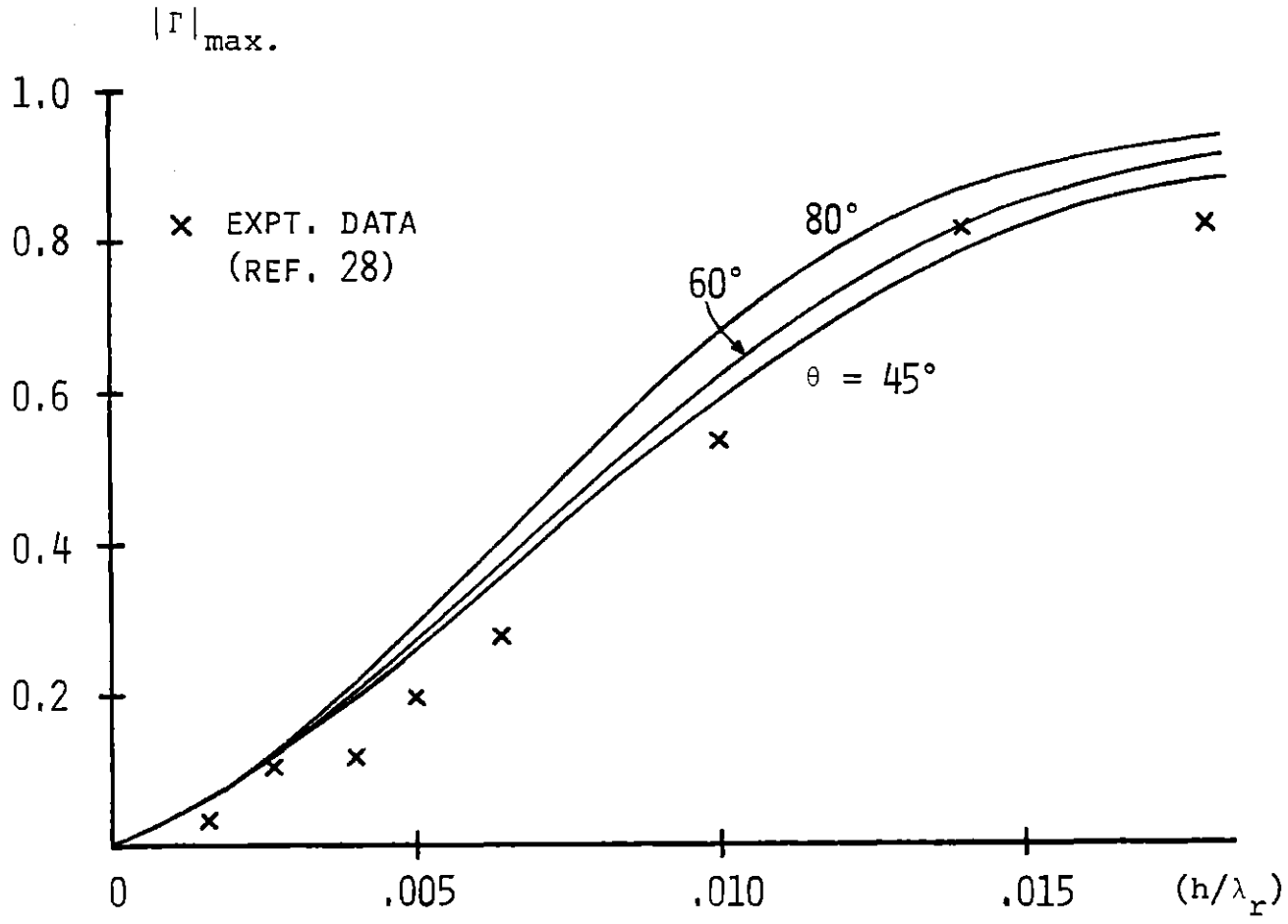

FIG. 5.6.4 DEPENDENCE OF MAXIMUM REFLECTION COEFFICIENT ON GROOVE DEPTH NEAR SECOND HARMONIC FOR 100 GROOVES ON Y-Z $LiNbO_3$ (ν = .335) WITH A GROOVE/STRIP RATIO OF 1.33.

5.7 Transmission Phase Response

The second-order reduction in the Bragg frequency of a grating is also manifested in the grating transmission phase response. The reduction of the surface-wave velocity (5.3.2), in the grating, results in an additional phase delay through the grating compared to that on the free surface. In addition, in the neighborhood of Bragg the grating has a strong first-order phase response.

Figure 5.7.1 shows the additional phase delay through a graing near Bragg, on Y - Z $LiNbO_3$, as measured by J. Melngailis (Lincoln Lab., unpublished). Also shown is the theoretical phase response, determined from the second-order theory and the modified coupled-wave equations (5.3.4). The agreement with experiment is very good; the theory even succeeds in closely predicting the structure of the observed ripples in the response.

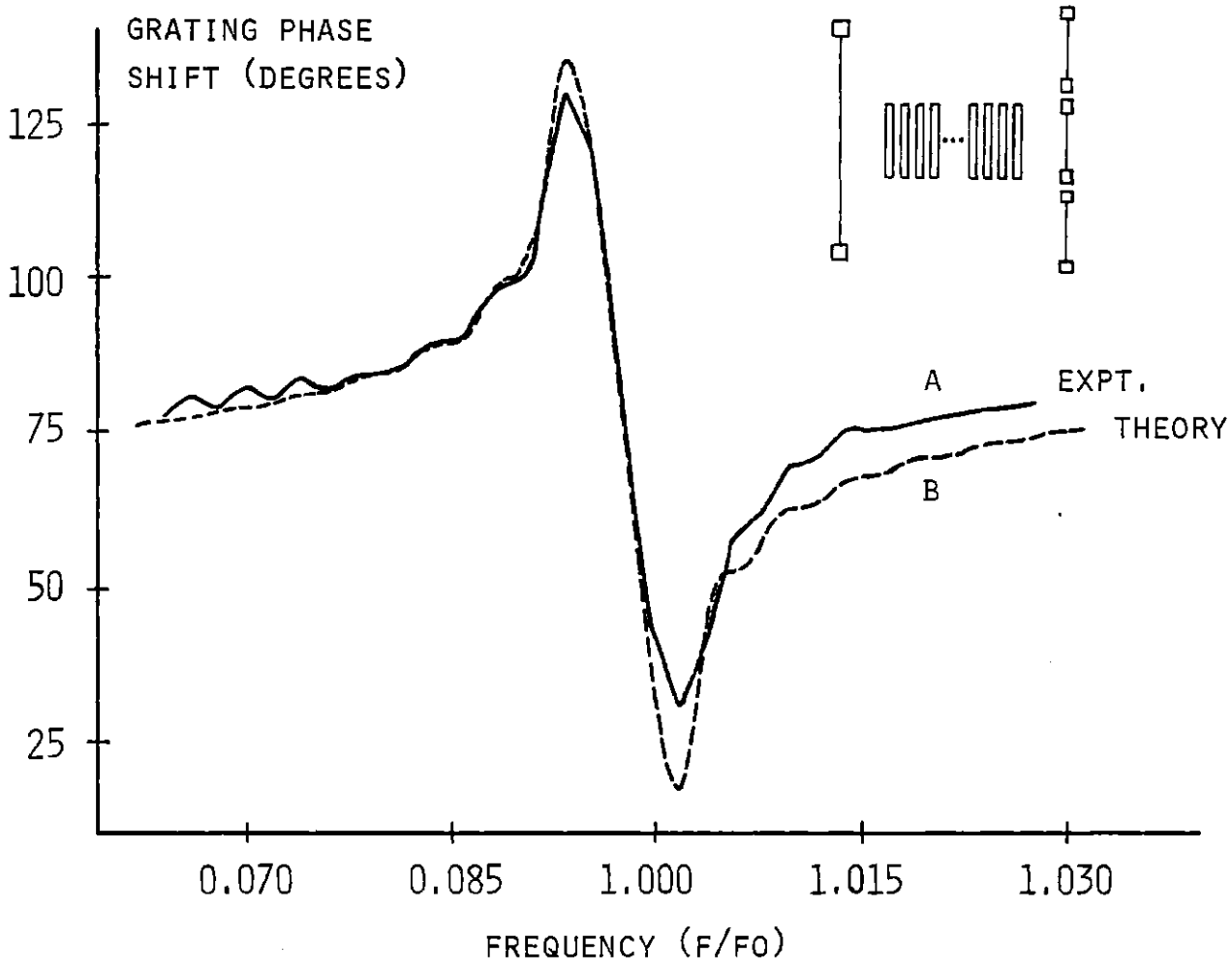

FIG. 5.7.1 GRATING PHASE SHIFT VS. FREQUENCY NEAR BRAGG (FO).
A: EXPERIMENT, 200 GROOVES ON Y-Z $LiNbO_3$
$(h/\lambda_r) \approx .016$ [J. MELNGAILIS, UNPUBLISHED].
B: THEORY, 200 GROOVES $\nu = .335$, $(h/\lambda_r) = .015$,
$\theta = 45°$ (ASSUMED).

I(b): Oblique Incidence

CHAPTER 6

REFLECTION COEFFICIENT AT OBLIQUE INCIDENCE

6.1 Introduction

SAW devices often employ gratings operating at oblique incidence. It is the purpose of this chapter to demonstrate that all the methods, presented in the previous chapters, for analyzing normal-incidence gratings, may also be used for analyzing oblique-incidence gratings. Following the approach of Chapter 3, the coupling coefficient of an oblique-incidence grating, and the single-groove reflection coefficient at oblique incidence, are determined to first order (in ε). The results are obtained in a relatively simple manner and are in agreement with existing alternate analyses. However, the analysis described here has the advantage that, as in Chapter 4, it may be easily extended to second order. The second-order frequency shift, and the second-order contributions to the reflection coefficient, may thereby be determined.

6.2 Determinantal Equations

As in Chapter 3 the determinantal equations, at the edges of each stop-band, may be determined by considering the boundary conditions on the surface of grating. Again the analysis is quasi-variational, in that only the zeroth-order amplitudes of the stresses in the grating are required to obtain the determinantal equations to $O(\varepsilon)$. At oblique incidence, in order to satisfy the boundary conditions completely, for each spatial dependency of the waves, three acoustic components are required. In addition to the longitudinal compressional-wave and the vertically-polarized shear-wave components, encountered in the normal-incidence analysis, a third, horizontally-polarized shear-wave component is excited at oblique incidence. The latter arises from the three-dimensional nature of the stresses in a grating at oblique incidence. For this case, there are finite stress components in the x, y and z directions. This contrasts with the case of normal incidence, already considered, in which there were no stress components in the y direction (i.e. parallel to the grating). To satisfy the stress-free boundary conditions on the surface of the grating, for the oblique-incidence analysis, all three directions must be considered.

Figure 6.2.1 shows a section of a grating, of infinite two-dimensional extent, in which the fundamental (i.e. zeroth

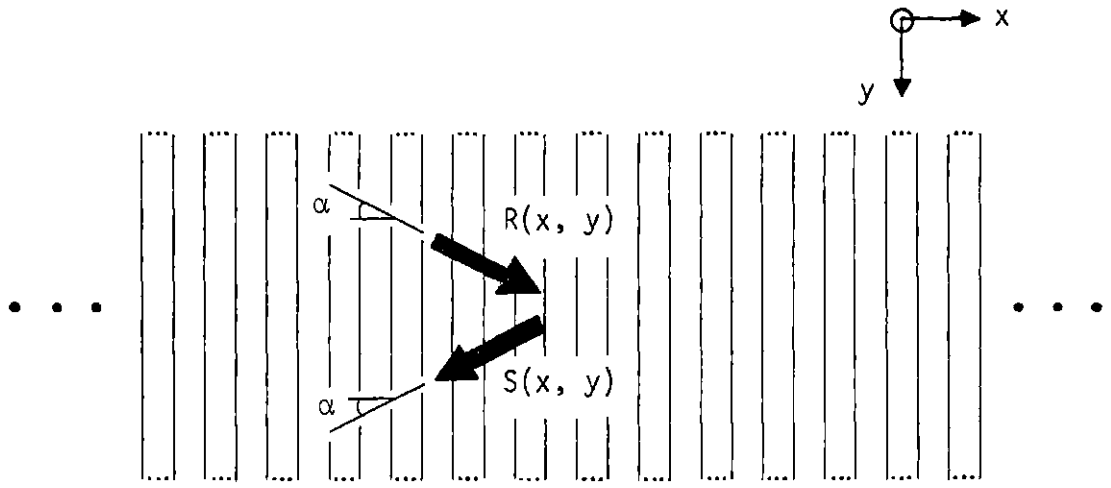

FIG. 6.2.1 GRATING WAVES PROPAGATING AT OBLIQUE INCIDENCE.

order) surface waves are propagating at oblique incidence to the grating. At the edges of the stop band, for the p-th harmonic, these waves have dependence $e^{\mp jk_r x \cos\alpha}\, e^{-jk_r y \sin\alpha}$, where k_r is the propagation constant of a free surface Rayleigh wave of frequency ω_o.

$$k_r = \omega_o/v_r = p\pi/(\Lambda \cos\alpha). \tag{6.2.1}$$

From coupling-of-modes theory, by a corresponding analysis to that for normal incidence in Section 3.1, we expect ω_o to be the center frequency of the stop band to $O(\varepsilon)$ [Fig. 3.1.2]. The frequency of the lowest harmonic response of the grating, with $p = 1$, is again referred to as Bragg.

From (A.4) the stress on the surface of the grating is, to $O(\varepsilon)$

$$\begin{aligned}\bar{\sigma}_s = {} & \{\sigma_{xz}(0) + \varepsilon\lambda_r[f(x)\ \sigma'_{xz}(0) - f'(x)\ \sigma_{xx}(0)]\}\ \hat{x} \\ & + \{\sigma_{yz}(0) + \varepsilon\lambda_r[f(x)\ \sigma'_{yz}(0) - f'(x)\ \sigma_{xy}(0)]\}\ \hat{y} \\ & + \{\sigma_{zz}(0) + \varepsilon\lambda_r[f(x)\ \sigma'_{zz}(0) - f'(x)\ \sigma_{xz}(0)]\}\ \hat{z}\end{aligned} \tag{6.2.2}$$

where

$$\sigma_{ij}(0) = \sigma_{ij}\Big|_{z=0}$$

and

$$\sigma'_{ij}(0) = \frac{\partial}{\partial z}\,\sigma_{ij}\Big|_{z=0}.$$

As in the normal-incidence analysis, let the normalized surface perturbation $f(x)$ be represented by the Fourier series (3.2.2). The derivative $f'(x)$ is then given by (3.2.3). For the case of oblique incidence we have, from (6.2.1)

$$k_g = 2\pi/\Lambda = \begin{cases} 2k_r \cos\alpha & \text{at Bragg} \\ (2/p)k_r \cos\alpha & \text{at } p \times \text{Bragg} \end{cases} \qquad (6.2.3)$$

As discussed above, at oblique incidence, for any specified propagation constant in the grating there are, in general, three acoustic components. We define the amplitudes of the acoustic waves with dependence $e^{\mp jk_r x \cos\alpha}\, e^{-jk_r y \sin\alpha}$ by $S_i^{\pm}$ respectively, where

$$i = \begin{cases} 1, & \text{for a compressional wave.} \\ 2, & \text{for a vertically-polarized (i.e. } \perp \text{ surface) shear wave.} \\ 3, & \text{for a horizontally-polarized (i.e. } \| \text{ surface) shear wave.} \end{cases}$$

To simplify the analysis the x and y-independent stress components of these waves, $\tilde{\sigma}_{ij}^{\pm}$ respectively, are defined by

$$\sigma_{ij}^{\pm} = \tilde{\sigma}_{ij}^{\pm} \, e^{\mp jk_r x \cos\alpha} \, e^{-jk_r y \sin\alpha} .$$

The surface of the grating is a free boundary and thus required to be stress free, i.e. $\bar{\sigma}_s = 0$. The only waves in the grating with finite zeroth-order amplitude are the compressional and vertically-polarized shear wave components $S_i^{\pm}$ $(i = 1, 2)$. To zeroth order these wave constitute two uncoupled Rayleigh waves (with amplitudes $S_1^{\pm}$). However, to first order it can be seen from (6.2.2) that as a consequence of the stress-free boundary requirement, these waves are coupled together by the Fourier component of the grating A_n, where $nk_g = 2k_r \cos\alpha$. For the stop-band at the p-th harmonic, from (6.2.3), $k_g = (2/p)k_r \cos\alpha$. Therefore, at the p-th harmonic, these waves are coupled together by the Fourier component A_p of the grating. The amplitudes of the horizontally-polarized shear wave components $S_3^{\pm}$, in the grating, are of first order (in ε).

To satisfy the boundary conditions on the surface of the grating to $O(\varepsilon)$, as in the case of normal incidence, in general, an infinite set of waves is required. These waves, or

Brillouin components, are all of first order and are generated by the interaction of the waves considered above with each spatial harmonic of the grating. However, as in the normal-incidence analysis, these wave amplitudes are not required to obtain the determinantal equations to $O(\varepsilon)$.

From (6.2.2), the stress-free boundary requirement $\bar{\sigma}_s \cdot \hat{x} = 0$ gives, to $O(\varepsilon)$

cf. $e^{-jk_r x \cos\alpha}\ e^{-jk_r y \sin\alpha}$ dep.

$$S_i^{+}\ \tilde{\sigma}^{+}_{ixz}(0) + \varepsilon\lambda_r\ A_p\ S_1^{-}\left[\frac{1}{2}\ \tilde{\sigma}^{-r'}_{xz}(0) + jk_r \cos\alpha\ \tilde{\sigma}^{-r}_{xx}(0)\right] = 0 \qquad \text{(i)}$$

cf. $e^{+jk_r x \cos\alpha}\ e^{-jk_r y \sin\alpha}$ dep.

$$S_i^{-}\ \tilde{\sigma}^{-}_{ixz}(0) + \varepsilon\lambda_r\ A_p\ S_1^{+}\left[\frac{1}{2}\ \tilde{\sigma}^{r'}_{xz}(0) - jk_r \cos\alpha\ \tilde{\sigma}^{r}_{xx}(0)\right] = 0 \qquad \text{(ii)}$$

the requirement $\bar{\sigma}_s \cdot \hat{y} = 0$ gives, to $O(\varepsilon)$

cf. $e^{-jk_r x \cos\alpha}\ e^{-jk_r y \sin\alpha}$ dep.

$$S_i^{+}\,\tilde{\sigma}^{+}_{iyz}(0) + \varepsilon\lambda_r\,A_p\,S_1^{-}\left[\frac{1}{2}\,\tilde{\sigma}^{-r'}_{yz}(0) + jk_r\cos\alpha\,\tilde{\sigma}^{-r}_{xy}(0)\right] = 0 \qquad \text{(iii)}$$

cf. $e^{+jk_r x\cos\alpha}\;e^{-jk_r y\sin\alpha}$ dep.

$$S_i^{-}\,\tilde{\sigma}^{-}_{iyz}(0) + \varepsilon\lambda_r\,A_p\,S_1^{+}\left[\frac{1}{2}\,\tilde{\sigma}^{r'}_{yz}(0) - jk_r\cos\alpha\,\tilde{\sigma}^{r}_{xy}(0)\right] = 0 \qquad \text{(iv)}$$

and the requirement $\bar{\sigma}_s \cdot \hat{z} = 0$ gives, to $O(\varepsilon)$

cf. $e^{-jk_r x\cos\alpha}\;e^{-jk_r y\sin\alpha}$ dep.

$$S_i^{+}\,\tilde{\sigma}^{+}_{izz}(0) + \varepsilon\lambda_r(A_p/2)\,S_1^{-}\,\tilde{\sigma}^{-r'}_{zz}(0) = 0 \qquad \text{(v)}$$

cf. $e^{+jk_r x\cos\alpha}\;e^{-jk_r y\sin\alpha}$ dep.

$$S_i^{-}\,\tilde{\sigma}^{-}_{izz}(0) + \varepsilon\lambda_r(A_p/2)\,S_1^{+}\,\tilde{\sigma}^{r'}_{zz}(0) = 0 \qquad \text{(vi)}$$

(6.2.4)

since $\sigma^{\pm r}_{xz}(0) = 0$.

The stress components of the acoustic waves are derived in Appendix F. They are stated in terms of θ, the angle between the propagation vector of the wave and the positive x axis. From Fig. 6.2.1, for the waves S_i^+, $\theta = \alpha$, and for the waves S_i^-, $\theta = (180 - \alpha)$. Equations (6.2.4), for the six undetermined wave amplitudes $S_i^{\pm}$ $(i = 1 \to 3)$, may be split into two uncoupled sets of equations, each in only three variables, by a transformation of variables. We define

$$S_i^T = \begin{cases} S_i^+ + S_i^-, & \text{for } i = 1, 2 \\ S_i^+ - S_i^-, & \text{for } i = 3 \end{cases}$$

$$S_i^D = \begin{cases} S_i^+ - S_i^-, & \text{for } i = 1, 2 \\ S_i^+ + S_i^-, & \text{for } i = 3. \end{cases} \qquad (6.2.5)$$

Referring to the stress components given in (F.5), (F.10), (F.14) and (F.16), we then obtain from (6.2.4)(i)-(ii), (iii)+(iv), and (v)+(vi) respectively,

$$S_i^T \tilde{\sigma}_{ixz}^+(0) - \varepsilon\lambda_r A_p S_1^T \left[\frac{1}{2} \tilde{\sigma}_{xz}^{r'}(0) - jk_r \cos\alpha \, \tilde{\sigma}_{xx}^r(0) \right] = 0$$

$$S_i^T \tilde{\sigma}^+_{iyz}(0) + \varepsilon\lambda_r A_p S_l^T\left[\frac{1}{2}\tilde{\sigma}^{r'}_{yz}(0) - jk_r \cos\alpha\, \tilde{\sigma}^r_{xy}(0)\right] = 0$$

$$S_i^T \tilde{\sigma}^+_{izz}(0) + \varepsilon\lambda_r(A_p/2) S_l^T \tilde{\sigma}^{r'}_{zz}(0) = 0 \qquad (6.2.6)$$

and from (6.2.4) (i)+(ii), (iii)-(iv), and (v)-(vi) respectively

$$S_i^D \tilde{\sigma}^+_{ixz}(0) + \varepsilon\lambda_r A_p S_l^D\left[\frac{1}{2}\tilde{\sigma}^{r'}_{xz}(0) - jk_r \cos\alpha\, \tilde{\sigma}^r_{xx}(0)\right] = 0$$

$$S_i^D \tilde{\sigma}^+_{iyz}(0) - \varepsilon\lambda_r A_p S_l^D\left[\frac{1}{2}\tilde{\sigma}^{r'}_{yz}(0) - jk_r \cos\alpha\, \tilde{\sigma}^r_{xy}(0)\right] = 0$$

$$S_i^D \tilde{\sigma}^+_{izz}(0) - \varepsilon\lambda_r(A_p/2) S_l^D \tilde{\sigma}^{r'}_{zz}(0) = 0. \qquad (6.2.7)$$

Equations (6.2.6) and (6.2.7) are independent sets of equations in the variables S_i^T $(i = 1 \to 3)$, and S_i^D $(i = 1 \to 3)$ respectively. In general, for $\varepsilon \neq 0$ the determinantal equations of each are different. Since both cannot then be satisfied simultaneously, either

$$S_i^D = 0 \qquad i = 1 \to 3$$

or

$$S_i^T = 0 \qquad i = 1 \to 3$$

to $O(\varepsilon)$.

Case 1. $S_i^D = 0$

For this case, we have from (6.2.5), to $O(\varepsilon)$

$$S_i^+ = S_i^-, \qquad \text{for } i = 1, 2$$

$$S_i^+ = -S_i^-, \qquad \text{for } i = 3.$$

This solution satisfies the determinantal equation of (6.2.6). Evaluating the stress components, in (6.2.6), from (F.5), (F.10), (F.14) and (F.16), we have, to $O(\varepsilon)$

$$\mu j k_r \cos\alpha \{2r + \varepsilon\lambda_r A_p [k_r^2 \sin^2\alpha - r_r^2 - q_r r_r + q_r^2(1 + \cos^2\alpha)]\} S_1^+ - \mu(k_r^2 + q^2)\cos\alpha\, S_2^+ + \mu q_r (k_r^2 - q_r^2)\sin\alpha\, S_3^+ = 0 \qquad \text{(i)}$$

$$\mu j k_r \sin\alpha \{2r + \varepsilon\lambda_r A_p [k_r^2 \cos^2\alpha - r_r^2 + q_r r_r - q_r^2\cos^2\alpha]\} S_1^+ - \mu(k_r^2 + q^2)\sin\alpha\, S_2^+$$

$$- \mu q_r (k_r^2 - q_r^2) \cos \alpha \, S_3^+ = 0 \qquad \text{(ii)}$$

$$\mu[(k_r^2 + q^2) - \varepsilon\lambda_r (A_p/2)(r_r - q_r)(k_r^2 + q_r^2)] S_1^+$$

$$+ 2\mu j k_r q \, S_2^+ = 0. \qquad \text{(iii)}$$

(6.2.8)

The first-order wave amplitude S_3^+ is easily eliminated. From (6.2.8) (i) $\cos \alpha$ + (ii) $\sin \alpha$ we obtain

$$jk_r[2r + \varepsilon\lambda_r A_p (2k_r^2 \sin^2\alpha \cos^2\alpha - r_r^2 - q_r r_r \cos 2\alpha$$

$$+ 2q_r^2 \cos^4\alpha)] \, S_1^+ - (k_r^2 + q^2) \, S_2^+ = 0. \qquad (6.2.9)$$

Equations (6.2.8) (iii) and (6.2.9) are now a pair of simultaneous equations for the wave amplitudes S_1^+ and S_2^+. For non-trivial solutions the determinant of these equations must be zero. From this requirement we obtain the determinantal equation, for this case, to $O(\varepsilon)$

$$(k_r^2 + q^2)^2 - 4k_r^2 qr = -\varepsilon\lambda_r \, 4k_r^2 q_r \cos^2\alpha [q_r (r_r - q_r)$$

$$- (k_r^2 - q_r^2) \sin^2\alpha]A_p. \qquad (6.2.10)$$

Case 2. $S_i^T = 0$

For this case, we have from (6.2.5) to $O(\varepsilon)$

$$S_i^+ = -S_i^-, \qquad \text{for } i = 1, 2$$

$$S_i^+ = S_i^-, \qquad \text{for } i = 3.$$

This solution satisfies the determinantal equation of (6.2.7). However, equations (6.2.7) are identical in form to those in (6.2.6), except for the replacement $\varepsilon \to -\varepsilon$. Thus, in this case, the determinantal equation is

$$(k_r^2 + q^2)^2 - 4k_r^2 qr = \varepsilon\lambda_r \, 4k_r^2 q_r \cos^2\alpha[q_r(r_r - q_r)$$

$$- (k_r^2 - q_r^2) \sin^2\alpha]A_p. \qquad (6.2.11)$$

6.3 First-Order Coupling and Reflection Coefficients

The determinantal equations at the edges of the stop-band, for the p-th harmonic, were determined from boundary conditions, to $O(\varepsilon)$, in Section 6.2. At ω_+, ω_- [Fig. 3.1.2], from (6.2.10) and (6.2.11)

$$(k_r^2 + q^2)^2 - 4k_r^2 qr = \pm\varepsilon\lambda_r\, 4k_r^2 q_r \cos^2\alpha [q_r(r_r - q_r) - (k_r^2 - q_r^2)\sin^2\alpha]A_p. \qquad (6.3.1)$$

However, from (D.6) the modified dispersion relation for waves at the edges of the stop-band is, to $O(\Delta\omega)$

$$(k_r^2 + q^2)^2 - 4k_r^2 qr = \frac{4k_r^2}{q_r r_r}(r_r - q_r)(k_r^2 r_r - k_r^2 q_r + 2q_r^2 r_r)(\Delta\omega/\omega_o) \qquad (6.3.2)$$

where $\Delta\omega = \omega - \omega_o$. Hence, from (6.3.1) and (6.3.2), for the stop-band of a grating at oblique incidence

$$\left(\frac{\Delta\omega}{\omega_o}\right) = \pm\varepsilon\lambda_r \frac{q_r^2 r_r \cos^2\alpha[q_r(r_r - q_r) - (k_r^2 - q_r^2)\sin^2\alpha]}{(r_r - q_r)(k_r^2 r_r - k_r^2 q_r + 2q_r^2 r_r)} A_p. \tag{6.3.3}$$

The stop-band is thus symmetric about the unperturbed center frequency ω_o, in agreement with first-order coupling-of-modes theory, and of width $2|\Delta\omega|$.

The coupling coefficient K, in an oblique-incidence grating, may now be deduced from the width of the stop-band, by coupling-of-modes theory as in Section 3.1. Corresponding to (3.1.6), at oblique incidence

$$2|K| = \frac{(\omega_+ - \omega_-)}{v_r \cos\alpha}$$

hence

$$|K| = \frac{k_r}{\cos\alpha}\left|\frac{\Delta\omega}{\omega_o}\right| .$$

Thus from (6.3.3)

$$|K| = \varepsilon\lambda_r \frac{k_r q_r^2 r_r \cos\alpha\,|[q_r(r_r - q_r) - (k_r^2 - q_r^2)\sin^2\alpha]|}{(r_r - q_r)(k_r^2 r_r - k_r^2 q_r + 2q_r^2 r_r)} A_p$$

or, in terms of the characteristic admittance Y_o (C.5)

$$|K| = \varepsilon\lambda_r \cos\alpha \frac{|[q_r(r_r - q_r) - k_2^2\sin^2\alpha]|}{8Y_o} A_p. \qquad (6.3.4)$$

For the case $\alpha = 0$, this expression is consistent with the coupling coefficient derived for a normal-incidence grating ((2.3.10) and (3.3.4)).

The single-groove reflection coefficient $2r$, is given by

$$2r = |K|\Lambda.$$

Thus, at the p-th harmonic

$$2r = |K| \frac{p\pi}{k_r \cos\alpha}.$$

From (6.3.4), replacing $\lambda_r = 2\pi/k_r$, we therefore determine that for a single oblique-incidence groove

$$2r = \varepsilon\pi^2 \frac{|[q_r(r_r - q_r) - k_2^2\sin^2\alpha]|}{4k_r^2 Y_o} pA_p$$

at the p-th harmonic (i.e. p × Bragg). This solution is in agreement with that derived by Otto et al., using a completely

different method of analysis.[14,49]

In the case of an "idealized" grating with a square-wave profile, $A_n = 2/n\pi$ for n odd, and $A_n = 0$ for n even. Thus, at Bragg and the odd harmonics

$$2r\Big|_{\substack{\text{square}\\\text{wave}}} = \varepsilon\pi \frac{|[q_r(r_r - q_r) - k_2{}^2\sin^2\alpha]|}{2k_r{}^2Y_o} \qquad (6.3.5)$$

and at the even harmonics,

$$2r\Big|_{\substack{\text{square}\\\text{wave}}} = 0$$

to $O(\varepsilon)$.

The single groove reflection coefficient (6.3.5), normalized to $(1/\cos\alpha)$ ($\propto$ groove width), is plotted in Fig. 6.3.1 as a function of the angle of incidence α, for $\nu = .335$, and $\nu = .41$. It is interesting to note that for $\alpha \approx 27°$ there is no reflection of the incident wave off the groove. In Fig. 6.3.2 the angle of incidence, for which there is no reflected wave, is plotted as a function of the Poisson ratio ν. It is not a strong function of the latter and is somewhat analogous to the Brewster angle, encountered in the oblique reflection of an electromagnetic wave from a dielectric boundary.

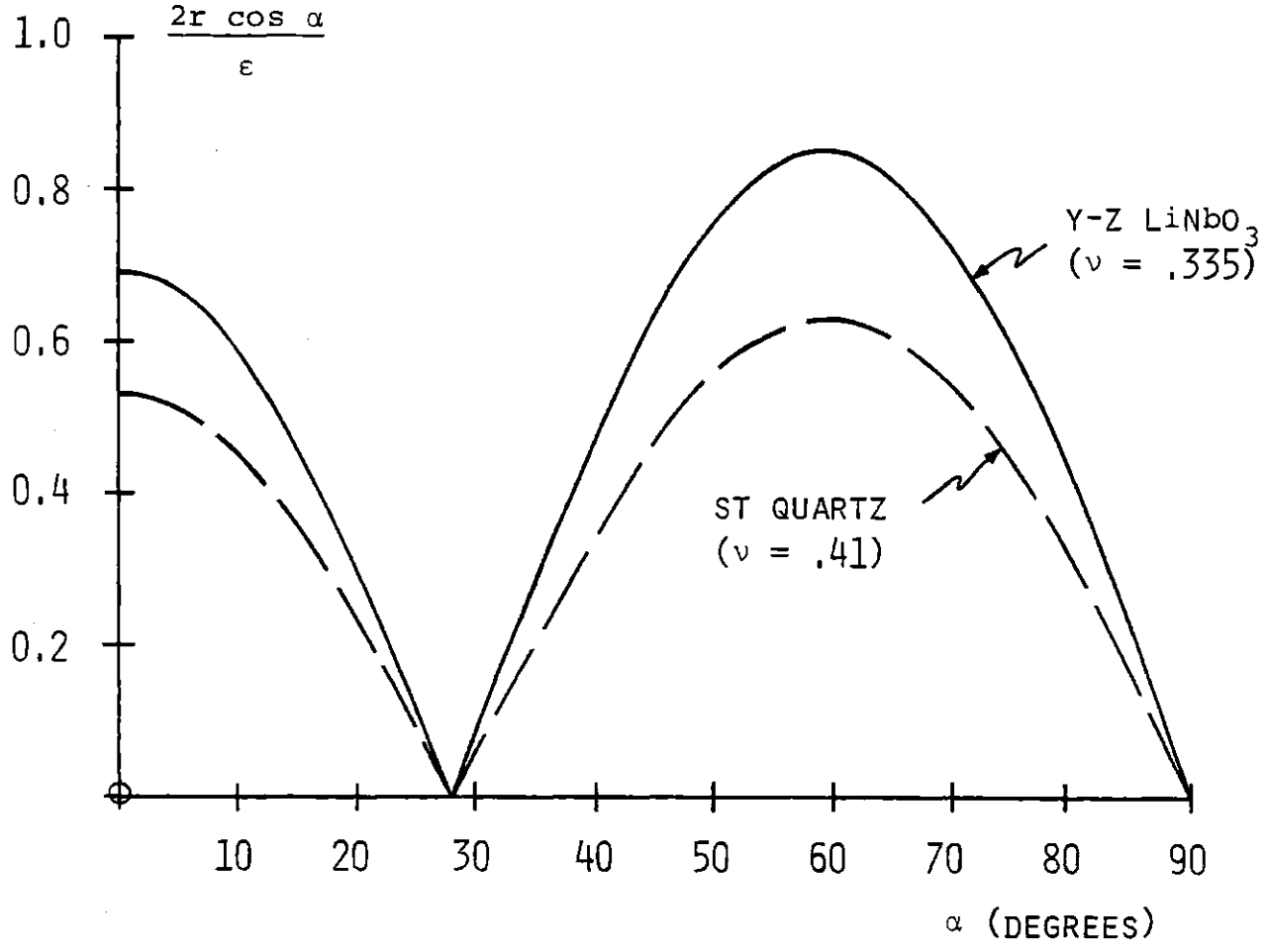

FIG. 6.3.1 NORMALIZED FIRST-ORDER GROOVE REFLECTION COEFFICIENT AT OBLIQUE INCIDENCE AS A FUNCTION OF THE ANGLE OF INCIDENCE.

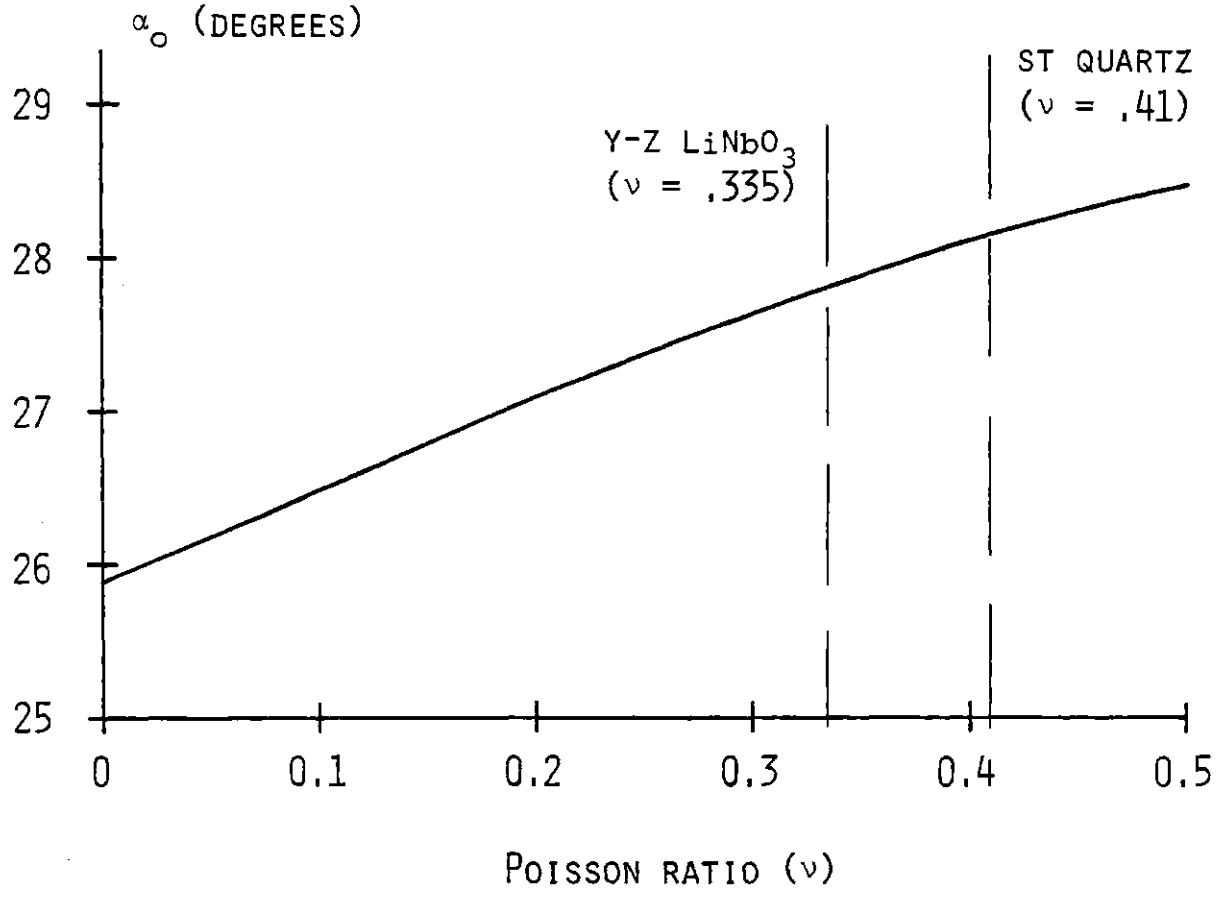

FIG. 6.3.2 OBLIQUE-INCIDENCE ANGLE FOR WHICH THE FIRST-ORDER GROOVE REFLECTION COEFFICIENT IS ZERO, AS A FUNCTION OF POISSON RATIO.

PART II

Closed-Form Analysis of Chirped Grating Structures

PART II

CLOSED-FORM ANALYSIS OF CHIRPED GRATING STRUCTURES

Preface

In part I the coupling coefficient K, of a SAW grating, was derived for both normal and oblique incidence, to second order (in ε). From a knowledge of K, the complete response of a constant-period normal-incidence grating may be easily determined. The solutions of the coupled-wave equations (3.1.1) are simple exponentials.[34,45] However, the analysis of constant-period gratings at oblique incidence is more complex. In addition, many SAW and optical devices employ gratings with chirped-spatial periods, both at normal and oblique incidence. The response of such structures, prior to this work, has never been analyzed in closed-form.

In part II we present closed-form analyses of gratings with a linear spatial chirp, at both normal and oblique incidence. The oblique-incidence solutions are particularly relevant to the analysis of the reflective-array-compressor (RAC). The latter is an important SAW device used for pulse compression. The exact solutions, derived here, permit a more detailed

analysis of the RAC than was previously possible, even using complex numerical computer analyses. Higher-order distortion effects in practical RAC devices are examined in detail using the new solutions. The coupling-of-modes solutions, being of a general nature, are also equally applicable to optical grating devices, such as bulk holograms.

CHAPTER 7

NORMAL-INCIDENCE CHIRPED GRATINGS

7.1 Introduction

Figure 7.1.1 shows a normal-incidence chirped grating. We shall consider only linear chirps, where the spatial period of the grating is a linear function of x, the penetration into the grating.

Kogelnik, in an expansion of his analysis of normal-incidence gratings, did consider gratings with a non-uniform, or chirped, period.[50] He also considered, simultaneously, gratings with a taper of the coupling strength. However, his analysis was based on a numerical approach. He transformed the governing coupled-wave equations for the grating into a non-linear first-order differential equation, or Ricatti equation, and then solved the latter numerically. No attempt was made to derive closed-form solutions for any of the gratings.

In this chapter we derive the exact closed-form solutions for the case of a normal-incidence grating with a linear spatial chirp. The solutions are mathematically complex, and, perhaps surprisingly, are more difficult to evaluate than the solutions

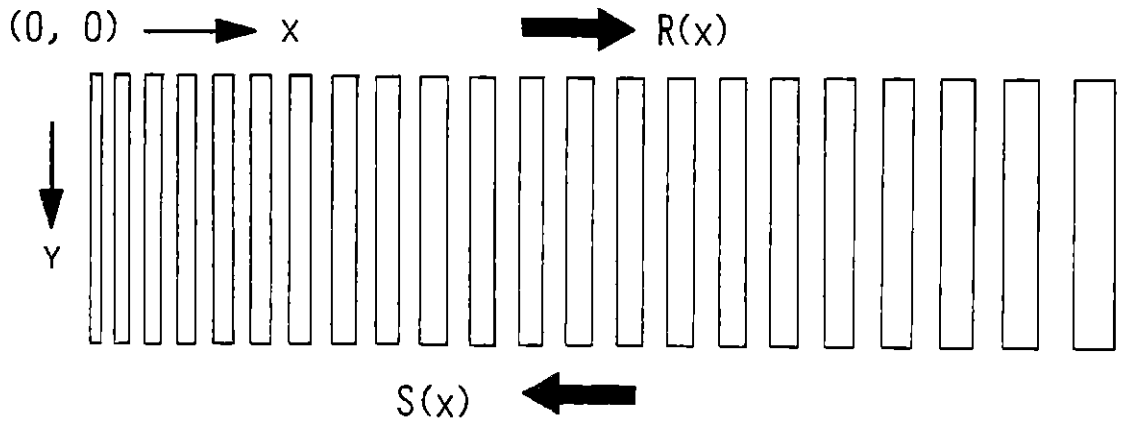

FIG. 7.1.1 NORMAL-INCIDENCE CHIRPED GRATING.

determined for oblique-incidence gratings, in the following chapters. However, they may be of use in studying the dependence on the various grating parameters, or in determining the limiting behavior of such a grating.

7.2 Exact Solutions

For the normal-incidence chirped grating structure shown in Fig. 7.1.1, which may be SAW, optical, or otherwise in nature, we define

$$k_g(x) = (2/p)(k_o - \delta x)$$

where $k_g(x) = 2\pi/\Lambda(x)$, and $\Lambda(x)$ is the local period of the grating. The chirp rate is specified by δ, and k_o is the local synchronous propagation constant at $x = 0$, for a wave at the p-th harmonic, i.e. $k_o = \omega_o(0)/v = p\pi/\Lambda(0)$. The initial detuning from synchronism we denote by Δ, where

$$\Delta = k_o - k = \frac{(\omega_o(0) - \omega)}{v}$$

and hence, the general detuning in the grating from the local synchronous frequency $\omega_o(x)$, is given by

$$\frac{(\omega_o(x) - \omega)}{v} = \Delta - \delta x. \qquad (7.2.1)$$

Defining the wave amplitudes as

$$R(x) = \tilde{R}(x)\ e^{j(\omega t - kx)}$$

$$S(x) = \tilde{S}(x)\ e^{j(\omega t + kx)}.$$

The coupled-wave equations are

$$\begin{aligned} \frac{d}{dx}\tilde{R}(x) &= K\, e^{-2j\Delta x + j\delta x^2}\, \tilde{S}(x) \\ \frac{d}{dx}\tilde{S}(x) &= K^*\, e^{2j\Delta x - j\delta x^2}\, \tilde{R}(x) \end{aligned} \qquad (7.2.2)$$

where K is the coupling coefficient/unit length. Observe, from the form of these equations, that the interaction between the two waves will be strongest at the point where the phase of K is stationary. This occurs at $x = \Delta/\delta$, which from (7.2.1) is, as expected, the local synchronous point in the grating.

From (7.2.2), we derive the second-order differential equation for $\tilde{S}(x)$

$$\left[\frac{d^2}{dx^2} - 2j(\Delta - \delta x)\frac{d}{dx} - |K|^2\right]\tilde{S}(x) = 0. \qquad (7.2.3)$$

This equation can be solved, in closed-form, in terms of (a)

parabolic cylinder functions, or (b) confluent hypergeometric functions.

(a) Parabolic cylinder functions.

Equation (7.2.3) can be transformed, by a suitable change of variables, into the standard form of the parabolic cylinder equation.[51] First, we introduce a new dependent variable $\hat{S}(x)$, where

$$\tilde{S}(x) = \hat{S}(x)\, e^{j\Delta x - j\frac{\delta}{2}x^2}. \qquad (7.2.4)$$

In terms of the new variable $\hat{S}(x)$, the differential equation (7.2.3) becomes

$$\left\{\frac{d^2}{dx^2} + [\delta^2(x - \Delta/\delta)^2 - (|K|^2 + j\delta)]\right\} \hat{S}(x) = 0. \qquad (7.2.5)$$

Defining a new independent variable

$$\xi = \sqrt{2j\delta}\ (x - \Delta/\delta) \qquad (7.2.6)$$

then transforms (7.2.5) into the standard form of the parabolic cylinder equation

$$\frac{d^2}{d\xi^2}\hat{S}(\xi) - \left[\frac{\xi^2}{4} + \left(\frac{1}{2} + \frac{|K|^2}{2j\delta}\right)\right]\hat{S}(\xi) = 0. \qquad (7.2.7)$$

This equation has two linearly-independent solutions $D_\nu(\pm j\xi)$, where

$$\nu = -j\,\frac{|K|^2}{2\delta}\,. \qquad (7.2.8)$$

Hence, the general solution for $\hat{S}(x)$, from (7.2.6) and (7.2.7) is

$$\hat{S}(x) = A\,D_\nu(j\sqrt{2j\delta}\,(x - \Delta/\delta)) + B\,D_\nu(-j\sqrt{2j\delta}\,(x - \Delta/\delta)) \qquad (7.2.9)$$

with ν given by (7.2.8). The constants A and B are determined from the boundary conditions

$$\tilde{R}(0) = 1$$
$$\tilde{S}(L) = 0.$$

Using these boundary conditions, and recursion and derivative relations for the parabolic cylinder functions,[51] we determine

$$A = j\,\frac{\sqrt{2j\delta}}{K}\left[D_{\nu-1}(-j\Delta\sqrt{2j/\delta}) + \frac{D_\nu(j\sqrt{2j\delta}\,(L - \Delta/\delta))}{D_\nu(-j\sqrt{2j\delta}\,(L - \Delta/\delta))}\,D_{\nu-1}(j\Delta\sqrt{2j/\delta})\right]^{-1}$$

$$B = -j\,\frac{\sqrt{2j\delta}}{K}\left[D_{\nu-1}(j\Delta\sqrt{2j/\delta}) + \frac{D_{\nu}(-j\sqrt{2j\delta}\ (L - \Delta/\delta))}{D_{\nu}(j\sqrt{2j\delta}\ (L - \Delta/\delta))}\,D_{\nu-1}(-j\Delta\sqrt{2j/\delta})\right]^{-1}$$

(7.2.10)

Thus, from (7.2.4), (7.2.9) and (7.2.10) one form, of the exact solution, for the reflection coefficient from a normal-incidence chirped grating is

$$\Gamma = \frac{S(0)}{R(0)} = j\,\frac{\sqrt{2j\delta}}{K}\,\{[D_{\nu}(-j\Delta\sqrt{2j/\delta})\ D_{\nu}(-j\sqrt{2j\delta}\ (L - \Delta/\delta))$$

$$- D_{\nu}(j\Delta\sqrt{2j/\delta})\ D_{\nu}(j\sqrt{2j\delta}\ (L - \Delta/\delta))]/[D_{\nu-1}(-j\Delta\sqrt{2j/\delta})$$

$$D_{\nu}(-j\sqrt{2j\delta}\ (L - \Delta/\delta)) + D_{\nu-1}(j\Delta\sqrt{2j/\delta})\ D_{\nu}(j\sqrt{2j\delta}\ (L - \Delta/\delta))]\}$$

(7.2.11)

where ν is given by (7.2.8).

(b) Confluent hypergeometric functions.

Equation (7.2.3) can also be transformed, by a change of variables, into the confluent hypergeometric differential equation (also known as Kummer's equation).[52] This requires

only a change in the independent variable. We define

$$\xi = -j\delta(x - \Delta/\delta)^2. \tag{7.2.12}$$

The differential equation (7.2.3) then becomes

$$\xi \frac{d^2}{d\xi^2} \tilde{S}(\xi) + \left(\frac{1}{2} - \xi\right) \frac{d}{d\xi} \tilde{S}(\xi) - \frac{j|K|^2}{4\delta} \tilde{S}(\xi) = 0 \tag{7.2.13}$$

which is the standard form of the confluent hypergeometric differential equation. The solutions are confluent hypergeometric functions. A general solution to (7.2.13) can be taken in the form

$$\tilde{S}(\xi) = A\ {}_1F_1\left(\frac{j|K|^2}{4\delta}\ ;\ \frac{1}{2}\ ;\ \xi\right) + B'\ \xi^{1/2}\ {}_1F_1\left(\frac{1}{2} + \frac{j|K|^2}{4\delta}\ ;\ \frac{3}{2}\ ;\ \xi\right)$$

Hence, from (7.2.12), the general solution for $\tilde{S}(x)$ is

$$\tilde{S}(x) = A\ {}_1F_1\left(\frac{j|K|^2}{4\delta}\ ;\ \frac{1}{2}\ ;\ -j\delta(x - \Delta/\delta)^2\right)$$

$$+ B\ (x - \Delta/\delta)\ {}_1F_1\left(\frac{1}{2} + \frac{j|K|^2}{4\delta}\ ;\ \frac{3}{2}\ ;\ -j\delta(x - \Delta/\delta)^2\right). \tag{7.2.14}$$

The constants A and B are again determined from the boundary conditions

$$\tilde{R}(0) = 1$$

$$\tilde{S}(L) = 0.$$

For these boundary conditions, using recursion and derivative relations for the confluent hypergeometric functions,[52] we determine

$$A = -\left[K \frac{\Delta}{\delta} {}_1F_1\left(1 + \frac{j|K|^2}{4\delta}; \frac{3}{2}; -j\frac{\Delta^2}{\delta}\right) + \frac{{}_1F_1\left(\frac{j|K|^2}{4\delta}; \frac{1}{2}; -j\delta\left(L - \frac{\Delta}{\delta}\right)^2\right) {}_1F_1\left(\frac{1}{2} + \frac{j|K|^2}{4\delta}; \frac{1}{2}; -j\frac{\Delta^2}{\delta}\right)}{K^*\left(L - \frac{\Delta}{\delta}\right) {}_1F_1\left(\frac{1}{2} + \frac{j|K|^2}{4\delta}; \frac{3}{2}; -j\delta\left(L - \frac{\Delta}{\delta}\right)^2\right)} \right]^{-1}$$

$$B = \left[\frac{1}{K^*} {}_1F_1\left(\frac{1}{2} + \frac{j|K|^2}{4\delta}; \frac{1}{2}; -j\frac{\Delta^2}{\delta}\right) + \frac{K\frac{\Delta}{\delta}\left(L - \frac{\Delta}{\delta}\right) {}_1F_1\left(\frac{1}{2} + \frac{j|K|^2}{4\delta}; \frac{3}{2}; -j\delta\left(L - \frac{\Delta}{\delta}\right)^2\right) {}_1F_1\left(1 + \frac{j|K|^2}{4\delta}; \frac{3}{2}; -j\frac{\Delta^2}{\delta}\right)}{{}_1F_1\left(\frac{j|K|^2}{4\delta}; \frac{1}{2}; -j\delta\left(L - \frac{\Delta}{\delta}\right)^2\right)} \right]^{-1}$$

(7.2.15)

Thus, from (7.2.14) and (7.2.15) an alternative, exact form, for the reflection coefficient from a normal-incidence chirped grating is

$$\Gamma = \frac{S(0)}{R(0)} = -K^{*}\left\{\left(L - \frac{\Delta}{\delta}\right) {}_1F_1\left(\frac{j|K|^2}{4\delta}; \frac{1}{2}; -j\frac{\Delta^2}{\delta}\right) {}_1F_1\left(\frac{1}{2} + \frac{j|K|^2}{4\delta}; \frac{3}{2}; -j\delta\left(L - \frac{\Delta}{\delta}\right)^2\right) + \frac{\Delta}{\delta} {}_1F_1\left(\frac{j|K|^2}{4\delta}; \frac{1}{2}; -j\delta\left(L - \frac{\Delta}{\delta}\right)^2\right) {}_1F_1\left(\frac{1}{2} + \frac{j|K|^2}{4\delta}; \frac{3}{2}; -j\frac{\Delta^2}{\delta}\right)\right\} \Big/ \left\{|K|^2 \frac{\Delta}{\delta}\left(L - \frac{\Delta}{\delta}\right) {}_1F_1\left(1 + \frac{j|K|^2}{4\delta}; \frac{3}{2}; -j\frac{\Delta^2}{\delta}\right) {}_1F_1\left(\frac{1}{2} + \frac{j|K|^2}{4\delta}; \frac{3}{2}; -j\delta\left(L - \frac{\Delta}{\delta}\right)^2\right) + {}_1F_1\left(\frac{j|K|^2}{4\delta}; \frac{1}{2}; -j\delta\left(L - \frac{\Delta}{\delta}\right)^2\right) {}_1F_1\left(\frac{1}{2} + \frac{j|K|^2}{4\delta}; \frac{1}{2}; -j\frac{\Delta^2}{\delta}\right)\right\} . \tag{7.2.16}$$

Forms (7.2.11) and (7.2.16), for the reflection coeffi-

cient, are mathematically equivalent. In any application, whichever is the more convenient form may be used.

CHAPTER 8

OBLIQUE-INCIDENCE CHIRPED GRATINGS

8.1 Introduction

Oblique-incidence gratings are used extensively in SAW and optical signal processing devices. In many of these applications the period of the gratings is also spatially chirped. However, previous to this work, no exact analysis of an oblique-incidence chirped grating has been performed.

Current analyses of oblique-incidence chirped grating structures usually assume that the reflection/groove, and the total reflection from the grating, are both very small. Two important effects in the grating are then ignored.

(i) Depletion of the transmitted wave through the grating.

(ii) Multiple-reflection effects within the grating.

These effects are illustrated in Fig. 8.1.1, for the case of 90° reflection. At each discontinuity in the grating (i.e. an up-step or a down-step in a grooved grating) a very small amount of the forward wave R is scattered into the secondary wave S. The power scattered into S results in a depletion of the forward wave R. This depletion is ignored in the low-reflection model, which thus does not satisfy power conservation.

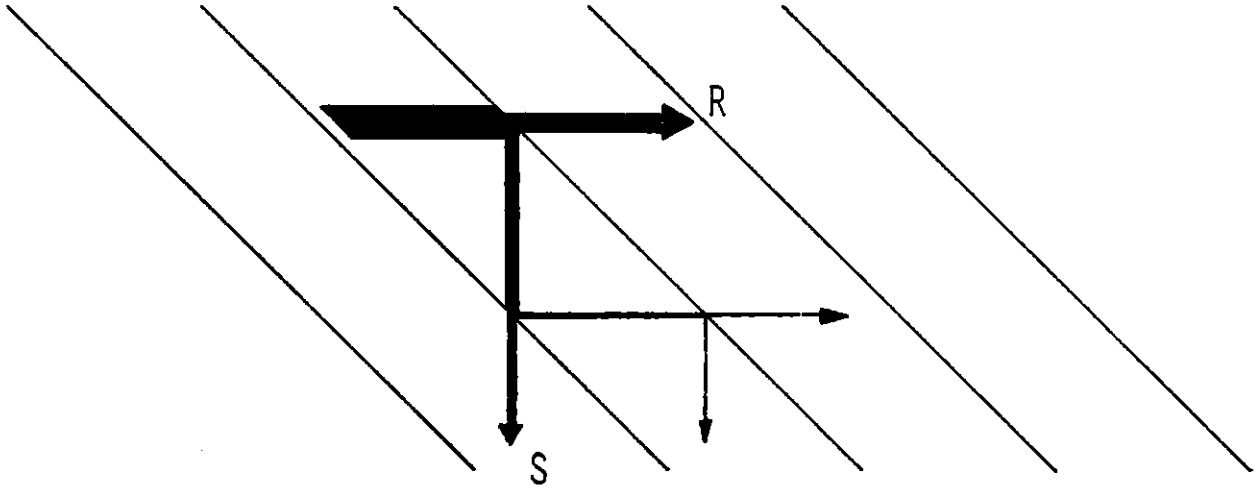

FIG. 8.1.1 DEPLETION AND MULTIPLE REFLECTIONS IN AN OBLIQUE-INCIDENCE GRATING.

Referring to Fig. 8.1.1, it is also apparent that, in general, R and S can interchange power many times across the width of the grating by a process of multiple reflection. These multiple reflections are also totally ignored in current low-reflection analyses. Modern signal processing devices frequently require strong grating reflection to achieve low insertion loss. The low-reflection model then becomes increasingly inaccurate for predicting the phase and amplitude response of the device.

An approach was suggested by Otto et al. for including depletion and multiple-reflection effects in the analysis of a constant-period oblique-incidence grating.[42] The technique consists of dividing the grating up into a large number of small unit cells, each containing one reflector [Fig. 1.2.3]. However, this approach is numerically intensive, gives little physical insight, and is unsuitable for chirped gratings.

In this chapter exact closed-form solutions are derived for an oblique-incidence grating with a linear spatial chirp. The solutions are particularly simple for the limiting case of a constant-period grating. Filter applications of oblique-incidence constant-period gratings are considered, and the reflective-array-compressor (RAC) is analyzed in greater detail than was possible with previous analyses.

8.2 Exact Solutions

For simplicity we will consider oblique reflection through 90°, for a grating with a linear chirp, in an isotropic medium [Fig. 8.2.1]. In this case, the grating reflectors are at 45° to the incident beam. For 90° reflection in practical anisotropic materials, the analysis remains valid with a simple scale change of one of the axes.[41] The grating structure may be SAW, optical, or otherwise in nature.

We define the grating period by

$$k_g(x, y) = p^{-1}[k_o - \delta(x - y)]$$

where $k_g(x, y) = 2\pi/\Lambda(x, y)$, and $\Lambda(x, y)$ is the local period of the grating measured along x or y [Fig. 8.2.1]. The chirp rate is specified by δ, and k_o is the local synchronous propagation constant along $(x - y) = 0$, for a wave at the p-th harmonic, i.e. $k_o = \omega_o(0, 0)/v = 2p\pi/\Lambda(0, 0)$. At the origin $(0, 0)$, the detuning from synchronism is denoted by Δ, where

$$\Delta = k_o - k = \frac{(\omega_o(0, 0) - \omega)}{v}$$

and k is the propagation constant of the wave. The detuning,

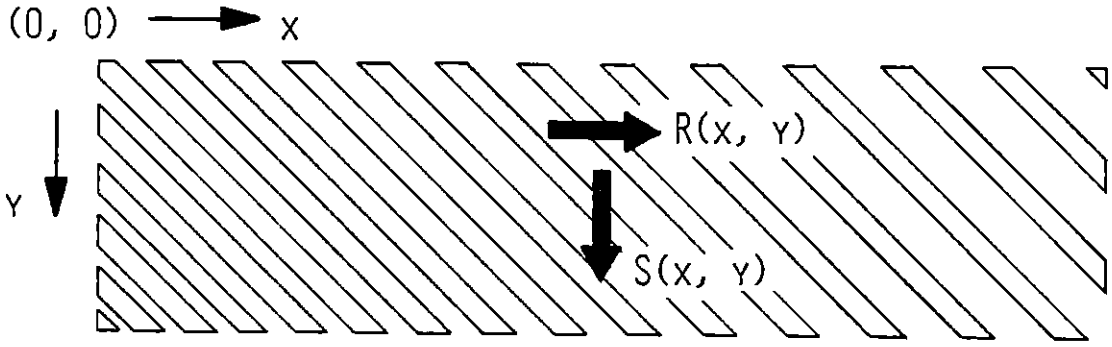

FIG. 8.2.1 45° OBLIQUE-INCIDENCE CHIRP GRATING

at a general point in the grating, from the local synchronous frequency $\omega_o(x, y)$, is given by

$$\frac{(\omega_o(x, y) - \omega)}{v} = \Delta - \delta(x - y). \tag{8.2.1}$$

The slowly-varying wave amplitudes $\tilde{R}(x, y)$ and $\tilde{S}(x, y)$ are defined by

$$\begin{aligned} R(x, y) &= \tilde{R}(x, y)\, e^{j(\omega t - kx)} \\ S(x, y) &= \tilde{S}(x, y)\, e^{j(\omega t - ky)}. \end{aligned} \tag{8.2.2}$$

In terms of these amplitudes, the coupled-wave equations for the oblique-incidence chirped grating are

$$\begin{aligned} \frac{\partial}{\partial x} \tilde{R}(x, y) &= - K\, e^{-j\Delta(x-y) + j \frac{\delta}{2} (x-y)^2}\, \tilde{S}(x, y) \\ \frac{\partial}{\partial y} \tilde{S}(x, y) &= K^*\, e^{j\Delta(x-y) - j \frac{\delta}{2} (x-y)^2}\, \tilde{R}(x, y) \end{aligned} \tag{8.2.3}$$

where K is the coupling coefficient/unit length. As a confirmation of the veracity of these equations, observe that they

predict the strongest wave interaction, in the grating, will occur where the phase of K is stationary with respect to x and y. This is determined to be the contour $(x - y) = \Delta/\delta$. As expected, we see from (8.2.1) that this is also the contour along which the grating is synchronous.

The coupled-wave equations (8.2.3) can be simplified by the change of variables

$$\tilde{R}(x, y) = \hat{R}(x, y)\, e^{j\Delta y + j\frac{\delta}{2} y^2}$$

$$\tilde{S}(x, y) = \hat{S}(x, y)\, e^{j\Delta x - j\frac{\delta}{2} x^2}. \qquad (8.2.4)$$

In terms of the new variables $\hat{R}(x, y)$ and $\hat{S}(x, y)$ the equations become

$$\frac{\partial}{\partial x} \hat{R}(x, y) = -K\, e^{-j\delta xy}\, \hat{S}(x, y)$$

$$\frac{\partial}{\partial x} \hat{S}(x, y) = K^*\, e^{j\delta xy}\, \hat{R}(x, y).$$

From these equations we derive the second-order partial differential equation for $\hat{R}(x, y)$

$$\left[\frac{\partial^2}{\partial x \partial y} + j\delta x \frac{\partial}{\partial x} + |K|^2\right] \hat{R}(x, y) = 0. \tag{8.2.5}$$

This equation is linear and of the hyperbolic type.[53]

A functionally-invariant solution may be determined for (8.2.5) using Riemann's method.[54,55] We assume a solution of the form

$$\hat{R}(x, y) = \int_0^y ds\ \psi(x)\ W(x(y - s)) + A\ W(xy) \tag{8.2.6}$$

where $\psi(s)$ is an arbitrary function. Such a solution is found to exist for a function $W(\zeta)$ satisfying the ordinary differential equation

$$\left[\zeta \frac{d^2}{d\zeta^2} + (1 + j\delta\zeta) \frac{d}{d\zeta} + |K|^2\right] W(\zeta) = 0. \tag{8.2.7}$$

A substitution

$$\xi = -j\delta\zeta \tag{8.2.8}$$

transforms this equation into

$$\xi \frac{d^2}{d\xi^2} W(\xi) + (1 - \xi) \frac{d}{d\xi} W(\xi) - \frac{|K|^2}{j\delta} W(\xi) = 0 \tag{8.2.9}$$

which can be identified as a confluent hypergeometric differential equation.[52]

A confluent hypergeometric equation was also encountered in the analysis of a normal-incidence chirped grating (7.2.13). In that case there were two acceptable solutions. The general solution was thus a linear combination of the two (7.2.14). However, in this case, there exists only one acceptable solution to the differential equation (8.2.9). The second solution exhibits a logorithmic singularity at the origin ($\xi = 0$) and therefore must be rejected. The general solution is thus

$$W(\xi) = {}_1F_1\left(\frac{|K|^2}{j\delta}; 1; \xi\right) \tag{8.2.10}$$

where ${}_1F_1(a; b; z)$ is again the confluent hypergeometric function (also called a Kummer function, or a degenerate hypergeometric function).

There is an essential difference between the normal and oblique-incidence cases. At normal incidence the coupled waves are collinear, and thus specifying only one boundary condition is insufficient to define the problem. Both waves exist at the input and output boundaries of the grating. Two boundary conditions are therefore required to determine their relative amplitude. However, in the oblique case, the boundary condition at

the input to the grating is entirely independent of the scattered wave S [Fig. 8.1.1]. The latter cannot couple, or scatter back to the input. Thus, we need only specify one boundary condition, in the oblique case, to define the problem. If we insist on specifying two arbitrary boundary conditions then sources are required in the grating. The singular solution, in the oblique case, represents these internal sources.

From (8.2.8) and (8.2.10) the function $W(\zeta)$, which satisfies the ordinary differential equation (8.2.7) is thus

$$W(\zeta) = {}_1F_1\left(\frac{|K|^2}{j\delta}\,;\,1\,;\,-j\delta\zeta\right) . \tag{8.2.11}$$

Hence, from (8.2.6) and (8.2.11), a general solution of the partial differential equation (8.2.5) is

$$\hat{R}(x,\,y) = \int_0^y ds\ \psi(s)\ {}_1F_1\left(\frac{|K|^2}{j\delta}\,;\,1\,;\,-j\delta x(y-s)\right)$$

$$+ A\ {}_1F_1\left(\frac{|K|^2}{j\delta}\,;\,1\,;\,-j\delta xy\right) . \tag{8.2.12}$$

The exact solutions for the grating waves, $R(x,\,y)$ and $S(x,\,y)$, are obtained from (8.2.2)-(8.2.4) and (8.2.12). In

(8.2.12), the arbitrary function $\psi(s)$ is chosen to satisfy the boundary condition along $x = 0$, while the constant A is determined from the boundary condition $S(x, 0) = 0$. Using recursion relations for the confluent hypergeometric functions,[52] we finally determine the exact solutions for the grating to be

$$R(x, y) = e^{j(\omega t - kx)} \left[R(0, y) - |K|^2 \, x \int_0^y ds \right.$$

$$e^{-j[\Delta(s - y) + \frac{\delta}{2}(s^2 - y^2)]}$$

$$\left. R(0, s) \; {}_1F_1\left(1 + \frac{|K|^2}{j\delta} ; 2 ; -j\delta x(y - s) \right) \right]$$

and

$$S(x, y) = K^* \, e^{j(\omega t - ky)} \int_0^y ds \; e^{-j[\Delta(s - x) + \frac{\delta}{2}(s - x)^2]}$$

$$R(0, s) \; {}_1F_1\left(- \frac{|K|^2}{j\delta} ; 1 ; j\delta x(y - s) \right) . \qquad (8.2.13)$$

These solutions for an oblique-incidence chirped grating are exact, in that they incorporate all orders of multiple

reflections and wave depletion within the grating. They are also valid for an arbitrary input wave profile, and for an arbitrary detuning between the input wave and the grating.

We shall now examine the implications of these solutions. We begin by considering gratings with a constant spatial period.

8.3 Constant-Period Gratings

For constant-period gratings the chirp parameter $\delta = 0$. From the series expansions of confluent hypergeometric functions, we find

$$\mathcal{L}_{\delta \to 0} \; {}_1F_1\left[1 + \frac{|K|^2}{j\delta} \; ; \; 2 \; ; \; -j\delta\xi\right] = \frac{J_1(2|K|\sqrt{\xi})}{|K|\sqrt{\xi}}$$

and

$$\mathcal{L}_{\delta \to 0} \; {}_1F_1\left[- \frac{|K|^2}{j\delta} \; ; \; 1 \; ; \; j\delta\xi\right] = J_o(2|K|\sqrt{\xi})$$

where $J_o(\zeta)$ and $J_1(\zeta)$ are the zeroth-order and first-order Bessel functions respectively. From (8.2.13), the exact solutions for a constant-period oblique-incidence grating are thus

$$R(x, y) = e^{j(\omega t - kx)} \left[R(0, y) - e^{j\Delta y} \; |K|\sqrt{x} \int_0^y ds \; e^{-j\Delta s} \right.$$

$$\left. R(0, s) \; \frac{J_1\left[2|K|\sqrt{x(y - s)}\right]}{\sqrt{y - s}} \right]$$

and

$$S(x, y) = K^* \; e^{j(\omega t - ky)} \; e^{j\Delta x} \int_0^y ds \; e^{-j\Delta s}$$

$$R(0, s) \; J_o\left[2|K|\sqrt{x(y - s)}\right] \; . \qquad (8.3.1)$$

These exact solutions, for an arbitrary input profile and arbitrary detuning Δ, clearly show the dependence of the grating response on the various grating parameters. In addition, they can be evaluated with much less computation than is required for the alternative unit-cell approach. Figure 8.3.1 shows the profile of the output wave, after transmission through an oblique-incidence grating at Bragg, and for small detuning from Bragg. Note the depletion and considerable distortions of the wave introduced by the grating.

For the case of Bragg excitation (i.e. $\Delta = 0$) and a uniform input wave profile $R(0, y) = 1$, the exact solutions are particularly simple. Under these conditions, the solutions (8.3.1) reduce to

$$R(x, y) = e^{j(\omega t - kx)} J_o(2|K|\sqrt{xy})$$

and

$$S(x, y) = e^{j(\omega t - ky)} \frac{K^*}{|K|} \sqrt{x/y}\, J_1(2|K|\sqrt{xy}). \qquad (8.3.2)$$

These solutions were also deduced by Bloch et al. by analogy with solutions obtained in holography.[39] They clearly illustrate the manner in which the transmitted wave, through the grating, will become distorted if the coupling coefficient K

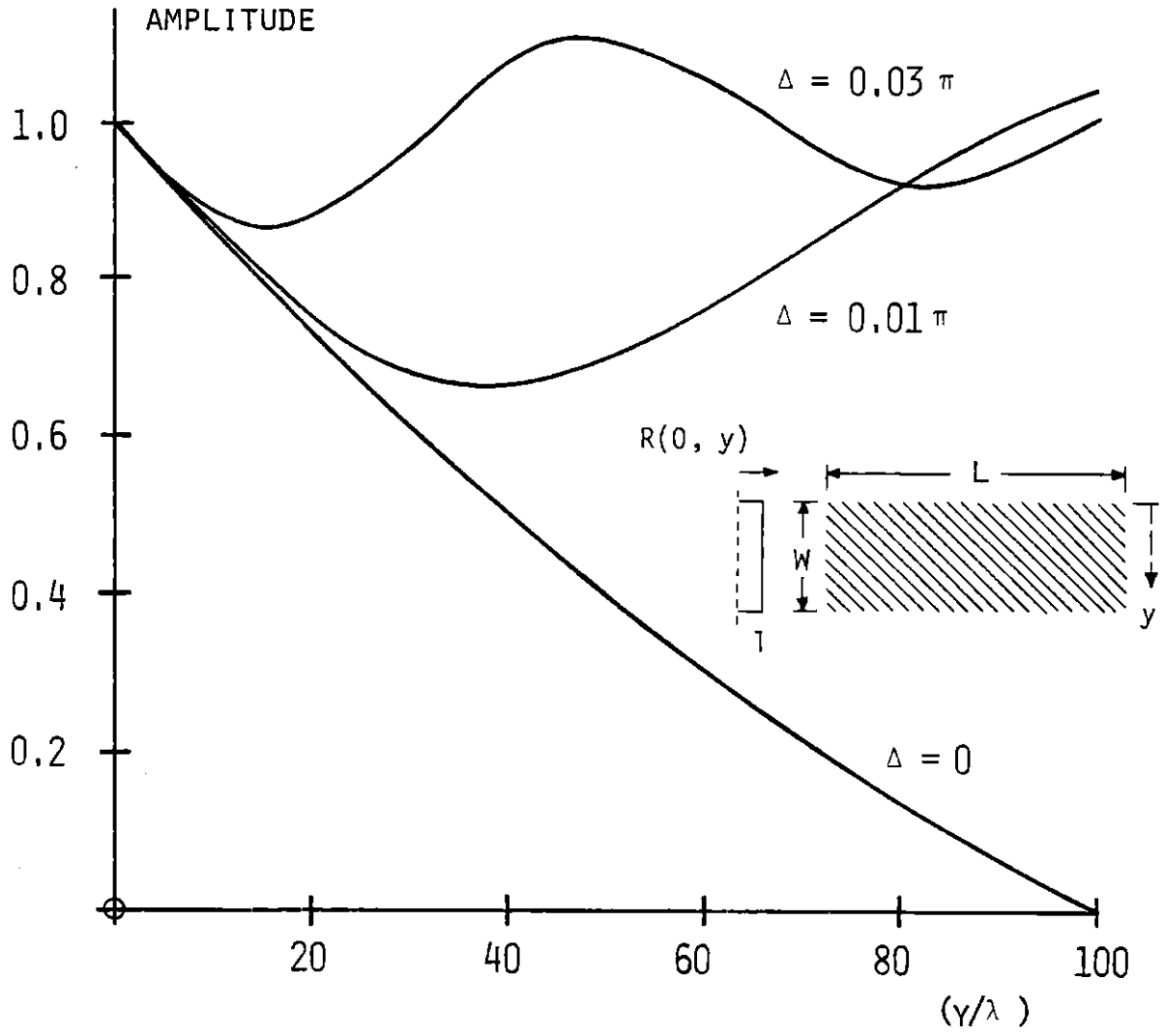

FIG. 8.3.1 AMPLITUDE PROFILE OF UNIFORM INCIDENT WAVE AFTER TRANSMISSION THROUGH A 45° CONSTANT-PERIOD OBLIQUE-INCIDENCE GRATING $(w/\lambda_r) = 100$, $(L/\lambda_r) = 400$).

and the grating dimensions are large enough.

As a possible application of this exact analysis we briefly consider the use of constant-period oblique-incidence gratings as filters. Either a bandstop or bandpass response may be realized. Figure 8.3.2 shows the configuration of such a SAW filter. For a bandstop response the output is taken from transducer 2, while for a bandpass response the output is taken from transducer 3. The filter bandwidth is reduced, for a given insertion loss, by increasing either the number of grooves or the width of the grating. This is illustrated in Fig. 8.3.3 which shows the theoretical bandstop characteristics of three practical gratings. Note that the bandwidth, of the response, appears to be much more sensitive to the width of the grating than to the number of grooves. This is partly due to multiple-reflection effects, which become more significant as the width of the grating is increased.

For the same grating considered in Fig. 8.3.3(b) we show the corresponding bandpass response from transducer 3 in Fig. 8.3.4(a). It is interesting to note that because of considerable phase distortion, across the wave front, much of the power scattered by the grating is not intercepted by the transducer. In Fig. 8.3.4(b) we show the true acoustic power scattered by the grating. The latter is seen to be much larger in amplitude,

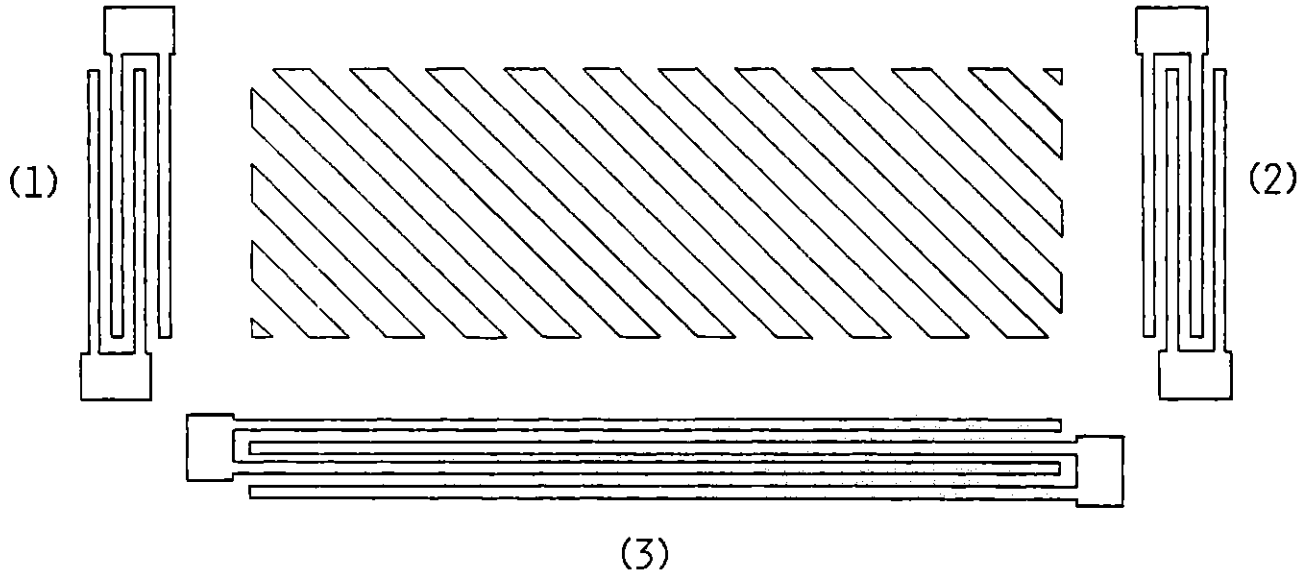

FIG. 8.3.2 OBLIQUE-INCIDENCE CONSTANT-PERIOD GRATING FILTER.

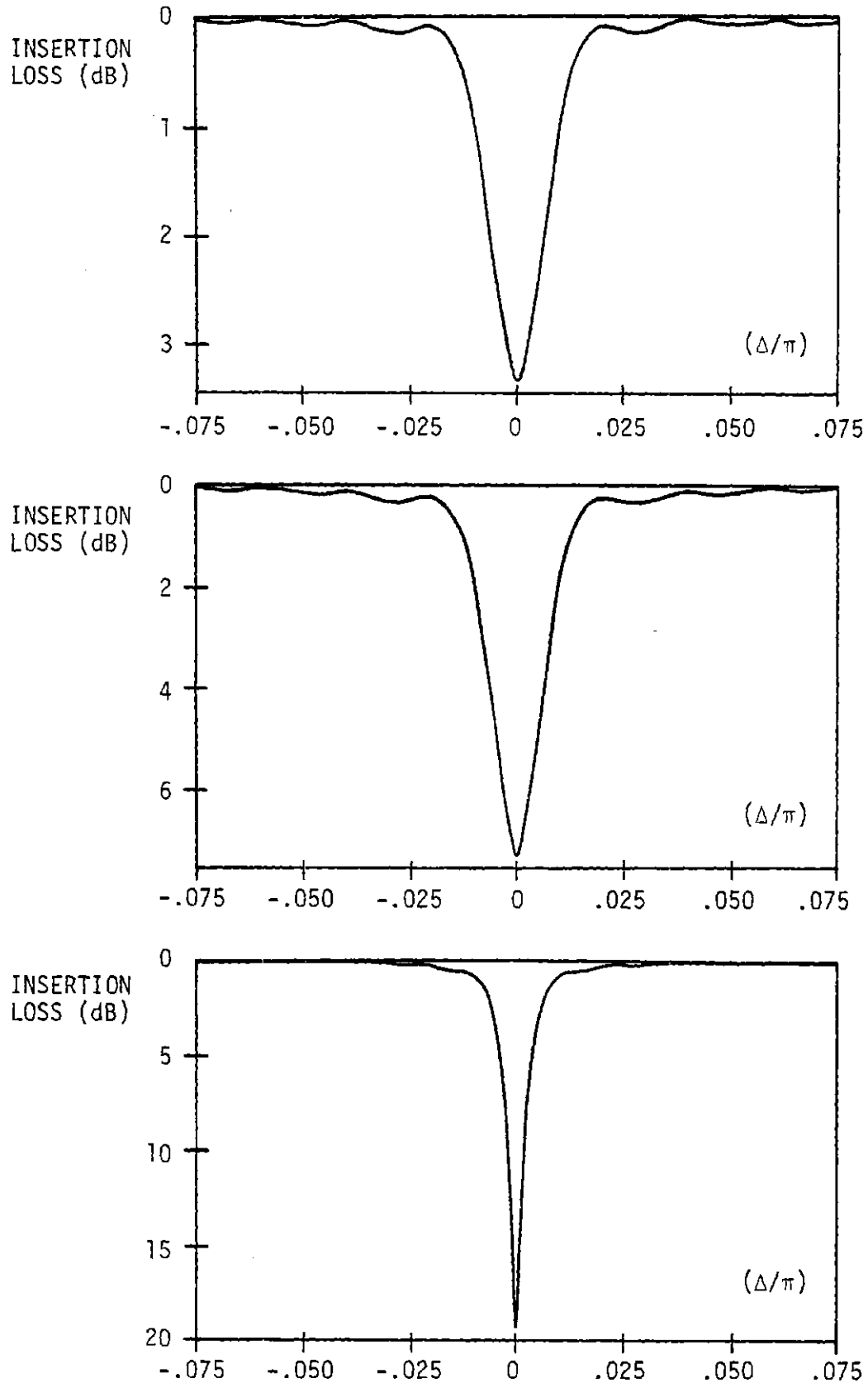

FIG. 8.3.3 BANDSTOP RESPONSE OF OBLIQUE-INCIDENCE GRATING FILTER ($K\lambda_r = 0.01$)

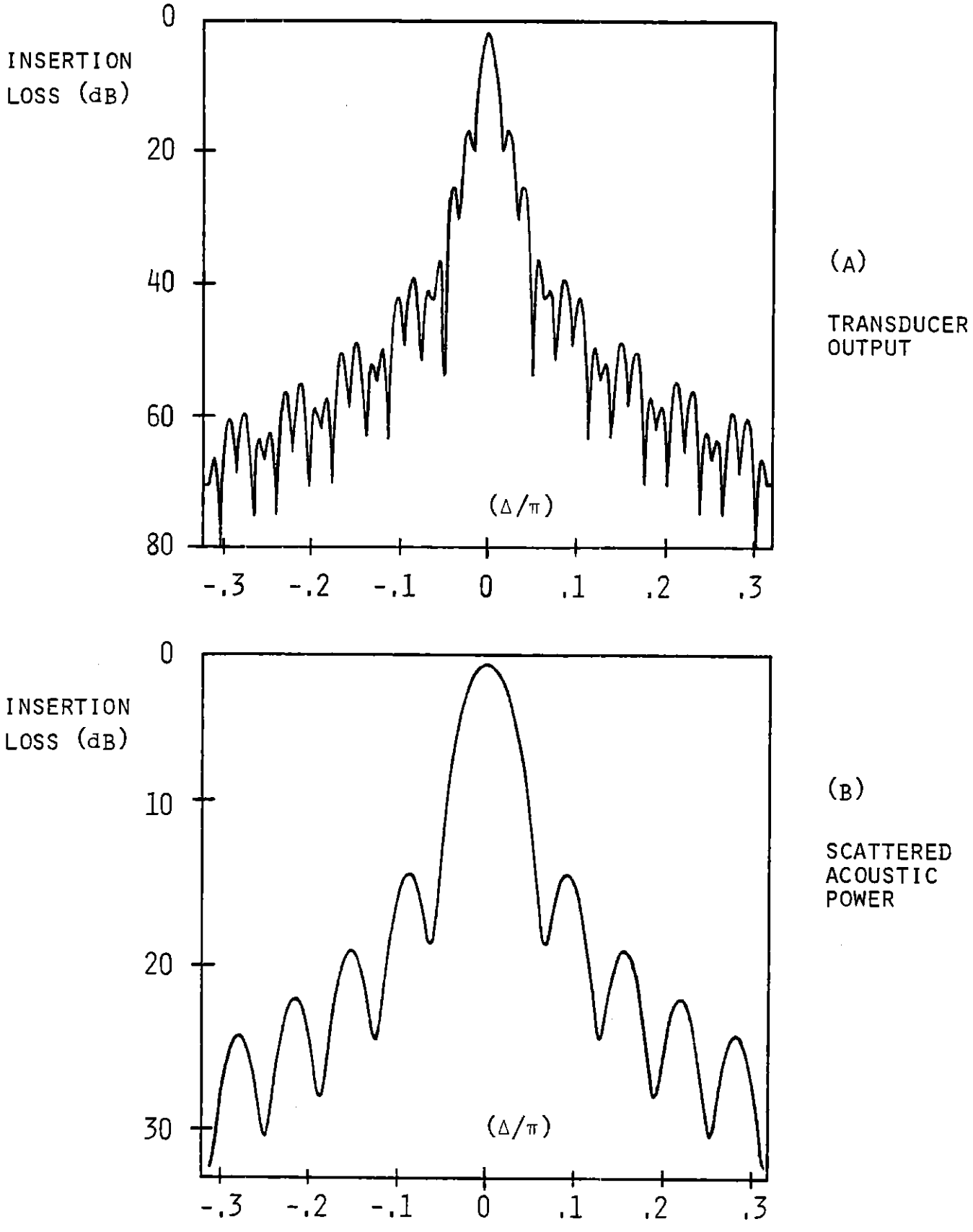

FIG. 8.3.4 BANDPASS RESPONSE OF OBLIQUE-INCIDENCE GRATING FILTER $((w/\lambda_r) = 100,\ (L/\lambda_r) = 400,\ K\lambda_r = 0.01)$.

and also to have a much wider bandwidth, than the electrical power from the transducer.

Before proceeding to consider the RAC we shall first digress to develop approximations to the exact chirped grating solutions given in (8.2.13).

8.4 Approximate Chirped Grating Solutions

In many cases the full exact solutions (8.2.13) may not be required for the analysis of practical gratings. If the coupling in the grating is small only the lowest-order terms in K need be considered. As a lowest-order approximation we obtain, to order K (i.e. $O(K)$)

$$R(x, y) = e^{j(\omega t - kx)} R(0, y)$$

and

$$S(x, y) = K^* e^{j(\omega t - ky)} \int_0^y ds\, e^{-j[\Delta(s - x) + \frac{\delta}{2}(s - x)^2]} R(0, s). \qquad (8.4.1)$$

These are the familiar solutions currently used extensively in RAC design.[41] The forward wave in the grating $R(x, y)$ is assumed to propagate through the grating unperturbed, and with no power loss. The scattered wave $S(x, y)$ is seen to be attributed to only one-order of reflection of $R(x, y)$, as all contributions of the order K^2 and above are ignored. For low-loss devices where the coupling may be somewhat tighter, these solutions may not be accurate enough. As we shall see,

much additional insight and accuracy in the design may be obtained by going to one higher-degree of approximation.

To include the contributions from the lowest-order of multiple reflections $(O(K^2))$, within the grating, it is necessary to expand the solutions (8.2.13) correct to $O(K^3)$. It can be shown that

$$ {}_1F_1\left[1 + \frac{|K|^2}{j\delta}\,;\, 2\,;\, -j\delta z\right] = e^{-j\frac{\delta}{2}z}\,\frac{\sin z}{z} + O(K^2) $$

and

$$ {}_1F_1\left[-\frac{|K|^2}{j\delta}\,;\, 1\,;\, j\delta z\right] = 1 - \frac{2|K|^2}{\delta}\int_0^{(\delta/2)z} d\xi\; e^{j\xi}\,\frac{\sin \xi}{\xi} + O(K^4) $$

where the last terms signify the order of the terms neglected. We thus obtain, to $O(K^3)$:

$$ R(x, y) = e^{j(\omega t - kx)}\left[R(0, y) - \frac{2|K|^2}{\delta}\int_0^y ds\; e^{j(y - s)[\Delta - \frac{\delta}{2}(x - y - s)]}\,R(0, s)\,\frac{\sin[(\delta/2)\,x(y - s)]}{(y - s)}\right] $$

and

$$S(x, y) = K^* e^{j(\omega t - ky)} \int_0^Y ds\, e^{-j[\Delta(s - x) + \frac{\delta}{2}(s - x)^2]} R(0, s)$$

$$\left[1 - \frac{2|K|^2}{\delta} \int_0^{(\delta/2)\, x(y-s)} d\xi\, e^{j\xi} \frac{\sin \xi}{\xi}\right] \qquad (8.4.2)$$

These solutions are more accurate for low-loss RAC design than the solutions (8.4.1) which are currently used. In many cases they are sufficiently accurate for the design of practical devices and are much simpler to evaluate than the exact solutions (8.2.13).

8.5 RAC Solutions

We have so far considered the response of only a single oblique-incidence chirped grating. In this section we apply the solutions obtained for such a grating to an analysis of the RAC. The RAC is a SAW dispersive filter which is used widely for pulse compression. In its simplest embodiment it consists of two 45° oblique-incidence chirped gratings through which the acoustic signal undergoes two 90° reflections [Fig. 8.5.1].

We begin by determining the exact response of a RAC, for a uniform input wave, using the exact oblique-incidence grating solutions (8.2.13). This solution is, however, difficult to evaluate, and of greater complexity than is required for the analysis of most practical devices. We therefore develop an approximate solution for the RAC response using the simpler, though approximate, grating solutions (8.4.2). In the following section the behavior of a practical RAC design is analyzed, in some detail, using these approximate solutions.

To obtain the response of a RAC [Fig. 8.5.1] we must consider reflection through two oblique-incidence gratings. It is convenient for the analysis to define the coordinate system, in each grating, with its origin at the center of the grating [Fig. 8.5.2]. Each grating is taken to be of width W and

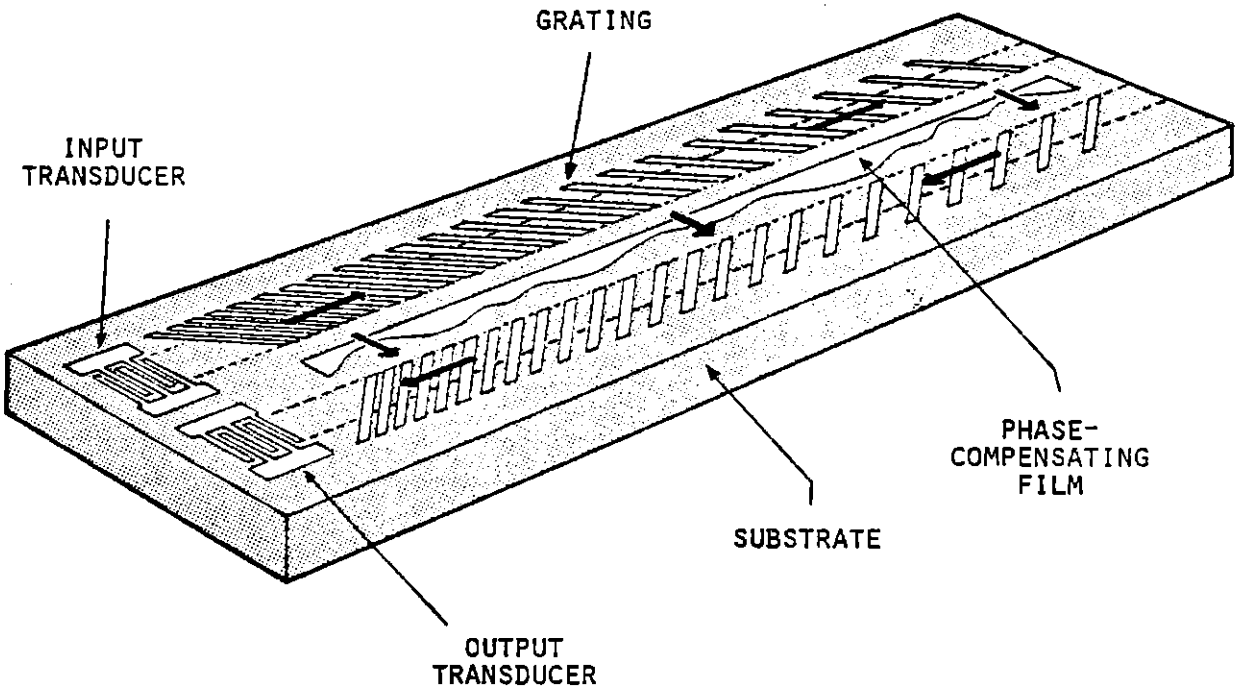

FIG. 8.5.1 RAC CONFIGURATION.

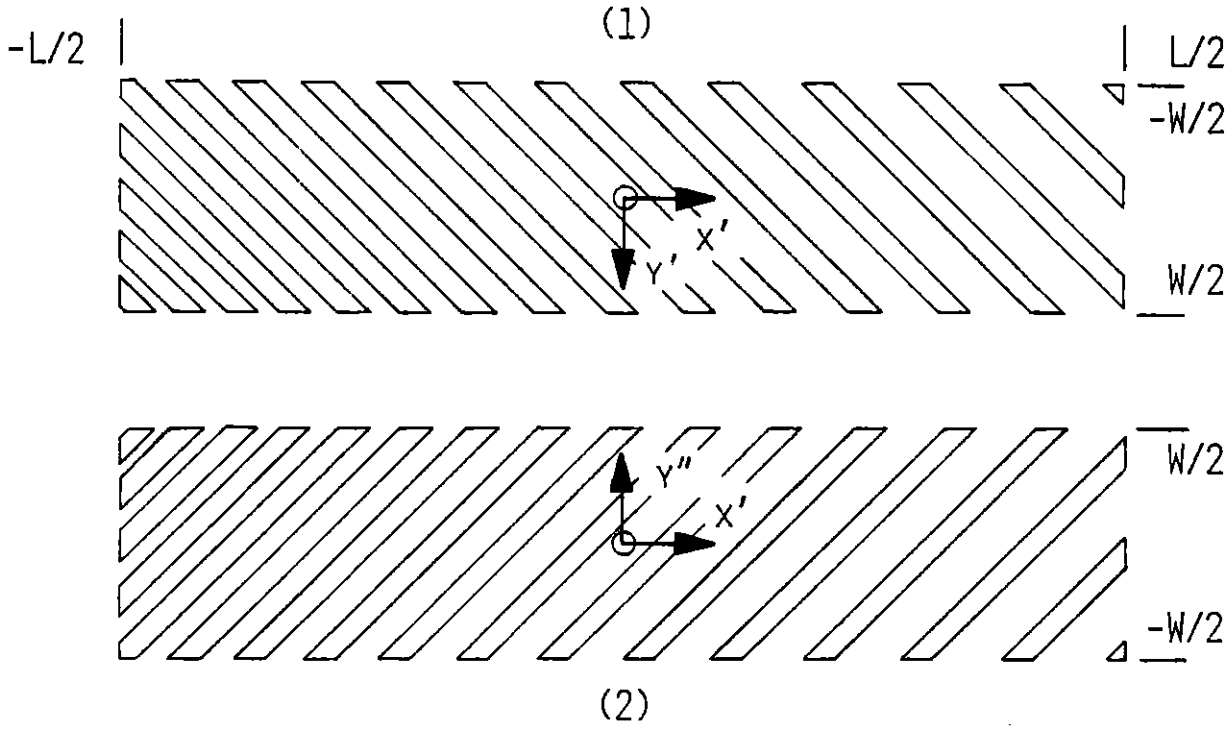

FIG. 8.5.2 RAC COORDINATE SYSTEM

length L. From (8.2.1) the synchronous detuning at the center of each grating Δ', is given by

$$\Delta' = \Delta - \delta\left(\frac{L}{2} - \frac{W}{2}\right) . \tag{8.5.1}$$

The output of the RAC, from a transducer at $x' = -L/2$ in grating (2), is given by

$$\bar{S} = \int_{-W/2}^{W/2} dy''\ S'(-L/2,\ y'')$$

where $S'(x', y'')$ is the wave in grating (2).

For the case of a uniform input wave to grating (1) ($R(-L/2, y') = 1$), ignoring frequency independent phase terms, we obtain using (8.2.13)

$$\bar{S} = |K|^2 \int_{-L/2}^{L/2} dx \left[\int_{-W/2}^{W/2} dy\ e^{-j[\Delta'(y - x) + \frac{\delta}{2}(y - x)^2]}\right.$$

$$\left. {}_1F_1\left(-\frac{|K|^2}{j\delta};\ 1\ ;\ j\delta(x + L/2)(W/2 - y)\right)\right]^2 \tag{8.5.2}$$

where Δ' is defined in (8.5.1). This is the response of a RAC for a uniform input. It includes all depletion and multiple

reflection effects in both gratings.

As discussed above, the exact solution (8.5.2) is usually not required for the analysis of most practical RAC designs. If the coupling is not too strong we may use the approximate grating solutions (8.4.2) to evaluate the output from the RAC. In this case we obtain the approximate solution

$$\bar{S} = |K|^2 \int_{-L/2}^{L/2} dx \left\{ \int_{-W/2}^{W/2} dy\, e^{-j[\Delta'(y - x) + \frac{\delta}{2}(y - x)^2]} \right.$$

$$\left. \left[1 - \frac{2|K|^2}{\delta} \int_0^{(\delta/2)(x + L/2)(W/2 - y)} d\xi\, e^{j\xi} \frac{\sin \xi}{\xi} \right] \right\}^2 \qquad (8.5.3)$$

This solution includes the effects of the lowest-order multiple reflections in each grating and is thus accurate to $O(K^5)$. It is much simpler to evaluate than the exact solution (8.5.2), and is accurate enough for the analysis of most practical devices.

8.6 Analysis of a Practical RAC

We will now consider the performance of a practical RAC design in the light of the new, more accurate, theoretical solutions presented in the previous sections. By way of illustration we shall consider a RAC with a linear FM downchirp, center frequency of 400 MHz, bandwidth 180 MHz, and 90 μs dispersive delay. A RAC with these specifications was considered by Otto et al., using the lowest-order approximate grating solutions (8.4.1), in a previous paper.[14]

For the analysis we shall use the approximate chirped grating and RAC solutions, (8.4.2) and (8.5.3) respectively, to evaluate the response of the device. These solutions include only the first order of multiple reflections in each grating. However, we shall show that these solutions provide important corrections to the response predicted a lowest-order analysis. The grating coupling coefficient K will be assumed independent of position (i.e. frequency). In practical devices this is usually achieved by depth weighting of the grooves.

In Fig. 8.6.1 we show a typical amplitude profile of the R-wave across the grating, for a wave in grating (1) at the center of its synchronous regime. The wave amplitude in the upper part of the grating has been partially depleted since it has passed through more grooves, close to synchronism, than

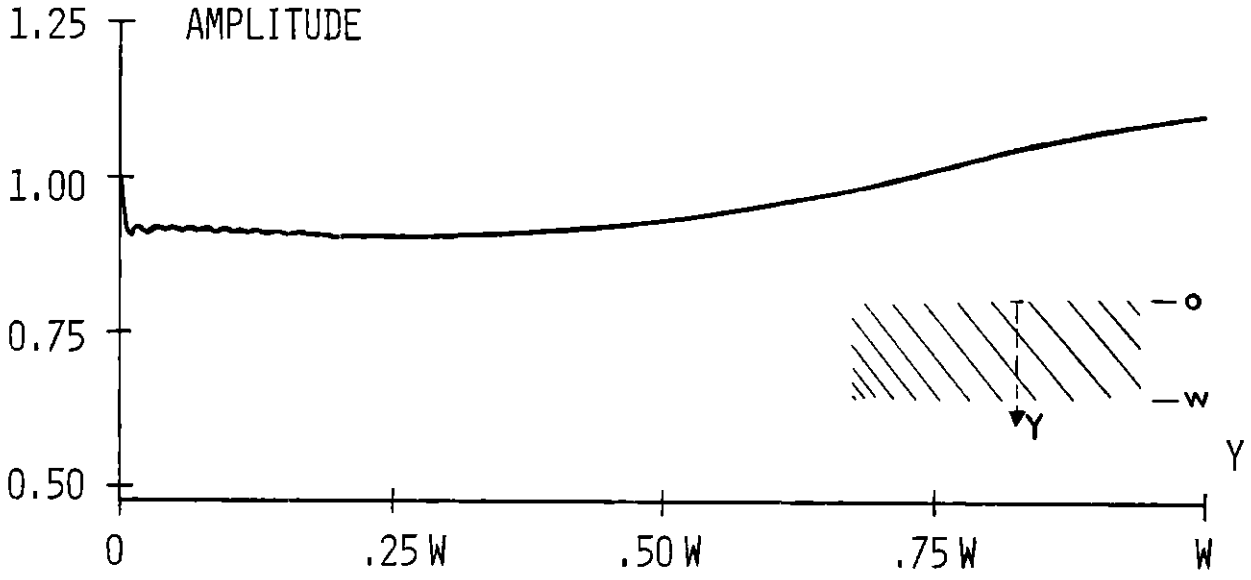

FIG. 8.6.1 SYNCHRONOUS AMPLITUDE PROFILE OF R-WAVE IN RAC (400 MHz)

the lower half. In addition, some additional energy has been "piled-up" in the lower half of the grating due to multiples. Beyond the synchronous region the amplitude profile of the R-wave again flattens out and merely shows a fairly uniform depletion caused by the coupling out of the S-wave. This behavior for the R-wave is physically more satisfying than the assumption of the lowest-order analysis, that the R-wave remains totally unperturbed.

A major advantage of the new analysis lies in predicting the phase response of the device. At any frequency the amplitude profile of the R-wave, across the center of its synchronous region, is almost identical with that shown in Fig. 8.6.1. However, the corresponding phase fronts of R depend strongly upon frequency.

In Fig. 8.6.2, we show the phase fronts of the R-wave for three frequencies, again each across the center of its synchronous region. As the wave travels under the grating its phase front becomes progressively distorted and delayed by multiple-reflection effects. Thus, frequencies that are synchronous far into the grating will suffer from increasing phase-distortions due to multiples. The tilting and distortion of the phase front of the R-wave results in a slight skewing, or tilt, in the amplitude and phase fronts of the S-wave

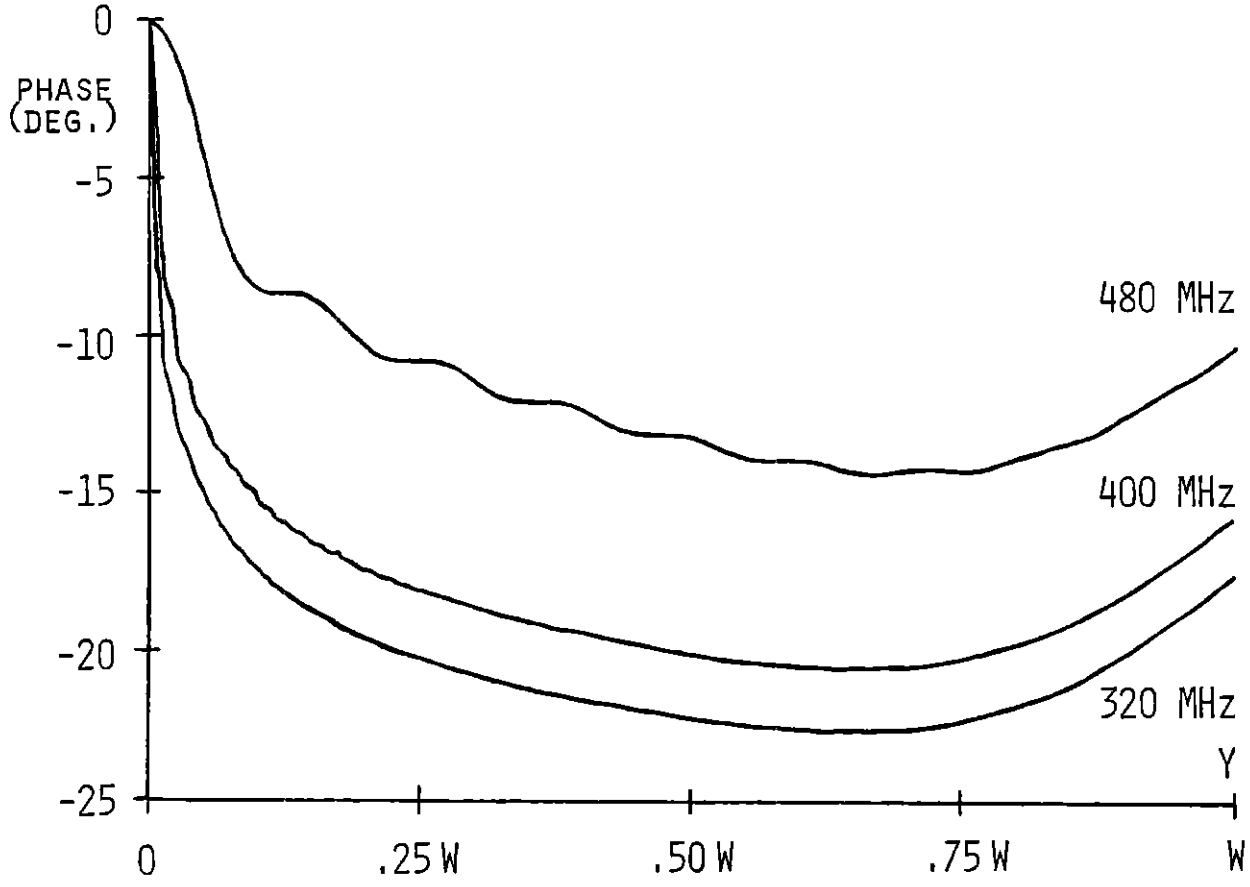

FIG. 8.6.2 PHASE FRONTS OF R-WAVE ACROSS THE CENTER OF THE SYNCHRONOUS REGION FOR EACH FREQUENCY

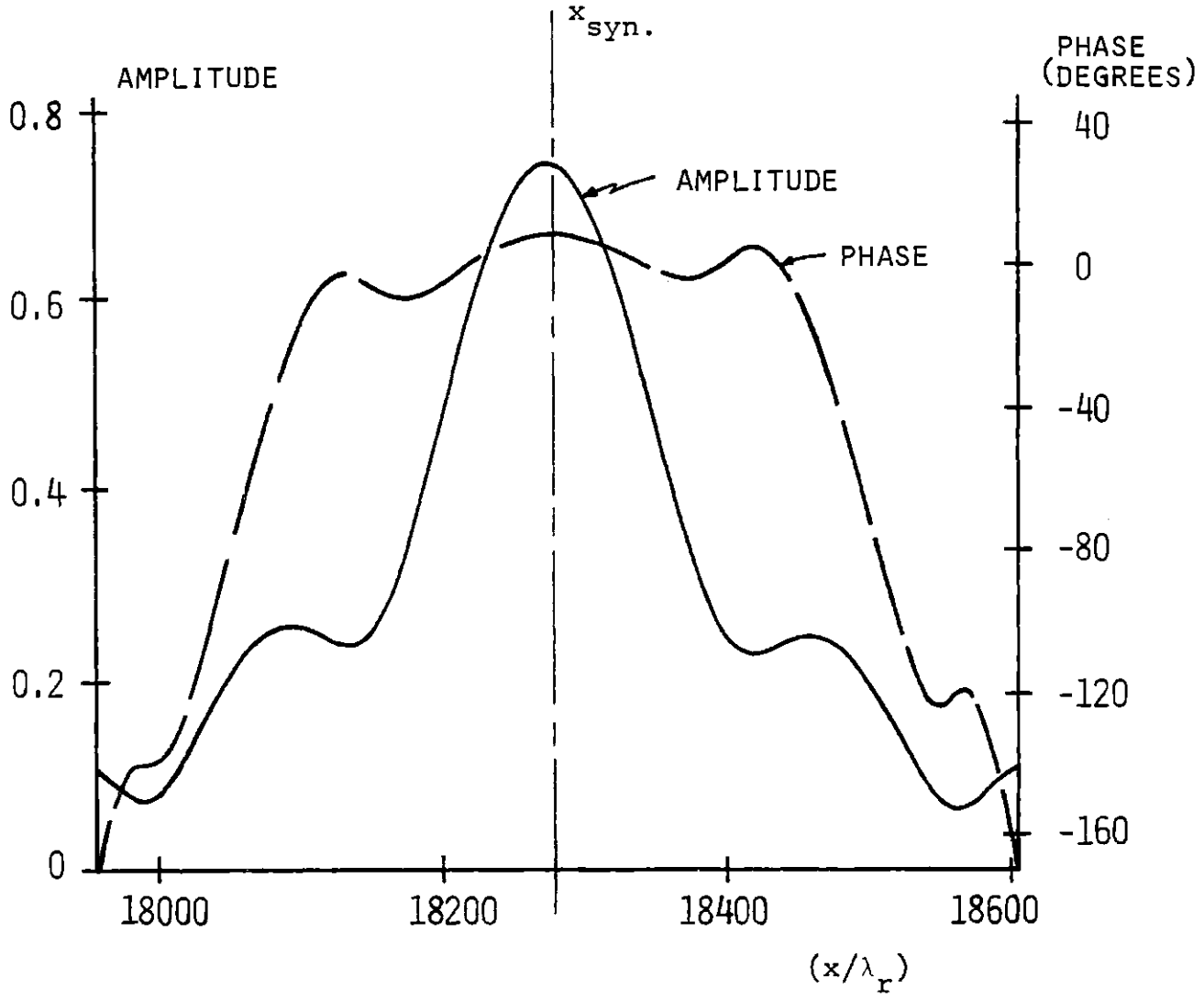

FIG. 8.6.3 AMPLITUDE AND PHASE OF S-WAVE BETWEEN GRATINGS (320 MHz).

between the gratings [Fig. 8.6.3]. However, this effect is only very small and has no significant effect on the overall RAC response. Of much greater importance is the progressive phase delay in the R-wave. In a downchirp device the latter results in an additional, increasing phase delay for decreasing frequency. The resultant additional phase delay in the RAC output, at any given frequency, is approximately twice the effective delay of the R-wave in the first grating. This is because a similar delay is suffered again by the wave in the second grating. Mathematically this is confirmed by (8.5.2), where we observe that the inner integral is squared.

Figure 8.6.4 shows the additional overall phase delay in the RAC response, due to multiples, determined from (8.5.3). As expected, the multiple reflections cause increasing additional phase delays for decreasing frequency. This phase delay is in addition to the quadratic behavior predicted by the lowest-order analysis. The effect of this distortion is two-fold, (1) it causes a change in the chirp-slope from the design expectation, and (2) it causes a phase-deviation from pure quadratic behavior. From (8.5.3) this additional phase delay can be seen to be approximately $\propto (1/\delta)$. Phase errors are typically observed in practical devices and usually necessitate a correcting phase-overlay film to be laid down between the two gratings.[56]

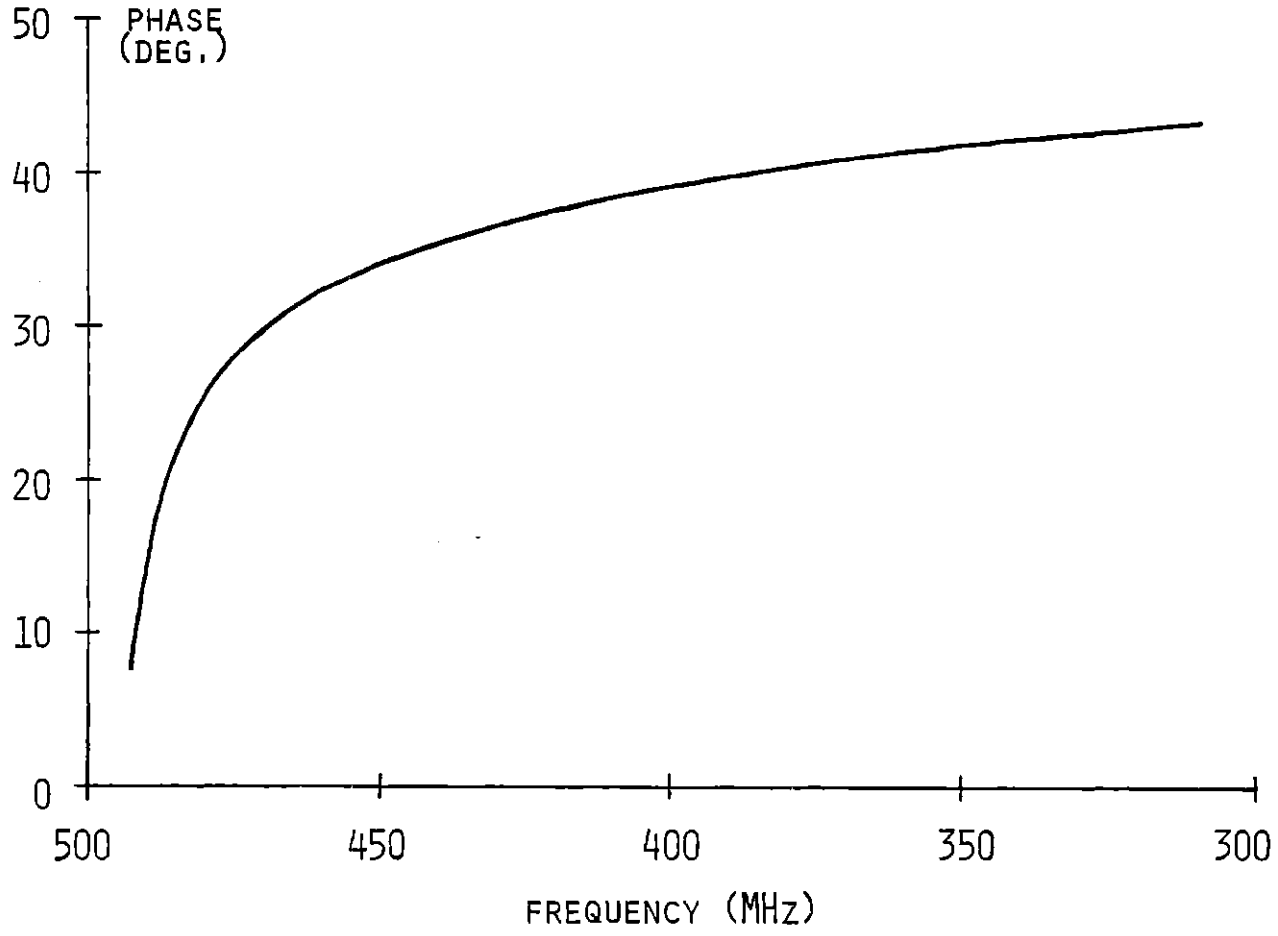

FIG. 8.6.4 ADDITIONAL PHASE DELAY IN RAC FROM IDEAL QUADRATIC

Figure 8.6.5 shows the amplitude response of the RAC, with and without, the correction for multiple reflections. The multiple reflections decrease the coupling through the RAC, especially at the high frequencies. This is because the grating is of constant width. At higher frequencies the grating is wider, in terms of wavelengths, and multiple reflections thus have more chance to introduce amplitude and phase distortions.

It has been reported, in the literature, that in practical down-chirp RAC devices there is frequently an unexplained amplitude rolloff at the lower frequencies.[14] From the analysis above it can be seen that for a constant K grating, even including multiples, such a rolloff in the coupling loss of the RAC is not predicted. However, there are several possible causes of such behavior.

(1) In practical devices K is not a constant. To compensate for propagation, diffraction and transducer losses the coupling constant is generally increased with distance into the grating.[14] For a downchirp device this means that the coupling is generally much stronger at the lower frequencies that at the higher frequencies. This tapering of K may contribute to the amplitude rolloff observed.

To illustrate this phenomenon, consider a "U"-path grating which consists of two constant-period (i.e. $\delta = 0$) oblique-incidence gratings. For the response at Bragg, we obtain from

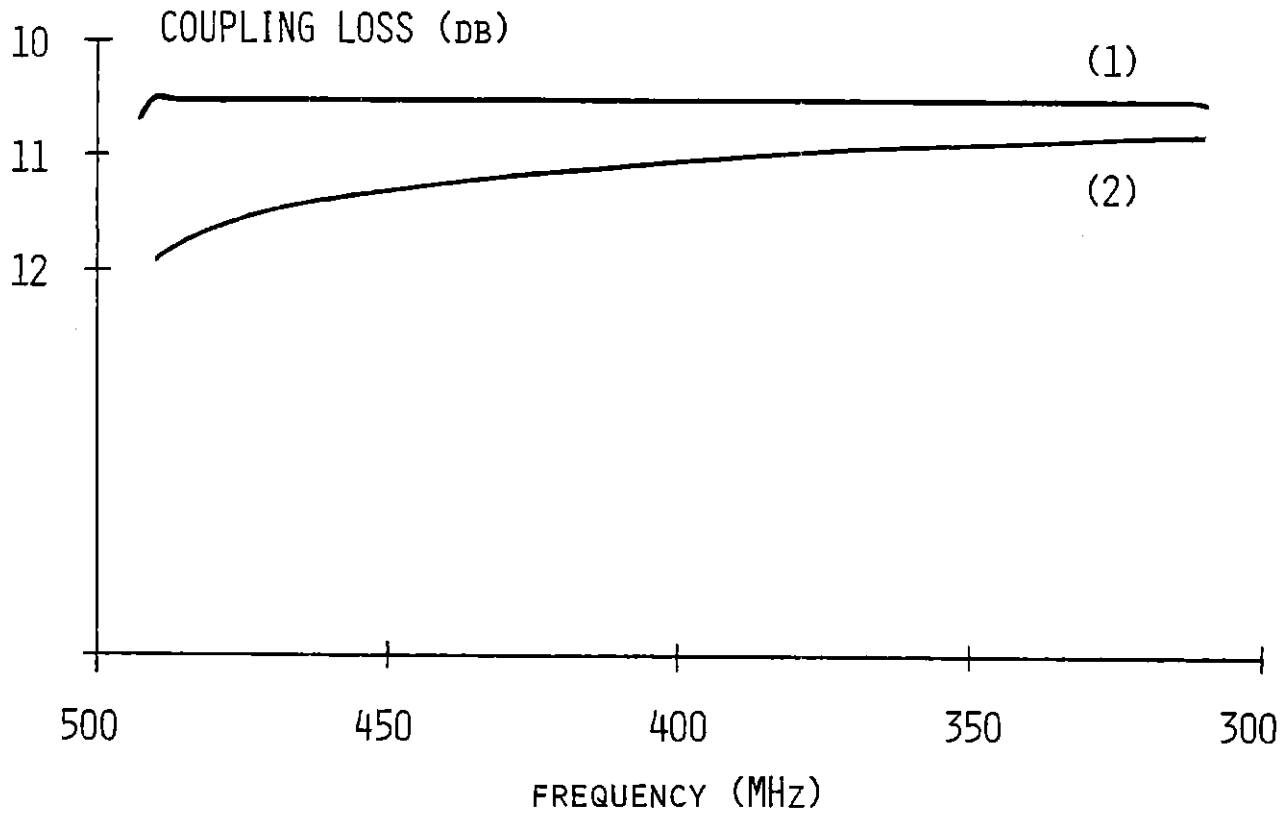

FIG. 8.6.5 COUPLING LOSS THROUGH RAC. (1) LOWEST-ORDER EXCLUDING MULTIPLES, (2) INCLUDING FIRST MULTIPLE REFLECTIONS IN EACH GRATING

the exact solution (8.5.2)

$$\bar{S} = |K|^2 \int_{-L/2}^{L/2} dx \left[\int_{-W/2}^{W/2} dy \; J_o\left(2|K| \sqrt{(x + L/2)(W/2 - y)} \right) \right]^2$$

$$= W\left[1 - J_o^2(2|K|\sqrt{WL}) - J_1^2(2|K|\sqrt{WL}) \right] .$$

The coupling loss through the structure is therefore

$$20 \log_{10}[1 - J_o^2(2|K|\sqrt{WL}) - J_1^2(2|K|\sqrt{WL})]. \qquad (8.6.1)$$

This is the exact solution for the coupling loss through a "U"-path grating at Bragg. From a lowest-order analysis the expected coupling loss would be

$$20 \log_{10}[|K|^2 \; WL]. \qquad (8.6.2)$$

Expanding (8.6.1), we have

$$20 \log_{10}[|K|^2 \; WL - \frac{1}{2} (|K|^2 \; WL)^2 + \ldots]. \qquad (8.6.3)$$

We observe, by comparing (8.6.2) and (8.6.3), that for a constant-period "U"-path grating, the lowest-order analysis under predicts the actual coupling loss of the structure. This error increases for tighter coupling values. In Fig. 8.6.6 the coupling loss predicted by (8.6.1) is plotted against that predicted by the lowest-order analysis (8.6.2). This curve was also obtained from many numerical computer runs using the unit-cell approach.[41] If this saturation effect, for increased coupling, is not taken into account in RAC design, the coupling at the lower frequencies (i.e. larger K) will be less than expected.

(2) Stored-energy effects have not been included in this analysis. In Part I we showed that in normal-incidence gratings these effects can cause the reflection/groove to become a strong function of the groove/strip ratio (Section 5.5). This is also expected to be the case for oblique-incidence gratings. Practical RAC Devices, using grooved reflectors, are generally fabricated with a fixed groove width. A change in the period is achieved by varying the spacing of the grooves. In actual RAC devices, therefore, the groove/strip ratio is not a constant. For high frequencies this ratio is generally > 1 and at low frequencies it is < 1. This effect may also cause an additional skewing of the amplitude response of the device. (It should be noted that the inclusion of stored-energy in the

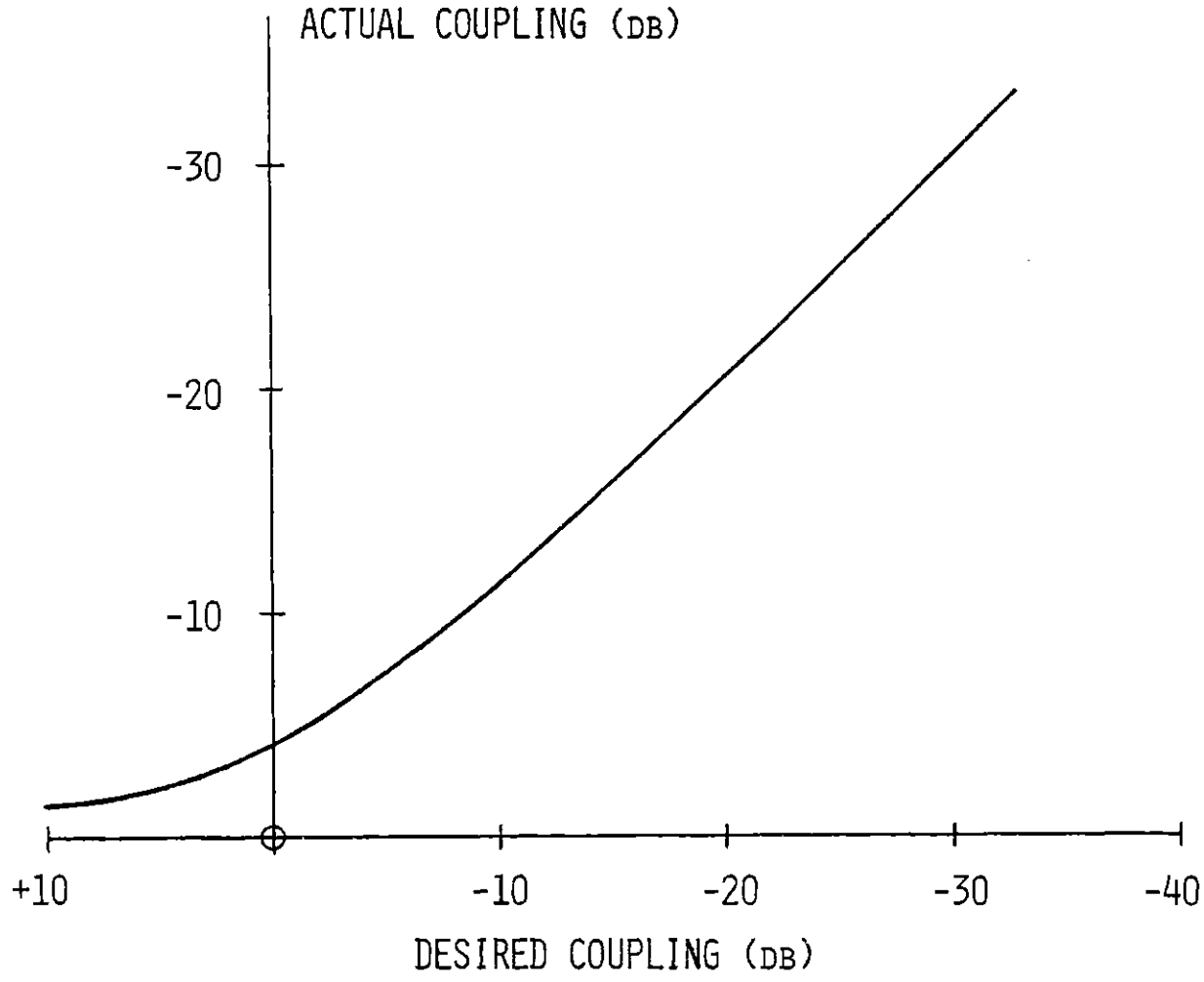

FIG. 8.6.6 COUPLING THROUGH A CONSTANT-PERIOD U-PATH GRATING. ACTUAL VERSUS LOWEST-ORDER PREDICTION.

analysis will also affect the phase response of the RAC.) [57]

(3) In long devices diffraction must also be correctly taken into account. Again, it will be responsible in a down-chirp device for additional loss at low frequencies.

APPENDIX A

STRESS COMPONENTS ON PERTURBED SURFACE

The stress on the perturbed surface of the grating is given by

$$\bar{\sigma}_s = \bar{\bar{\sigma}} \cdot \hat{z}' \qquad \text{(A.1)}$$

where $\bar{\bar{\sigma}}$ is the stress tensor of the acoustic wave on the surface, and $\hat{z}'$ is a unit vector normal to the surface (Fig. A.1). The surface is defined by $z = \varepsilon\lambda_r f(x)$. Thus we write

$$s = z - \varepsilon\lambda_r f(x)$$

and hence

$$\nabla_s = \hat{z} - \hat{x}\, \varepsilon\lambda_r f'(x).$$

Since ∇_s is normal to the surface, it follows that

$$\hat{z}' = \frac{\hat{z} - \hat{x}\, \varepsilon\lambda_r f'(x)}{\sqrt{1 + (\varepsilon\lambda_r f'(x))^2}} .$$

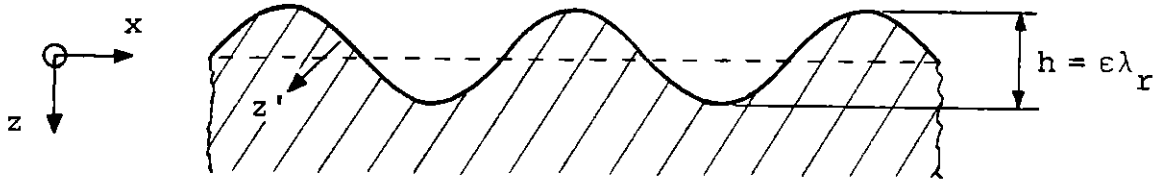

FIG. A.1 PERTURBED GRATING BOUNDARY

From (A.1) the stress on the surface of the grating is therefore

$$\bar{\sigma}_s = \begin{bmatrix} \sigma_{xx} & \sigma_{xy} & \sigma_{xz} \\ \sigma_{xy} & \sigma_{yy} & \sigma_{yz} \\ \sigma_{xz} & \sigma_{yz} & \sigma_{zz} \end{bmatrix} \cdot \begin{bmatrix} -\varepsilon\lambda_r f'(x) \\ 0 \\ 1 \end{bmatrix} \frac{1}{\sqrt{1 + (\varepsilon\lambda_r f'(x))^2}} .$$

To $O(\varepsilon^2)$, we have

$$\begin{aligned} \bar{\sigma}_s = & \left[- \varepsilon\lambda_r f'(x) \sigma_{xx} + \left(1 - \frac{1}{2} (\varepsilon\lambda_r f'(x))^2\right) \sigma_{xz} \right] \hat{x} \\ & + \left[- \varepsilon\lambda_r f'(x) \sigma_{xy} + \left(1 - \frac{1}{2} (\varepsilon\lambda_r f'(x))^2\right) \sigma_{yz} \right] \hat{y} \\ & + \left[- \varepsilon\lambda_r f'(x) \sigma_{xz} + \left(1 - \frac{1}{2} (\varepsilon\lambda_r f'(x))^2\right) \sigma_{zz} \right] \hat{z}. \end{aligned} \quad (A.2)$$

The stress tensor components σ_{ij}, on the surface of the grating, may be expanded in terms of the stress components $\sigma_{ij}(0)$ on the unperturbed surface at $z = 0$. We write the expansion as

$$\sigma_{ij} = \sigma_{ij}(0) + \varepsilon\lambda_r f(x) \sigma'_{ij}(0) + \frac{1}{2} (\varepsilon\lambda_r f(x))^2 \sigma''_{ij}(0) + \ldots$$

where

$$\sigma'_{ij}(0) \equiv \frac{\partial}{\partial z} \sigma_{ij}\Big|_{z=0}$$

and

$$\sigma''_{ij}(0) \equiv \frac{\partial^2}{\partial z^2} \sigma_{ij}\Big|_{z=0} \qquad \text{etc.}$$

Introducing these expansions into (A.2) we obtain, to $O(\varepsilon^2)$

$$\bar{\sigma}_s = \{\sigma_{xz}(0) + \varepsilon\lambda_r[f(x)\ \sigma'_{xz}(0) - f'(x)\ \sigma_{xx}(0)]$$

$$- (\varepsilon\lambda_r)^2[f(x)\ f'(x)\ \sigma'_{xx}(0) + \frac{1}{2}\ (f'(x))^2\ \sigma_{xz}(0)$$

$$- \frac{1}{2}\ (f(x))^2\ \sigma''_{xz}(0)]\}\ \hat{x}$$

$$+ \{\sigma_{yz}(0) + \varepsilon\lambda_r[f(x)\ \sigma'_{yz}(0) - f'(x)\ \sigma_{xy}(0)]$$

$$- (\varepsilon\lambda_r)^2[f(x)\ f'(x)\ \sigma'_{xy}(0) + \frac{1}{2}\ (f'(x))^2\ \sigma_{yz}(0)$$

$$- \frac{1}{2}\ (f(x))^2\ \sigma''_{yz}(0)]\}\ \hat{y}$$

$$+ \{\sigma_{zz}(0) + \varepsilon\lambda_r[f(x)\ \sigma'_{zz}(0) - f'(x)\ \sigma_{xz}(0)]$$

$$- (\varepsilon\lambda_r)\ [f(x)\ f'(x)\ \sigma'_{xz}(0) + \frac{1}{2}\ (f'(x))^2\ \sigma_{zz}(0)$$

$$- \frac{1}{2} (f(x))^2 \sigma''_{zz}(0)]\} \hat{z} \qquad (A.3)$$

and, to $O(\varepsilon)$

$$\bar{\sigma}_s = \{\sigma_{xz}(0) + \varepsilon\lambda_r[f(x)\ \sigma'_{xz}(0) - f'(x)\ \sigma_{xx}(0)]\}\ \hat{x}$$

$$+ \{\sigma_{yz}(0) + \varepsilon\lambda_r[f(x)\ \sigma'_{yz}(0) - f'(x)\ \sigma_{xy}(0)]\}\ \hat{y}$$

$$+ \{\sigma_{zz}(0) + \varepsilon\lambda_r[f(x)\ \sigma'_{zz}(0) - f'(x)\ \sigma_{xz}(0)]\}\ \hat{z}. \qquad (A.4)$$

A Rayleigh wave satisfies the stree free boundary conditions on the surface $z = 0$. Thus, for a Rayleigh wave

$$\sigma^r_{xz}(0) = \sigma^r_{yz}(0) = \sigma^r_{zz}(0) = 0.$$

For a Rayleigh wave, with no y dependence, the stress on the perturbed surface of the grating is thus, to $O(\varepsilon)$

$$\bar{\sigma}_s{}^r = \varepsilon\lambda_r[f(x)\ \sigma^{r'}_{xz}(0) - f'(x)\ \sigma^r_{xx}(0)]\ \hat{x} + \varepsilon\lambda_r\ f(x)\ \sigma^{r'}_{zz}(0)\ \hat{z}.$$

(A.5)

APPENDIX B

ACOUSTIC WAVE COMPONENTS FOR NORMAL-INCIDENCE ANALYSIS

Rayleigh waves are the acoustic surface wave solutions for a half-space (or infinite substrate) with a free boundary surface. The wave energy is confined closely to the surface of the substrate, with the wave amplitude decaying exponentially into the bulk. Rayleigh waves are hybrid waves. They are a combination of a compressional (or longitudinal) wave with a vertically polarized shear (or transverse) wave. Together the two waves satisfy the stress-free boundary conditions (i.e. $\bar{\bar{\sigma}} \cdot \hat{z}' = 0$) on the free surace of the solid.

We develop here the stress tensor components and displacements of (a) a compressional wave, (b) a shear wave, and (c) a Rayleigh wave, propagating on the free surface boundary of an isotropic, perfectly elastic solid. The solid is taken to occupy the half-space region $z > 0$, with mass density ρ and elastic Lame constants λ and μ. The direction of wave propagation is taken to be along x, at an angular frequency ω. The compressional wave number k_1, and shear wave number k_2 of the solid are given by[58]

$$k_1 = \omega \left(\frac{\rho}{\lambda + 2\mu} \right)^{1/2} \qquad \text{(B.1)}$$

$$k_2 = \omega(\rho/\mu)^{1/2}. \tag{B.2}$$

(a) Compressional Wave

The compressional wave is a longitudinal wave. Its displacement $\bar{u}$ is thus derivable from a scalar potential

$$\bar{u} = \nabla\phi \tag{B.3}$$

where the scalar potential ϕ, obeys the wave equation

$$(\nabla^2 + k_1^2)\phi = 0. \tag{B.4}$$

For a plane wave, with no dependence on the coordinate y, the stress components are given in terms of the scalar potential ϕ, by[59]

$$\begin{aligned}
\sigma_{xx} &= \lambda\left(\frac{\partial^2\phi}{\partial x^2} + \frac{\partial^2\phi}{\partial z^2}\right) + 2\mu\,\frac{\partial^2\phi}{\partial x^2} \\
\sigma_{zz} &= \lambda\left(\frac{\partial^2\phi}{\partial x^2} + \frac{\partial^2\phi}{\partial z^2}\right) + 2\mu\,\frac{\partial^2\phi}{\partial z^2} \\
\sigma_{xz} &= 2\mu\,\frac{\partial^2\phi}{\partial x\partial z}\,.
\end{aligned} \tag{B.5}$$

We are interested in identifying plane wave solutions, propagating in the +x direction, and decaying in the +z direction. We therefore assume a scalar potential of the form

$$\phi = S_1 \, e^{-jkx} \, e^{-rz} \tag{B.6}$$

where a time dependence of $e^{j\omega t}$ is understood. For this potential function to be a solution of the wave equation (B.4) we require

$$k_1^2 = k^2 - r^2. \tag{B.7}$$

For propagating bulk waves the decay constant r must be pure imaginary. This condition requires $|k| < k_1$.

The displacements and stress components of the compressional wave are easily obtained by introducing solution (B.6) into (B.3) and (B.5). We find

$$u_x = - jkS_1 \, e^{-jkx} \, e^{-rz}$$

$$u_z = - rS_1 \, e^{-jkx} \, e^{-rz}$$

and

$$\sigma_{xx} = - \mu(k_2^2 + 2r^2)S_1 \, e^{-jkx} \, e^{-rz} \qquad (B.8)$$

$$\sigma_{zz} = (2k^2 - k_2^2)S_1 \, e^{-jkx} \, e^{-rz}$$

$$\sigma_{xz} = 2\mu jkrS_1 \, e^{-jkx} \, e^{-rz}.$$

(b) Shear Wave

The shear wave is a transverse wave. We therefore require a vector potential to describe its displacement. We define

$$\bar{u} = \nabla \times \bar{\psi} \qquad (B.9)$$

where the potential $\bar{\psi}$, satisfies the wave equation

$$(\nabla^2 + k_2^2)\bar{\psi} = 0. \qquad (B.10)$$

For a plane wave, with no y-dependence, i.e. $\partial/\partial y = 0$, and no displacement along the y axis, only the y-component of the vector potential ψ_y, is non-zero. The stress components are given in terms of this potential by[59]

$$\sigma_{xx} = - 2\mu \frac{\partial^2 \psi_y}{\partial x \partial z}$$

$$\sigma_{zz} = 2\mu \frac{\partial^2 \psi_y}{\partial x \partial z} \tag{B.11}$$

$$\sigma_{xz} = \mu \left(\frac{\partial^2 \psi_y}{\partial x^2} - \frac{\partial^2 \psi_y}{\partial z^2} \right) .$$

We again seek plane wave solutions propagating in the +x direction, and decaying in the +z direction. We thus assume a solution for ψ_y of the form

$$\psi_y = S_2 \, e^{-jkx} \, e^{-qz}. \tag{B.12}$$

This solution is seen to satisfy the wave equation (B.10) ($\psi_x = \psi_z = 0$), with the decay constant q determined by

$$k_2^2 = k^2 - q^2. \tag{B.13}$$

Again q will be pure imaginary for propagating bulk waves. This requires $|k| < k_2$.

The displacements and stress components of the shear wave are obtained by introducing solution (B.12) into (B.9) and (B.11). We find

$$u_x = qS_2 \, e^{-jkx} \, e^{-qz}$$

$$u_z = - jkS_2 \, e^{-jkx} \, e^{-qz}$$

and

$$\sigma_{xx} = - 2\mu jkqS_2 \, e^{-jkx} \, e^{-qz} \tag{B.14}$$

$$\sigma_{zz} = 2\mu jkqS_2 \, e^{-jkx} \, e^{-qz}$$

$$\sigma_{xz} = - \mu(k^2 + q^2)S_2 \, e^{-jkx} \, e^{-qz}.$$

(c) Rayleigh Wave

The Rayleigh wave is a combination of a compressional wave with a vertically polarized shear wave. The particular ratio of the shear/compressional wave amplitudes, and the Rayleigh wave dispersion relation, are obtained by requiring the free boundary at $z = 0$ to be stress free. Using the results of the previous two sections, the displacements and the stress tensor components may then be determined.

The stress free conditions on the boundary, for a Rayleigh wave with no dependence on the y coordinate, require

$$\sigma^r_{zz} = \sigma^r_{xz} = 0 \tag{B.15}$$

at $z = 0$.

The compressional wave amplitude is S_1, and the shear

wave amplitude is S_2. We denote the decay constant of the compressional wave by r_r, and the decay constant of the shear wave by q_r. From (B.7) and (B.13)

$$r_r^2 = k_r^2 - k_1^2 \tag{B.16}$$

$$q_r^2 = k_r^2 - k_2^2 \tag{B.17}$$

where $k_r = 2\pi/\lambda_r$ is the propagation constant of the Rayleigh wave. Introducing the stress components of the compressional and shear waves, from (B.8) and (B.14), into (B.15) gives

$$(k_r^2 + q_r^2)S_1 + 2jk_r q_r S_2 = 0$$

$$2jk_r r_r S_1 - (k_r^2 + q_r^2)S_2 = 0.$$

From these equations we obtain the determinantal equation

$$(k_r^2 + q_r^2)^2 - 4k_r^2 q_r r_r = 0 \tag{B.18}$$

and the ratio of the wave amplitudes to be

$$\frac{S_2}{S_1} = j\,\frac{(k_r^2 + q_r^2)}{2k_r q_r} \equiv \frac{2jk_r r_r}{(k_r^2 + q_r^2)}\,. \tag{B.19}$$

The displacements and stress components of the Rayleigh wave are now obtained from (B.8), (B.14) and (B.19). The results are

$$u_x^r = -jS_1 \left(k_r e^{-r_r z} - \frac{k_r^2 + q_r^2}{2k_r} e^{-q_r z} \right) e^{-jk_r x}$$

$$u_z^r = -S_1 \left(r_r e^{-r_r z} - \frac{k_r^2 + q_r^2}{2q_r} e^{-q_r z} \right) e^{-jk_r x} \qquad \text{(B.20)}$$

and

$$\sigma_{xx}^r = -\mu S_1 [(k_r^2 - q_r^2 + 2r_r^2) e^{-r_r z} - (k_r^2 + q_r^2) e^{-q_r z}] e^{-jk_r x}$$

$$\sigma_{zz}^r = \mu S_1 (k_r^2 + q_r^2)(e^{-r_r z} - e^{-q_r z}) e^{-jk_r x}$$

$$\sigma_{xz}^r = 2\mu j S_1 k_r r_r (e^{-r_r z} - e^{-q_r z}) e^{-jk_r x}.$$

APPENDIX C

RAYLEIGH WAVE POWER FLOW

The complex Poynting vector of an acoustic wave $\bar{P}_a$, is given by[60]

$$\bar{P}_a = - \bar{\bar{\sigma}} \cdot \frac{\partial}{\partial t} \bar{u}.$$

Thus, the time average power flow of a Rayleigh wave, per unit width, is given by

$$P_r = - \frac{1}{2} \int_0^{+\infty} dz \; Re\left\{ \bar{\bar{\sigma}}^r \cdot \frac{\partial}{\partial t} \bar{u}^{r*} \right\}$$

$$= - \frac{1}{2} \int_0^{+\infty} dz \; Re[j\omega(\sigma_{xx}^r \; u_x^{r*} + \sigma_{xz}^r \; u_z^{r*})]. \qquad (C.1)$$

The displacement and stress components for a forward propagating Rayleigh wave are given in (B.20). Substituting in (C.1) we have

$$P_r = - \frac{\mu\omega}{2} |S_1|^2 \int_0^{+\infty} dz \Big\{ [(k_r^2 - q_r^2 + 2r_r^2) e^{-r_r z}$$

$$- (k_r^2 + q_r^2)e^{-q_r z}] \left\{ k_r e^{-r_r z} - \frac{k_r^2 + q_r^2}{2k_r} e^{-q_r z} \right\}$$

$$+ 2k_r r_r (e^{-r_r z} - e^{-q_r z}) \left\{ r_r e^{-r_r z} - \frac{k_r^2 + q_r^2}{2k_r} e^{-q_r z} \right\} \Bigg\} .$$

Evaluating the integral, and making judicious use of the dispersion relation (B.18), we obtain

$$P_r = \frac{\mu\omega}{2} |S_1|^2 \frac{(k_r^2 - q_r^2)^3}{(k_r^2 + q_r^2)^2} \frac{(k_r^6 + 5k_r^2 q_r^4 + 2q_r^6)}{8k_r^3 q_r^3} . \qquad (C.2)$$

If we define the Rayleigh wave power flow to be [61]

$$P_r = 2\omega\mu\, k_2^2 Y_o |S_1|^2 \qquad (C.3)$$

where Y_o is a dimensionless quantity and plays the role of a characteristic admittance, then from (C.2)

$$Y_o = \left(\frac{k_r^2 - q_r^2}{k_r^2 + q_r^2} \right)^2 \frac{(k_r^6 + 5k_r^2 q_r^4 + 2q_r^6)}{32k_r^3 q_r^3} . \qquad (C.4)$$

Using the dispersion relation (B.18) we may also derive the alternate form

$$Y_o = k_2^4 \frac{(k_r^2 r_r - k_r^2 q_r + 2q_r^2 r_r)}{32 k_r^3 q_r^3 r_r} . \qquad (C.5)$$

APPENDIX D

PERTURBED SURFACE-WAVE DISPERSION RELATION

On the free boundary of an infinite isotropic solid the surface-wave solutions are Rayleigh waves. Rayleigh waves are dispersionless with a propagation constant $k_r = \omega/v_r$, where ω is the angular frequency of the wave and v_r is the Rayleigh wave velocity. As shown in Appendix B, the propagation constant k_r satisfies the determinantal equation (B.18)

$$(k_r^2 + q_r^2)^2 - 4k_r^2 q_r r_r = 0 \qquad (D.1)$$

where r_r and q_r are the decay constants of the compressional wave and the shear wave respectively.

By contrast, in a grating, coupling between counter-propagating surface-waves causes dispersion as shown in Fig. 3.1.1. The surface-wave solutions in a grating are no longer Rayleigh waves and do not satisfy the free-surface dispersion relation (D.1). A surface wave of a given frequency experiences a perturbation of its propagation constant within the grating (Fig. 3.1.1). Conversely, a surface wave with a given propagation constant is perturbed in frequency within the grating

(Fig. 3.1.2).

Consider a surface wave propagating in a grating with a propagation constant k_r, and with an angular frequency ω. The frequency differs from that of a Rayleigh wave ω_o, having the same propagation constant, by an amount $\Delta\omega$, where

$$\omega = \omega_o + \Delta\omega \tag{D.2}$$

and $\Delta\omega$ is of $O(\varepsilon)$ (or above). Let the decay constants of the compressional and the shear wave components be r and q respectively. Because the frequency of the wave differs from that of a Rayleigh wave $r \neq r_r$, $q \neq q_r$. However, the decay constants r and q may be Taylor expanded in terms of the frequency perturbation $\Delta\omega$. The expansions take the form

$$r = r_r + \Delta\omega \left.\frac{dr}{d\omega}\right|_{\omega=\omega_o} + \frac{(\Delta\omega)^2}{2} \left.\frac{d^2r}{d\omega^2}\right|_{\omega=\omega_o} + \ldots$$

$$q = q_r + \Delta\omega \left.\frac{dq}{d\omega}\right|_{\omega=\omega_o} + \frac{(\Delta\omega)^2}{2} \left.\frac{d^2q}{d\omega^2}\right|_{\omega=\omega_o} + \ldots$$

Using such expansions and the determinantal equation (D.1) the modified dispersion relation for waves in the grating may

be obtained in the form

$$(k_r^2 + q^2)^2 - 4k_r^2 qr = a_1 \Delta\omega + a_2 (\Delta\omega)^2 + \ldots$$

We now proceed to determine the exact form of this dispersion relation.

From (B.2) and (B.13)

$$k_{2r} = (k_r^2 - q_r^2)^{1/2} = (\rho/\mu)^{1/2} \omega_o$$

thus, from (D.2)

$$k_2 = (k_r^2 - q^2)^{1/2} = (\rho/\mu)^{1/2} (\omega_o + \Delta\omega) = k_{2r}(1 + \Delta\omega/\omega_o).$$

Hence,

$$q^2 = (k_r^2 - k_2^2) = q_r^2 - (k_r^2 - q_r^2)(\Delta\omega/\omega_o)(2 + \Delta\omega/\omega_o) \qquad (D.3)$$

and, to $O((\Delta\omega)^2)$

$$q = q_r - \frac{(k_r^2 - q_r^2)}{q_r} \left(\frac{\Delta\omega}{\omega_o}\right) \left[1 + \frac{1}{2} \left(\frac{k_r^2}{q_r^2}\right) \left(\frac{\Delta\omega}{\omega_o}\right)\right] . \qquad (D.4)$$

Similarly, to $O((\Delta\omega)^2)$

$$r = r_r - \frac{(k_r^2 - r_r^2)}{r_r}\left(\frac{\Delta\omega}{\omega_o}\right)\left[1 + \frac{1}{2}\left(\frac{k_r^2}{r_r}\right)\left(\frac{\Delta\omega}{\omega_o}\right)\right] . \qquad (D.5)$$

From (D.1) and (D.3)-(D.5), the dispersion relation for perturbed surface waves in the grating is determined to be, to $O((\Delta\omega)^2)$

$$(k_r^2 + q^2)^2 - 4k_r^2 qr = \frac{4k_r^2}{q_r r_r}(r_r - q_r)(k_r^2 r_r - k_r^2 q_r + 2q_r^2 r_r)$$

$$(\Delta\omega/\omega_o) + \frac{2k_r^2}{q_r^3 r_r^3}(r_r - q_r)[k_r^4(r_r - q_r)(q_r + r_r)^2$$

$$+ k_r^2 q_r^2 r_r^2 (r_r - q_r) + 10q_r^4 r_r^3](\Delta\omega/\omega_o)^2 . \qquad (D.6)$$

APPENDIX E

FIRST-ORDER BRILLOUIN COMPONENTS AND SECOND-ORDER DETERMINANTAL EQUATIONS IN NORMAL-INCIDENCE GRATING

(a) Brillouin Wave Amplitudes

The amplitudes of the Brillouin components are obtained, to $O(\varepsilon)$, by considering only those terms with the corresponding spatial dependence in (4.2.3) and (4.2.4). As in Section 3.2 the x-independent stress components of each wave $\tilde{\sigma}_{ij}^{\pm(n)}$, $\tilde{\sigma}_{ij}^{\pm(-n)}$ are defined by

$$\sigma_{ij}^{\pm(n)} = \tilde{\sigma}_{ij}^{\pm(n)} \, e^{\mp j(k_r + nk_g)x} \qquad (n = 1 \to \infty)$$

$$\sigma_{ij}^{\pm(-n)} = \tilde{\sigma}_{ij}^{\pm(-n)} \, e^{\mp j(k_r - nk_g)x} \qquad (n = 1 \to \bar{p}).$$

We consider the two sets of Brillouin components, $S_i^{\pm(n)}$ and $S_i^{\pm(-n)}$, separately.

(a.1) Brillouin components $S_i^{\pm(n)}$, with $|k| > k_r$.

These components are all non-radiating. From (4.2.3), to

$O(\varepsilon)$:

cf. $e^{-j(k_r + nk_g)x}$ dep.

$$S_i^{+(n)}\ \tilde{\sigma}_{ixz}^{+(n)}(0) + \frac{\varepsilon\lambda_r}{2}\left[A_n\ S_1^{+}\ \tilde{\sigma}_{xz}^{r'}(0) + A_{n+p}\ S_1^{-}\ \tilde{\sigma}_{xz}^{-r'}(0)\right]$$

$$+ \varepsilon\lambda_r j\ \frac{k_r}{p}\left[nA_n\ S_1^{+}\ \tilde{\sigma}_{xx}^{r}(0) + (n+p)A_{n+p}\ S_1^{-}\ \tilde{\sigma}_{xx}^{-r}(0)\right]$$

$$= 0 \qquad \text{(i)}$$

cf. $e^{+j(k_r + nk_g)x}$ dep.

$$S_i^{-(n)}\ \tilde{\sigma}_{ixz}^{-(n)}(0) + \frac{\varepsilon\lambda_r}{2}\left[A_n\ S_1^{-}\ \tilde{\sigma}_{xz}^{-r'}(0) + A_{n+p}\ S_1^{+}\ \tilde{\sigma}_{xz}^{r'}(0)\right]$$

$$- \varepsilon\lambda_r j\ \frac{k_r}{p}\left[nA_n\ S_1^{-}\ \tilde{\sigma}_{xx}^{-r}(0) + (n+p)A_{n+p}\ S_1^{+}\ \tilde{\sigma}_{xx}^{r}(0)\right]$$

$$= 0 \qquad \text{(ii)}$$

and from (4.2.4), to $O(\varepsilon)$

cf. $e^{-j(k_r + nk_g)x}$ dep.

$$S_i^{+(n)}\ \tilde{\sigma}_{izz}^{+(n)}(0) + \frac{\varepsilon\lambda_r}{2}\left[A_n\ S_1^{+}\ \tilde{\sigma}_{zz}^{r'}(0) + A_{n+p}\ S_1^{-}\ \tilde{\sigma}_{zz}^{-r'}(0)\right] = 0 \qquad \text{(iii)}$$

cf. $e^{+j(k_r + nk_g)x}$ dep.

$$S_i^{-(n)}\ \tilde{\sigma}_{izz}^{-(n)}(0) + \frac{\varepsilon\lambda_r}{2}\left[A_n\ S_1^{-}\ \tilde{\sigma}_{zz}^{-r'}(0) + A_{n+p}\ S_1^{+}\ \tilde{\sigma}_{zz}^{r'}(0)\right] = 0 \qquad \text{(iv)}$$

(E.1)

since $\sigma_{xz}^{\pm r}(0) = 0$.

By reciprocity $\sigma_{ij}^{-r} = \sigma_{ij}^{r*}$, and $\sigma_{ij}^{-(n)} = \sigma_{ij}^{+(n)*}$ for all the compressional and shear wave Brillouin components. Before solving (E.1), for the wave amplitudes, it is expedient to introduce a transformation of variables, of corresponding form to that used for the propagating waves in Section 3.2. In addition to (3.2.7), for the Brillouin components we define,

$$S_i^{(n)^T} = S_i^{+(n)} + S_i^{-(n)*}$$

$$S_i^{(n)D} = S_i^{+(n)} - S_i^{-(n)*}. \tag{E.2}$$

Then, from (E.1) (i)+(ii)*, and (iii)+(iv)* respectively,

$$S_i^{(n)T}\,\tilde{\sigma}_{ixz}^{+(n)}(0) + \frac{\varepsilon\lambda_r}{2}\left[A_n\,S_1^{T}\,\tilde{\sigma}_{xz}^{r'}(0) + A_{n+p}\,S_1^{T*}\,\tilde{\sigma}_{xz}^{r*'}(0)\right]$$

$$+ \varepsilon\lambda_r j\,\frac{k_r}{p}\left[nA_n\,S_1^{T}\,\tilde{\sigma}_{xx}^{r}(0) + (n+p)A_{n+p}\,S_1^{T*}\,\tilde{\sigma}_{xx}^{r*}(0)\right] = 0$$

$$S_i^{(n)T}\,\tilde{\sigma}_{izz}^{+(n)}(0) + \frac{\varepsilon\lambda_r}{2}\left[A_n\,S_1^{T}\,\tilde{\sigma}_{zz}^{r'}(0) + A_{n+p}\,S_1^{T*}\,\tilde{\sigma}_{zz}^{r*'}(0)\right] = 0$$

(E.3)

and from (E.1) (i)-(ii)*, and (iii)-(iv)* respectively,

$$S_i^{(n)D}\,\tilde{\sigma}_{ixz}^{+(n)}(0) + \frac{\varepsilon\lambda_r}{2}\left[A_n\,S_1^{D}\,\tilde{\sigma}_{xz}^{r'}(0) - A_{n+p}\,S_1^{D*}\,\tilde{\sigma}_{xz}^{r*'}(0)\right]$$

$$+ \varepsilon\lambda_r j\,\frac{k_r}{p}\left[nA_n\,S_1^{D}\,\tilde{\sigma}_{xx}^{r}(0) - (n+p)A_{n+p}\,S_1^{D*}\,\tilde{\sigma}_{xx}^{r*}(0)\right] = 0$$

$$S_i^{(n)D}\,\tilde{\sigma}_{izz}^{+(n)}(0) + \frac{\varepsilon\lambda_r}{2}\left[A_n\,S_1^{D}\,\tilde{\sigma}_{zz}^{r'}(0) - A_{n+p}\,S_1^{D*}\,\tilde{\sigma}_{zz}^{r*'}(0)\right] = 0.$$

(E.4)

Equations (E.3) and (E.4) are two independent pairs of equations for the amplitudes $S_1^{(n)T}$, $S_2^{(n)T}$ and $S_1^{(n)D}$, $S_2^{(n)D}$, respectively.

Case 1: $S_i^{+} = S_i^{-*}$

For this case from (3.2.7), $S_1^{D} = 0$. Thus, from equations (E.4)

$$S_i^{(n)D} = 0 \rightarrow S_i^{+(n)} = S_i^{-(n)*} \qquad (n = 1 \rightarrow \infty)$$

to $O(\varepsilon)$. Substituting in (E.3), and evaluating the stress components from (B.8), (B.14), and (B.20) gives (for S_1^{+} real)

$$S_1^{+(n)}\, 2jk_n r_n - S_2^{+(n)}(k_n^2 + q_n^2)$$

$$= \varepsilon\lambda_r j(r_r - q_r)[k_n(r_r + q_r)(A_n + A_{n+p}) - k_r q_r(A_n - A_{n+p})]S_1^{+}$$

$$S_1^{+(n)}(k_n^2 + q_n^2) + S_2^{+(n)}\, 2jk_n q_n = \frac{\varepsilon\lambda_r}{2}(r_r - q_r)(k_r^2 + q_r^2)$$

$$(A_n + A_{n+p})S_1^{+}. \qquad (E.5)$$

Here k_n is the propagation constant of the Brillouin waves

$$k_n = k_r + nk_g = k_r(1 + 2n/p) \tag{E.6}$$

and r_n and q_n are the decay constants of the corresponding compressional and shear wave components. From (B.7) and (B.13)

$$\begin{aligned} r_n &= (k_n^2 - k_1^2)^{1/2} \\ q_n &= (k_n^2 - k_2^2)^{1/2}. \end{aligned} \tag{E.7}$$

The determinant of equations (E.5) is

$$D(k_n) = (k_n^2 + q_n^2)^2 - 4k_n^2 q_n r_n. \tag{E.8}$$

Since k_r satisfies the Rayleigh wave determinantal equation (B.18), $D(k_n) \neq 0$ for $n \neq 0$. Defining

$$\begin{aligned} A_n^+ &= A_n + A_{n+p} \\ A_n^- &= A_n - A_{n+p} \end{aligned} \tag{E.9}$$

from (E.5) the amplitudes of the Brillouin components for this

case are, to $O(\varepsilon)$:

$$\frac{S_1^{+(n)}}{S_1^{+}} = -\varepsilon\lambda_r \frac{(r_r - q_r)}{D(k_n)} \left\{ \left[2k_n^2 q_n (r_r + q_r) - \frac{1}{2}(k_n^2 + q_n^2)(k_r^2 + q_r^2) \right] A_n^{+} - 2k_n q_n k_r q_r A_n^{-} \right\}$$

$$\frac{S_2^{+(n)}}{S_1^{+}} = -\varepsilon\lambda_r j \frac{(r_r - q_r)}{D(k_n)} \left\{ k_n [(k_n^2 + q_n^2)(r_r + q_r) - r_n(k_r^2 + q_r^2)] A_n^{+} - (k_n^2 + q_n^2) k_r q_r A_n^{-} \right\} . \qquad (E.10)$$

Case 2: $S_i^{+} = -S_i^{-*}$

For this case from (3.2.7) $S_1^{T} = 0$. Thus, from equations (E.3)

$$S_i^{(n)T} = 0 \rightarrow S_i^{+(n)} = -S_i^{-(n)*} \qquad (n = 1 \rightarrow \infty)$$

to $O(\varepsilon)$. The wave amplitudes may now be obtained from (E.4). Comparing (E.4) with (E.3) we observe that the equations are of identical form, except for the replacement $A_{n+p} \rightarrow -A_{n+p}$.

Thus, by analogy with (E.10), in this case the amplitudes of the Brillouin components are, to $O(\varepsilon)$:

$$\frac{S_1^{+(n)}}{S_1^{+}} = -\varepsilon\lambda_r \frac{(r_r - q_r)}{D(k_n)} \left\{ \left[2k_n^2 q_n (r_r + q_r) - \frac{1}{2}(k_n^2 + q_n^2)(k_r^2 + q_r^2) \right] A_n^{-} - 2k_n q_n k_r q_r A_n^{+} \right\}$$

$$\frac{S_2^{+(n)}}{S_1^{+}} = -\varepsilon\lambda_r j \frac{(r_r - q_r)}{D(k_n)} \left\{ k_n [(k_n^2 + q_n^2)(r_r + q_r) - r_n(k_r^2 + q_r^2)] A_n^{-} - (k_n^2 + q_n^2) k_r q_r A_n^{+} \right\} \qquad \text{(E.11)}$$

(a.2) Brillouin components $S_i^{\pm(-n)}$, with $|k| < k_r$.

This set of Brillouin waves, in general, is comprised of both non-radiating and radiating components. From (4.2.3), to $O(\varepsilon)$:

cf. $e^{-j(k_r - nk_g)x}$ dep.

$$S_i^{+(-n)} \tilde{\sigma}_{ixz}^{+(-n)}(0) + \frac{\varepsilon\lambda_r}{2} [A_n S_1^{+} \tilde{\sigma}_{xz}^{r'}(0) + A_{p-n} S_1^{-} \tilde{\sigma}_{xz}^{-r'}(0)]$$

$$- \varepsilon\lambda_r j \frac{k_r}{p} [nA_n S_1^{+} \tilde{\sigma}_{xx}^{r}(0) - (p - n)A_{p-n} S_1^{-} \tilde{\sigma}_{xx}^{-r}(0)] = 0$$

(i)

cf. $e^{+j(k_r - nk_g)x}$ dep.

$$S_i^{-(-n)} \tilde{\sigma}_{ixz}^{-(-n)}(0) + \frac{\varepsilon\lambda_r}{2} [A_n S_1^{-} \tilde{\sigma}_{xz}^{-r'}(0) + A_{p-n} S_1^{+} \tilde{\sigma}_{xz}^{r'}(0)]$$

$$+ \varepsilon\lambda_r j \frac{k_r}{p} [nA_n S_1^{-} \tilde{\sigma}_{xx}^{-r}(0) - (p - n)A_{p-n} S_1^{+} \tilde{\sigma}_{xx}^{r}(0)] = 0$$

(ii)

and from (4.2.4), to $O(\varepsilon)$

cf. $e^{-j(k_r - nk_g)x}$ dep.

$$S_i^{+(-n)} \tilde{\sigma}_{izz}^{+(-n)}(0) + \frac{\varepsilon\lambda_r}{2} [A_n S_1^{+} \tilde{\sigma}_{zz}^{r'}(0) + A_{p-n} S_1^{-} \tilde{\sigma}_{zz}^{-r'}(0)] = 0$$

(iii)

cf. $e^{+j(k_r - nk_g)x}$ dep.

$$S_i^{-(-n)}\ \tilde{\sigma}_{izz}^{-(-n)}(0) + \frac{\varepsilon\lambda_r}{2}\left[A_n\ S_1^{-}\ \tilde{\sigma}_{zz}^{-r'}(0) + A_{p-n}\ S_1^{+}\ \tilde{\sigma}_{zz}^{r'}(0)\right] = 0 \qquad \text{(iv)} \qquad \text{(E.12)}$$

since $\sigma_{xz}^{\pm r}(0) = 0$.

As in the previous analysis, by reciprocity, $\sigma_{ij}^{-r} = \sigma_{ij}^{r*}$. However, the radiative components now also propagate in the direction $+z$ (into the bulk), as well as along x. Therefore, for this set of Brillouin waves, $\sigma_{ij}^{-(-n)} = \sigma_{ij}^{+(-n)*}$ only for the non-radiating components. In general, for the radiative components $\sigma_{ij}^{-(-n)}(0) = \pm\ \sigma_{ij}^{+(-n)*}(0)$, and $\sigma_{ij}^{-(-n)'}(0) = \pm\ \sigma_{ij}^{+(-n)'}(0)$, where the correct choice of sign for each component can be determined by reference to Appendix B. These waves, therefore, cannot be separated into two sets of solutions, with $S_i^{+(-n)} = S_i^{-(-n)*}$ and $S_i^{+(-n)} = -\ S_i^{-(-n)*}$, in the same manner as the other grating waves already considered.

We define the propagation constant of the Brillouin waves in the x direction to be k_{-n}, thus

$$k_{-n} = k_r - nk_g = k_r(1 - 2n/p). \qquad \text{(E.13)}$$

As discussed in Section 4.2 all the shear wave components will

be radiative, in any isotropic solid, for $p \leq 15$. The z-dependence of the shear waves is therefore taken to be $e^{-jq_{-n}z}$, where from (B.13)

$$q_{-n} = (k_2^2 - k_{-n}^2)^{1/2}. \tag{E.14}$$

The compressional waves will, in general, comprise both radiating and non-radiating components, depending on the harmonic p, and the material Poisson ratio ν. In most isotropic solids, however, the single compressional Brillouin component for $p = 2, 3$ is radiative. We therefore choose to take the z-dependence of the compressional waves to be $e^{-jr_{-n}z}$, where from (B.7)

$$r_{-n} = (k_1^2 - k_{-n}^2)^{1/2}. \tag{E.15}$$

For non-radiating compressional waves r_{-n} will be pure imaginary. To simplify the form of the solutions, corresponding to (E.9), we define

$$\begin{aligned} A_{-n}^{+} &= A_n + A_{p-n} \\ A_{-n}^{-} &= A_n - A_{p-n}. \end{aligned} \tag{E.16}$$

Case 1: $S_i^+ = S_i^{-*}$

Evaluating the stress components in (E.12), from (B.8), (B.14) and (B.20), we have, for this case, from (i) and (iii) respectively

$$S_1^{+(-n)}\ 2k_{-n}r_{-n} + S_2^{+(-n)}(k_{-n}^2 - q_{-n}^2)$$

$$= -\varepsilon\lambda_r j(r_r - q_r)[k_{-n}(r_r + q_r)A_{-n}^+ - k_r q_r\ A_{-n}^-]S_1^+$$

$$S_1^{+(-n)}(k_{-n}^2 - q_{-n}^2) - S_2^{+(-n)}\ 2k_{-n}q_{-n}$$

$$= \frac{\varepsilon\lambda_r}{2}(r_r - q_r)(k_r^2 + q_r^2)A_{-n}^+\ S_1^+ \qquad \text{(E.17)}$$

and, from (ii) and (iv) respectively

$$S_1^{-(-n)}\ 2k_{-n}r_{-n} - S_2^{-(-n)}(k_{-n}^2 - q_{-n}^2) =$$

$$-\varepsilon\lambda_r j(r_r - q_r)[k_{-n}(r_r + q_r)A_{-n}^+ - k_r q_r\ A_{-n}^-]S_1^+$$

$$S_1^{-(-n)}(k_{-n}^2 - q_{-n}^2) + S_2^{-(-n)}\ 2k_{-n}q_{-n} = \frac{\varepsilon\lambda_r}{2}\ (r_r - q_r)$$

$$(k_r{}^2 + q_r{}^2)A_{-n}^{+}\ S_1{}^{+}. \tag{E.18}$$

The determinant of both pairs of equations is

$$D(k_{-n}) = (k_{-n}^2 - q_{-n}^2)^2 + 4k_{-n}^2 q_{-n} r_{-n}. \tag{E.19}$$

Again, since k_r satisfies the Rayleigh wave determinantal equation (B.18), $D(k_{-n}) \neq 0$ for $n \neq 0$. From (E.17), the amplitudes of the forward propagating (+x) Brillouin waves are, to $O(\varepsilon)$

$$\frac{S_1^{+(-n)}}{S_1{}^{+}} = \varepsilon\lambda_r\ \frac{(r_r - q_r)}{D(k_{-n})}\left\{\left[-2k_{-n}^2 j\ q_{-n}(r_r + q_r)\right.\right.$$

$$\left.\left. + \frac{1}{2}\ (k_{-n}^2 - q_{-n}^2)(k_r{}^2 + q_r{}^2)\right]A_{-n}^{+} + 2k_{-n} j\ q_{-n}k_r q_r A_{-n}^{-}\right\}$$

$$\frac{S_2^{+(-n)}}{S_1{}^{+}} = -\ \varepsilon\lambda_r j\ \frac{(r_r - q_r)}{D(k_{-n})}\left\{k_{-n}[(k_{-n}^2 - q_{-n}^2)(r_r + q_r)\right.$$

$$\left. - jr_{-n}(k_r{}^2 + q_r{}^2)]A_{-n}^{+} - (k_{-n}^2 - q_{-n}^2)k_r q_r\ A_{-n}^{-}\right\} \tag{E.20}$$

From (E.18), we find that for the reverse propagating (-x) Brillouin waves

$$S_1^{-(-n)} = S_1^{+(-n)}$$
$$S_2^{-(-n)} = -S_2^{+(-n)}. \qquad \text{(E.21)}$$

(Relations (E.21) hold for both radiating and non-radiating components.)

Case 2. $S_i^{+} = -S_i^{-*}$

For this case, reference to equations (E.12) shows that the amplitudes of the forward propagating Brillouin waves will be identical to those for Case 1, except for the replacement $A_{p-n} \to -A_{p-n}$. Thus, to $O(\varepsilon)$:

$$\frac{S_1^{+(-n)}}{S_1^{+}} = \varepsilon\lambda_r \frac{(r_r - q_r)}{D(k_{-n})} \left\{ \left[-2k_{-n}^2 jq_{-n}(r_r + q_r) + \frac{1}{2}(k_{-n}^2 - q_{-n}^2) \right.\right.$$
$$\left.\left. (k_r^2 + q_r^2) \right] A_{-n}^{-} + 2k_{-n} jq_{-n} k_r q_r A_{-n}^{+} \right\}$$

$$\frac{S_2^{+(-n)}}{S_1^{+}} = -\varepsilon\lambda_r j \frac{(r_r - q_r)}{D(k_{-n})} \left\{ k_{-n}[(k_{-n}^2 - q_{-n}^2)(r_r + q_r) \right.$$

$$- jr_{-n}(k_r^2 + q_r^2)]A_{-n}^{-} - (k_{-n}^2 - q_{-n}^2)k_r q_r A_{-n}^{+}\Big\} \qquad \text{(E.22)}$$

Also, by analogy with (E.21), in this case, for the reverse propagating Brillouin waves

$$S_1^{-(-n)} = -S_1^{+(-n)}$$
$$\text{(E.23)}$$
$$S_2^{-(-n)} = S_2^{+(-n)}.$$

(Again, relations (E.23) hold for both radiating and non-radiating components.)

This concludes the determination of the amplitudes of all the Brillouin components, in the grating, to $O(\varepsilon)$.

(b) Determinantal Equations

The determinantal equations, at the edges of the stop-bands, are obtained by considering the terms in (4.3.2) and (4.3.3) with the spatial dependence $e^{-jk_r x}$. We use the notation defined in Sections 3.2 and 4.2. For the stop-band at the p-th harmonic (i.e. p × Bragg) we obtain from (3.1.8) and (4.3.2), to $O(\varepsilon^2)$:

cf. $e^{-jk_r x}$ dep.

$$S_i^+ \tilde{\sigma}_{ixz}^+(0) + \varepsilon\lambda_r A_p S_i^- \left[\frac{1}{2}\tilde{\sigma}_{ixz}^{-\prime}(0) + jk_r \tilde{\sigma}_{ixx}^-(0)\right]$$

$$+ \varepsilon\lambda_r \sum_{n=1}^{\infty} \left\{A_n S_i^{+(n)} \left[\frac{1}{2}\tilde{\sigma}_{ixz}^{+(n)\prime}(0) - j\frac{n}{p} k_r \tilde{\sigma}_{ixx}^{+(n)}(0)\right]\right.$$

$$\left. + A_{n+p} S_i^{-(n)} \left[\frac{1}{2}\tilde{\sigma}_{ixz}^{-(n)\prime}(0) + j\frac{(n+p)}{p} k_r \tilde{\sigma}_{ixx}^{-(n)}(0)\right]\right\}$$

$$+ \varepsilon\lambda_r \sum_{n=1}^{\bar{p}} \left\{A_n S_i^{+(-n)} \left[\frac{1}{2}\tilde{\sigma}_{ixz}^{+(-n)}(0) + j\frac{n}{p} k_r \tilde{\sigma}_{ixx}^{+(-n)}(0)\right]\right.$$

$$\left. + \delta(n - p/2) A_{p-n} S_i^{-(-n)} \left[\frac{1}{2}\tilde{\sigma}_{ixz}^{-(-n)\prime}(0) + j\frac{(p-n)}{p} k_r \tilde{\sigma}_{ixx}^{-(-n)}(0)\right]\right\} + \frac{(\varepsilon\lambda_r)^2}{2} \left\{\frac{1}{2}\sum_{n=1}^{\infty} A_n^2 S_1^+ \tilde{\sigma}_{xz}^{r\prime\prime}(0)\right.$$

$$+ j\frac{k_r}{p}\left[\sum_{n=1}^{p-1} nA_n A_{p-n} + \sum_{n=p+1}^{\infty} nA_n A_{n-p} - \sum_{n=1}^{\infty} nA_n A_{n+p}\right]$$

$$S_1^- \tilde{\sigma}_{xx}^{-r\prime}(0) + \frac{1}{4}\left[\sum_{n=1}^{p-1} A_n A_{p-n} + \sum_{n=p+1}^{\infty} A_n A_{n-p}\right.$$

$$\left.\left. + \sum_{n=1}^{\infty} A_n A_{n+p}\right] S_1^- \tilde{\sigma}_{xz}^{-r\prime\prime}(0)\right\} = 0$$

and from (4.3.3), to $O(\varepsilon^2)$:

cf. $e^{-jk_r x}$ dep.

$$S_i^{+}\,\tilde{\sigma}_{izz}^{+}(0) + \varepsilon\lambda_r A_p S_i^{-}\left[\frac{1}{2}\tilde{\sigma}_{izz}^{-'}(0) + jk_r\,\tilde{\sigma}_{ixz}^{-}(0)\right]$$

$$+ \varepsilon\lambda_r \sum_{n=1}^{\infty}\left\{A_n S_i^{+(n)}\left[\frac{1}{2}\tilde{\sigma}_{izz}^{+(n)'}(0) - j\frac{n}{p}k_r\,\tilde{\sigma}_{ixz}^{+(n)}(0)\right]\right.$$

$$\left. + A_{n+p} S_i^{-(n)}\left[\frac{1}{2}\tilde{\sigma}_{izz}^{-(n)'}(0) + j\frac{(n+p)}{p}k_r\,\tilde{\sigma}_{ixz}^{-(n)}(0)\right]\right\}$$

$$+ \varepsilon\lambda_r \sum_{n=1}^{\bar{p}}\left\{A_n S_i^{+(-n)}\left[\frac{1}{2}\tilde{\sigma}_{izz}^{+(-n)'}(0) + j\frac{n}{p}k_r\,\tilde{\sigma}_{ixz}^{+(-n)}(0)\right]\right.$$

$$+ \delta(n - p/2)A_{p-n} S_i^{-(-n)}\left[\frac{1}{2}\tilde{\sigma}_{izz}^{-(-n)'}(0) + j\frac{(p-n)}{p}k_r\right.$$

$$\left.\left.\tilde{\sigma}_{ixz}^{-(-n)}(0)\right]\right\} + \frac{(\varepsilon\lambda_r)^2}{2}\left\{\frac{1}{2}\sum_{n=1}^{\infty} A_n^2 S_1^{+}\,\tilde{\sigma}_{zz}^{r''}(0)\right.$$

$$+ j\frac{k_r}{p}\left[\sum_{n=1}^{p-1} nA_nA_{p-n} + \sum_{n=p+1}^{\infty} nA_nA_{n-p} - \sum_{n=1}^{\infty} nA_nA_{n+p}\right]$$

$$\left. S_1^{-}\,\tilde{\sigma}_{xz}^{-r'}(0) + \frac{1}{4}\left[\sum_{n=1}^{p-1} A_nA_{p-n} + \sum_{n=p+1}^{\infty} A_nA_{n-p}\right.\right.$$

$$+ \sum_{n=1}^{\infty} A_n A_{n+p} \Big] S_1^- \tilde{\sigma}_{zz}^{-r''}(0) \Big\} = 0 \qquad \text{(E.24)}$$

where $\bar{p}$ is defined in (4.2.5), and

$$\delta(n - p/2) = \begin{cases} 0, & \text{for } n = p/2 \\ 1, & \text{otherwise.} \end{cases} \qquad \text{(E.25)}$$

By reciprocity, as before, $\tilde{\sigma}_{ij}^{-r} = \tilde{\sigma}_{ij}^{r*}$ and $\tilde{\sigma}_{ij}^{-(n)} = \tilde{\sigma}_{ij}^{+(n)*}$, since these stress components in the grating are all non-radiating. We now derive the determinantal equations at the upper and lower edges of the stop-band, ω_+ and ω_- respectively, from (E.24), to $O(\varepsilon^2)$.

Case 1. ω_-

At ω_-, from the first-order analysis in Sections 3.2 and 4.2, we have

$$S_i^+ = S_i^{-*}$$

and

$$S_i^{+(n)} = S_i^{-(n)*} \qquad (n = 1 \to \infty)$$

to $O(\varepsilon)$. Substituting in equations (E,24), we have, for this

case, to $O(\varepsilon^2)$:

$$S_i^+ \tilde{\sigma}_{ixz}^+(0) + \varepsilon\lambda_r A_p S_i^{+*}\left[\frac{1}{2}\tilde{\sigma}_{ixz}^{+*'}(0) + jk_r \tilde{\sigma}_{ixx}^{+*}(0)\right]$$

$$+ \varepsilon\lambda_r \sum_{n=1}^{\infty}\left\{A_n S_i^{+(n)}\left[\frac{1}{2}\tilde{\sigma}_{ixz}^{+(n)'}(0) - j\frac{n}{p}k_r \tilde{\sigma}_{ixx}^{+(n)}(0)\right]\right.$$

$$\left. + A_{n+p} S_i^{+(n)*}\left[\frac{1}{2}\tilde{\sigma}_{ixz}^{+(n)*'}(0) + j\frac{(n+p)}{p}k_r \tilde{\sigma}_{ixx}^{+(n)*}(0)\right]\right\}$$

$$+ \varepsilon\lambda_r \sum_{n=1}^{\bar{p}}\left\{A_n S_i^{+(-n)}\left[\frac{1}{2}\tilde{\sigma}_{ixz}^{+(-n)'}(0) + j\frac{n}{p}k_r \tilde{\sigma}_{ixx}^{+(-n)}(0)\right]\right.$$

$$\left. + \delta(n - p/2)A_{p-n} S_i^{-(-n)}\left[\frac{1}{2}\tilde{\sigma}_{ixz}^{-(-n)'}(0) + j\frac{(p-n)}{p}k_r \tilde{\sigma}_{ixx}^{-(-n)}(0)\right]\right\} + \frac{(\varepsilon\lambda_r)^2}{2}\left\{\frac{1}{2}\sum_{n=1}^{\infty} A_n^2 S_1^+ \tilde{\sigma}_{xz}^{r''}(0)\right.$$

$$+ jk_r\left[\sum_{n=1}^{p-1}(n/p)A_n A_{p-n} + \sum_{n=1}^{\infty} A_n A_{n+p}\right] S_1^+ \tilde{\sigma}_{xx}^{r*'}(0)$$

$$\left. + \frac{1}{4}\left[\sum_{n=1}^{p-1} A_n A_{p-n} + 2\sum_{n=1}^{\infty} A_n A_{n+p}\right] S_1^+ \tilde{\sigma}_{xz}^{r*''}(0)\right\} = 0$$

$$S_i^+ \tilde{\sigma}_{izz}^+(0) + \varepsilon\lambda_r A_p S_i^{+*}\left[\frac{1}{2}\tilde{\sigma}_{izz}^{+*'}(0) + jk_r \tilde{\sigma}_{ixz}^{+*}(0)\right]$$

$$+ \varepsilon\lambda_r \sum_{n=1}^{\infty} \left\{ A_n \, S_i^{+(n)} \left[\frac{1}{2} \tilde{\sigma}_{izz}^{+(n)\prime}(0) - j \frac{n}{p} k_r \tilde{\sigma}_{ixz}^{+(n)}(0) \right] \right.$$

$$\left. + A_{n+p} \, S_i^{+(n)*} \left[\frac{1}{2} \tilde{\sigma}_{izz}^{+(n)*\prime}(0) + j \frac{(n+p)}{p} k_r \tilde{\sigma}_{ixz}^{+(n)*}(0) \right] \right\}$$

$$+ \varepsilon\lambda_r \sum_{n=1}^{\bar{p}} \left\{ A_n \, S_i^{+(-n)} \left[\frac{1}{2} \tilde{\sigma}_{izz}^{+(-n)\prime}(0) + j \frac{n}{p} k_r \tilde{\sigma}_{ixz}^{+(-n)}(0) \right] \right.$$

$$\left. + \delta(n - p/2) A_{p-n} \, S_i^{-(-n)} \left[\frac{1}{2} \tilde{\sigma}_{izz}^{-(-n)\prime}(0) + j \frac{(p-n)}{p} k_r \right. \right.$$

$$\left. \left. \tilde{\sigma}_{ixz}^{-(-n)}(0) \right] \right\} + \frac{(\varepsilon\lambda_r)^2}{2} \left\{ \frac{1}{2} \sum_{n=1}^{\infty} A_n^2 \, S_1^+ \tilde{\sigma}_{zz}^{r\prime\prime}(0) \right.$$

$$+ jk_r \left[\sum_{n=1}^{p-1} (n/p) A_n A_{p-n} + \sum_{n=1}^{\infty} A_n A_{n+p} \right] S_1^+ \tilde{\sigma}_{xz}^{r*\prime}(0)$$

$$\left. + \frac{1}{4} \left[\sum_{n=1}^{p-1} A_n A_{p-n} + 2 \sum_{n=1}^{\infty} A_n A_{n+p} \right] S_1^+ \tilde{\sigma}_{zz}^{r*\prime\prime}(0) \right\} = 0 \quad \text{(E.26)}$$

where the amplitudes of the reverse propagating Brillouin components, with $|k| < k_r$, are related to the forward propagating components by (E.21)

In Section 4.2, the amplitudes of all the forward propagating waves were determined in terms of the forward compressional wave amplitude S_1^+, to $O(\varepsilon)$. Equations (E.26) may therefore

be written, to $O(\varepsilon^2)$, as a pair of simultaneous equations for the wave amplitudes S_1^+ and S_2^+. Using (4.2.1), and evaluating the stress components of the zeroth-order waves from (B.8), (B.14) and (B.20), we obtain

$$\left\{2\mu jk_r r - \varepsilon\lambda_r \mu jk_r A_p(r-q)(2q+r) + \frac{(\varepsilon\lambda_r)^2}{2}\mu jk_r(r_r - q_r)\right.$$

$$\left[r_r(r_r+q_r)\left(\sum_{n=1}^{\infty} A_n^2 - \frac{1}{2}\sum_{n=1}^{p-1} A_n A_{p-n}\right) - (k_r^2 - q_r r_r\right.$$

$$\left. - q_r^2)A_p^2 + (k_r^2 + q_r^2 + r_r^2 + q_r r_r)\sum_{n=1}^{\infty} A_n A_{n+p}\right.$$

$$\left. + (k_r^2 + q_r^2 + 2r_r^2 + 2q_r r_r)\sum_{n=1}^{p-1}(n/p)A_n A_{p-n}\right]$$

$$\left. + (\varepsilon\lambda_r)^2\mu\, T_1\right\} S_1^+ - \mu(k_r^2 + q^2)S_2^+ = 0$$

$$\left\{\mu(k_r^2+q^2) - \varepsilon\lambda_r\mu(A_p/2)(r-q)(k_r^2+q^2) + \frac{(\varepsilon\lambda_r)^2}{4}\mu(r_r - q_r)\right.$$

$$\left[(k_r^2+q_r^2)(r_r+q_r)\left(\sum_{n=1}^{\infty} A_n^2 + \frac{1}{2}\sum_{n=1}^{p-1} A_n A_{p-n}\right)\right.$$

$$\left. + (7k_r^2 q_r + 4k_r^2 r_r - q_r^3)A_p^2\right.$$

$$- (3k_r^2 r_r - k_r^2 q_r - q_r^2 r_r - q_r^3) \sum_{n=1}^{\infty} A_n A_{n+p}$$

$$- 4k_r^2 r_r \sum_{n=1}^{p-1} (n/p) A_n A_{p-n} \Bigg] + (\varepsilon\lambda_r)^2 \mu \, T_2 \Bigg\} S_1^+$$

$$+ 2\mu j k_r q \, S_2^+ = 0 \qquad \text{(E.27)}$$

where

$$T_1 = \sum_{n=1}^{\infty} \left\{ A_n \, \bar{S}_i^{+(n)} \left[\frac{1}{2} \tilde{\sigma}_{ixz}^{+(n)\prime}(0) - j \frac{n}{p} k_r \tilde{\sigma}_{ixx}^{+(n)}(0) \right] \right.$$

$$\left. + A_{n+p} \, \bar{S}_i^{+(n)*} \left[\frac{1}{2} \tilde{\sigma}_{ixz}^{+(n)*\prime}(0) + j \frac{(n+p)}{p} k_r \tilde{\sigma}_{ixx}^{+(n)*}(0) \right] \right\}$$

$$+ \sum_{n=1}^{\bar{p}} \left\{ A_n \, \bar{S}_i^{+(-n)} \left[\frac{1}{2} \tilde{\sigma}_{ixz}^{+(-n)\prime}(0) + j \frac{n}{p} k_r \tilde{\sigma}_{ixx}^{+(-n)}(0) \right] \right.$$

$$+ \delta(n - p/2) A_{p-n} \, \bar{S}_i^{-(-n)} \left[\frac{1}{2} \tilde{\sigma}_{ixz}^{-(-n)\prime}(0) + j \frac{(p-n)}{p} k_r \right.$$

$$\left. \left. \tilde{\sigma}_{ixx}^{-(-n)}(0) \right] \right\}$$

$$T_2 = \sum_{n=1}^{\infty} \left\{ A_n \, \bar{S}_i^{+(n)} \left[\frac{1}{2} \tilde{\sigma}_{izz}^{+(n)\prime}(0) - j \frac{n}{p} k_r \tilde{\sigma}_{ixz}^{+(n)}(0) \right] \right.$$

$$+ A_{n+p}\ \bar{S}_i^{+(n)*}\left[\frac{1}{2}\ \tilde{\sigma}_{izz}^{+(n)*'}(0) + j\ \frac{(n+p)}{p}\ k_r\ \tilde{\sigma}_{ixz}^{+(n)*}(0)\right]\Bigg\}$$

$$+ \sum_{n=1}^{\bar{p}}\Bigg\{A_n\ \bar{S}_i^{+(-n)}\left[\frac{1}{2}\ \tilde{\sigma}_{izz}^{+(-n)'}(0) + j\ \frac{n}{p}\ k_r\ \tilde{\sigma}_{ixz}^{+(-n)}(0)\right]$$

$$+ \delta(n - p/2)A_{p-n}\ \bar{S}_i^{-(-n)}\left[\frac{1}{2}\ \tilde{\sigma}_{izz}^{-(-n)'}(0) + j\ \frac{(p-n)}{p}\ k_r\right.$$

$$\left.\tilde{\sigma}_{ixz}^{-(-n)}(0)\right]\Bigg\} \qquad \text{(E.28)}$$

and the normalized amplitudes of the Brillouin waves $\bar{S}_i^{+(n)}$, $\bar{S}_i^{\pm(-n)}$ are defined by

$$S_i^{+(n)} = \varepsilon\lambda_r\mu\ S_1^{+}\ \bar{S}_i^{+(n)}$$

$$\bar{S}_i^{\pm(-n)} = \varepsilon\lambda_r\mu\ S_1^{+}\ \bar{S}_i^{\pm(-n)}. \qquad \text{(E.29)}$$

The Brillouin wave amplitudes $S_i^{+(n)}$, $S_i^{\pm(-n)}$ are given, for this case, by (E.10) and (E.20), (E.21) respectively.

For non-trivial solutions, for S_1^{+} and S_2^{+}, the determinant of equations (E.27) must be zero. This requirement gives, to $O(\varepsilon^2)$:

$$(k_r^2 + q^2)^2 - 4k_r^2 qr = -\varepsilon\lambda_r\, 4k_r^2 q^2 (r - q) A_p$$

$$- (\varepsilon\lambda_r)^2 k_r^2 (r_r - q_r) \Big\{ (3k_r^2 q_r + k_r^2 r_r + q_r^2 r_r - q_r^3) A_p^2$$

$$- (k_r^2 + q_r^2)(r_r + q_r) \sum_{n=1}^{\infty} A_n A_{n+p} + \sum_{n=1}^{p-1} A_n A_{p-n}$$

$$\Big[q_r r_r (r_r + q_r) - (n/p)(k_r^2 r_r + k_r^2 q_r + 2q_r r_r^2$$

$$+ 3q_r^2 r_r + q_r^3) \Big] \Big\} - (\varepsilon\lambda_r)^2 [2jk_r q_r T_1 + (k_r^2 + q_r^2) T_2]$$

(E.30)

where the first-order determinantal equation (3.2.11) has been utilized to simplify the relation. This is the required determinantal equation, to $O(\varepsilon^2)$, at the lower edge of the stop-band ω_-.

Case 2. ω_+

At ω_+, from the first-order analysis, we have

$$S_i^+ = -S_i^{-*}$$

and

$$S_i^{+(n)} = -S_i^{-(n)*} \qquad (n = 1 \to \infty)$$

to $O(\varepsilon)$. Substituting in equations (E.24), we have, for this case, to $O(\varepsilon^2)$:

$$S_i^{+}\,\tilde{\sigma}_{ixz}^{+}(0) - \varepsilon\lambda_r A_p S_i^{+*}\left[\frac{1}{2}\,\tilde{\sigma}_{ixz}^{+*'}(0) + jk_r\,\tilde{\sigma}_{ixx}^{+*}(0)\right]$$

$$+ \varepsilon\lambda_r \sum_{n=1}^{\infty}\left\{A_n S_i^{+(n)}\left[\frac{1}{2}\,\tilde{\sigma}_{ixz}^{+(n)'}(0) - j\,\frac{n}{p}\,k_r\,\tilde{\sigma}_{ixx}^{+(n)}(0)\right]\right.$$

$$\left. - A_{n+p} S_i^{+(n)*}\left[\frac{1}{2}\,\tilde{\sigma}_{ixz}^{+(n)*'}(0) + j\,\frac{(n+p)}{p}\,k_r\,\tilde{\sigma}_{ixx}^{+(n)*}(0)\right]\right\}$$

$$+ \varepsilon\lambda_r \sum_{n=1}^{\bar{p}}\left\{A_n S_i^{+(-n)}\left[\frac{1}{2}\,\tilde{\sigma}_{ixz}^{+(-n)'}(0) + j\,\frac{n}{p}\,k_r\,\tilde{\sigma}_{ixx}^{+(-n)}(0)\right]\right.$$

$$\left. + \delta(n - p/2)A_{p-n} S_i^{-(-n)}\left[\frac{1}{2}\,\tilde{\sigma}_{ixz}^{-(-n)'}(0) + j\,\frac{(p-n)}{p}\,k_r\right.\right.$$

$$\left.\left.\tilde{\sigma}_{ixx}^{-(-n)}(0)\right]\right\} + \frac{(\varepsilon\lambda_r)^2}{2}\left\{\frac{1}{2}\sum_{n=1}^{\infty} A_n^2\, S_1^{+}\,\tilde{\sigma}_{xz}^{r''}(0)\right.$$

$$\left. - j\,\frac{k_r}{p}\left[\sum_{n=1}^{p-1} nA_nA_{p-n} + \sum_{n=p+1}^{\infty} nA_nA_{n-p} - \sum_{n=1}^{\infty} nA_nA_{n+p}\right]\right.$$

$$S_1^+ \tilde{\sigma}_{xx}^{r*'}(0) - \frac{1}{4}\left[\sum_{n=1}^{p-1} A_n A_{p-n} + \sum_{n=p+1}^{\infty} A_n A_{n-p} + \sum_{n=1}^{\infty} A_n A_{n+p}\right] S_1^+ \tilde{\sigma}_{xz}^{r*''}(0)\Bigg\} = 0$$

$$S_i^+ \tilde{\sigma}_{izz}^+(0) - \varepsilon\lambda_r A_p S_i^{+*}\left[\frac{1}{2}\tilde{\sigma}_{izz}^{+*'}(0) + jk_r \tilde{\sigma}_{ixz}^{+*}(0)\right]$$

$$+ \varepsilon\lambda_r \sum_{n=1}^{\infty}\left\{A_n S_i^{+(n)}\left[\frac{1}{2}\tilde{\sigma}_{izz}^{+(n)'}(0) - j\frac{n}{p}k_r \tilde{\sigma}_{ixz}^{+(n)}(0)\right]\right.$$

$$\left. - A_{n+p} S_i^{+(n)*}\left[\frac{1}{2}\tilde{\sigma}_{izz}^{+(n)*'}(0) + j\frac{(n+p)}{p}k_r \tilde{\sigma}_{ixz}^{+(n)*}(0)\right]\right\}$$

$$+ \varepsilon\lambda_r \sum_{n=1}^{\bar{p}}\left\{A_n S_i^{+(-n)}\left[\frac{1}{2}\tilde{\sigma}_{izz}^{+(-n)'}(0) + j\frac{n}{p}k_r \tilde{\sigma}_{ixz}^{+(-n)}(0)\right]\right.$$

$$\left. + \delta(n - p/2)A_{p-n} S_i^{-(-n)}\left[\frac{1}{2}\tilde{\sigma}_{izz}^{-(-n)'}(0) + j\frac{(p-n)}{p}k_r \tilde{\sigma}_{ixz}^{-(-n)}(0)\right]\right\} + \frac{(\varepsilon\lambda_r)^2}{2}\left\{\frac{1}{2}\sum_{n=1}^{\infty} A_n^2 S_1^+ \tilde{\sigma}_{zz}^{r''}(0)\right.$$

$$\left. - j\frac{k_r}{p}\left[\sum_{n=1}^{p-1} nA_n A_{p-n} + \sum_{n=p+1}^{\infty} nA_n A_{n-p} - \sum_{n=1}^{\infty} nA_n A_{n+p}\right]\right.$$

$$S_1^+ \tilde{\sigma}_{xz}^{r*'}(0) - \frac{1}{4}\left[\sum_{n=1}^{p-1} A_n A_{p-n} + \sum_{n=p+1}^{\infty} A_n A_{n-p} + \sum_{n=1}^{\infty} A_n A_{n+p}\right]$$

$$S_1^+ \tilde{\sigma}_{zz}^{r*''}(0)\Big\} = 0 \qquad \text{(E.31)}$$

where the amplitudes of the reverse propagating Brillouin components, with $|k| < k_r$, are related to the forward propagating components by (E.23).

As in the previous case, equations (E.31) may be written, to $O(\varepsilon^2)$, as a pair of simultaneous equations for the wave amplitudes S_1^+ and S_2^+. Using (4.2.2), and evaluating the stress components of the zeroth-order waves from (B.8), (B.14) and (B.20), we obtain

$$\Bigg\{2\mu jk_r r + \varepsilon\lambda_r \mu jk_r A_p(r-q)(2q+r) + \frac{(\varepsilon\lambda_r)^2}{2}\mu jk_r(r_r - q_r)$$

$$\Bigg[r_r(r_r+q_r)\left(\sum_{n=1}^{\infty} A_n^2 + \frac{1}{2}\sum_{n=1}^{p-1} A_n A_{p-n}\right)$$

$$-(k_r^2 - q_r r_r - q_r^2)A_p^2 - (k_r^2 + q_r^2 + r_r^2 + q_r r_r)$$

$$\sum_{n=1}^{\infty} A_n A_{n+p} - (k_r^2 + q_r^2 + 2r_r^2 + 2q_r r_r)\sum_{n=1}^{p-1}(n/p)A_n A_{p-n}\Bigg]$$

$$+ (\varepsilon\lambda_r)^2\mu\, T_3\Bigg\} S_1^+ - \mu(k_r^2 + q^2)S_2^+ = 0$$

$$\left\{\mu(k_r^2 + q^2) + \varepsilon\lambda_r\mu(A_p/2)(r - q)(k_r^2 + q^2) + \frac{(\varepsilon\lambda_r)^2}{4}\mu(r_r - q_r)\right.$$

$$\left[(k_r^2 + q_r^2)(r_r + q_r)\left(\sum_{n=1}^{\infty} A_n^2 - \frac{1}{2}\sum_{n=1}^{p-1} A_n A_{p-n}\right)\right.$$

$$+ (7k_r^2 q_r + 4k_r^2 r_r - q_r^3)A_p^2$$

$$+ (3k_r^2 r_r - k_r^2 q_r - q_r^2 r_r - q_r^3)\sum_{n=1}^{\infty} A_n A_{n+p}$$

$$\left.+ 4k_r^2 r_r \sum_{n=1}^{p-1}(n/p)A_n A_{p-n}\right] + (\varepsilon\lambda_r)^2\mu\, T_4\Bigg\}\, S_1^+$$

$$+ 2\mu j k_r q\, S_2^+ = 0 \qquad \text{(E.32)}$$

where

$$T_3 = \sum_{n=1}^{\infty}\left\{A_n\, \bar{S}_i^{+(n)}\left[\frac{1}{2}\tilde{\sigma}_{ixz}^{+(n)\prime}(0) - j\frac{n}{p}k_r\,\tilde{\sigma}_{ixx}^{+(n)}(0)\right]\right.$$

$$\left. - A_{n+p}\,\bar{S}_i^{+(n)*}\left[\frac{1}{2}\tilde{\sigma}_{ixz}^{+(n)*\prime}(0) + j\frac{(n+p)}{p}k_r\,\tilde{\sigma}_{ixx}^{+(n)*}(0)\right]\right\}$$

$$+ \sum_{n=1}^{\bar{p}}\left\{A_n\,\bar{S}_i^{+(-n)}\left[\frac{1}{2}\tilde{\sigma}_{ixz}^{+(-n)\prime}(0) + j\frac{n}{p}k_r\,\tilde{\sigma}_{ixx}^{+(-n)}(0)\right]\right.$$

$$+ \delta(n - p/2) A_{p-n} \bar{S}_i^{-(-n)} \left[\frac{1}{2} \tilde{\sigma}_{ixz}^{-(-n)'}(0) \right.$$

$$\left. + j \frac{(p - n)}{p} k_r \tilde{\sigma}_{ixx}^{-(-n)}(0) \right] \Bigg\}$$

$$T_4 = \sum_{n=1}^{\infty} \left\{ A_n \bar{S}_i^{+(n)} \left[\frac{1}{2} \tilde{\sigma}_{izz}^{+(n)'}(0) - j \frac{n}{p} k_r \tilde{\sigma}_{ixz}^{+(n)}(0) \right] \right.$$

$$\left. - A_{n+p} \bar{S}_i^{+(n)*} \left[\frac{1}{2} \tilde{\sigma}_{izz}^{+(n)*'}(0) + j \frac{(n + p)}{p} k_r \tilde{\sigma}_{ixz}^{+(n)*}(0) \right] \right\}$$

$$+ \sum_{n=1}^{\bar{p}} \left\{ A_n \bar{S}_i^{+(-n)} \left[\frac{1}{2} \tilde{\sigma}_{izz}^{+(-n)'}(0) + j \frac{n}{p} k_r \tilde{\sigma}_{ixz}^{+(-n)}(0) \right] \right.$$

$$+ \delta(n - p/2) A_{p-n} \bar{S}_i^{-(-n)} \left[\frac{1}{2} \tilde{\sigma}_{izz}^{-(-n)'}(0) \right.$$

$$\left. \left. + j \frac{(p - n)}{p} k_r \tilde{\sigma}_{ixz}^{-(-n)}(0) \right] \right\} . \qquad \text{(E.33)}$$

The normalized Brillouin wave amplitudes $\bar{S}_i^{+(n)}$, $\bar{S}_i^{\pm(-n)}$ are defined, as before, by (E.29). For this case, the Brillouin wave amplitudes $S_i^{+(n)}$, $S_i^{\pm(-n)}$ are given by (E.11) and (E.22), (E.23) respectively.

For non-trivial solutions, for S_1^+ and S_2^+, we require the determinant of equations (E.32) to be zero. This gives to

$O(\varepsilon^2)$:

$$(k_r^2 + q^2)^2 - 4k_r^2 qr = \varepsilon\lambda_r\, 4k_r^2 q^2 (r - q) A_p$$

$$- (\varepsilon\lambda_r)^2 k_r^2 (r_r - q_r) \Big\{ (3k_r^2 q_r + k_r^2 r_r + q_r^2 r_r - q_r^3) A_p^2$$

$$+ (k_r^2 + q_r^2)(r_r + q_r) \sum_{n=1}^{\infty} A_n A_{n+p}$$

$$- \sum_{n=1}^{p-1} A_n A_{p-n} [q_r r_r (r_r + q_r) - (n/p)(k_r^2 r_r + k_r^2 q_r$$

$$+ 2q_r r_r^2 + 3q_r^2 r_r + q_r^3)] \Big\} - (\varepsilon\lambda_r)^2 [2jk_r q_r\, T_3$$

$$+ (k_r^2 + q_r^2) T_4] \qquad \text{(E.34)}$$

where we have made use of the first-order determinantial equation (3.2.12). This is the determinantal equation, to $O(\varepsilon^2)$, at the upper edge of the stop-band ω_+.

APPENDIX F

ACOUSTIC-WAVE COMPONENTS FOR OBLIQUE-INCIDENCE ANALYSIS

In this Appendix, the propagation of acoustic plane-waves on the free-surface boundary of an isotropic solid is considered, when the direction of propagation is not along one of the co-ordinate axes. The solid is taken to occupy the infinite half space $z > 0$ and to have mass density ρ and Lame constants λ and μ. The surface coordinates are thus x and y. We assume that the direction of propagation of the waves makes an angle θ with the $+x$ axis [Fig. F.1].

Four types of acoustic waves are considered. They are (a) a compressional wave, (b) a vertically-polarized shear wave, (c) a horizontally-polarized shear wave, and (d) a Rayleigh wave. The compressional wave and the shear waves are all bulk wave components, which alone do not satisfy the stress-free boundary conditions. The Rayleigh wave is a hybrid wave which satisfies the boundary conditions on the free surface. It is a combination of a compressional wave with a vertically-polarized shear wave. In general, in an oblique-incidence grating, there are propagating waves of all four types considered above. The stress tensor components and displacements of each type of wave are determined in the following sections.

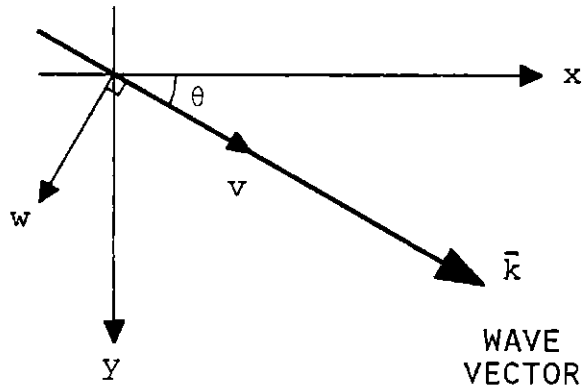

FIG. F.1 COORDINATES FOR PROPAGATION AT OBLIQUE INCIDENCE.

(a) Compressional Wave.

As in Appendix B, the displacement $\bar{u}$ may be determined from a scalar potential ϕ [(B.3) and (B.4)]. In terms of the scalar potential, the stress components are given by[62]

$$\sigma_{xx} = \lambda\left(\frac{\partial^2\phi}{\partial x^2} + \frac{\partial^2\phi}{\partial y^2} + \frac{\partial^2\phi}{\partial z^2}\right) + 2\mu\,\frac{\partial^2\phi}{\partial x^2}$$

$$\sigma_{yy} = \lambda\left(\frac{\partial^2\phi}{\partial x^2} + \frac{\partial^2\phi}{\partial y^2} + \frac{\partial^2\phi}{\partial z^2}\right) + 2\mu\,\frac{\partial^2\phi}{\partial y^2}$$

$$\sigma_{zz} = \lambda\left(\frac{\partial^2\phi}{\partial x^2} + \frac{\partial^2\phi}{\partial y^2} + \frac{\partial^2\phi}{\partial z^2}\right) + 2\mu\,\frac{\partial^2\phi}{\partial z^2}$$

$$\sigma_{yz} = 2\mu\,\frac{\partial^2\phi}{\partial y\partial z}$$

$$\sigma_{xz} = 2\mu\,\frac{\partial^2\phi}{\partial x\partial z}$$

$$\sigma_{xy} = 2\mu\,\frac{\partial^2\phi}{\partial x\partial y}\,. \qquad \text{(F.1)}$$

We seek plane wave solutions, propagating in the direction $+v$ [Fig. F.1], and decaying in z. The scalar potential is

therefore taken as

$$\phi = S_1 \, e^{-j\bar{k} \cdot \bar{v}} \, e^{-rz} \qquad \text{(F.2)}$$

(ignoring the time dependence $e^{j\omega t}$). For (F.2) to satisfy the wave equation (B.4) we require

$$k_1^2 = k^2 - r^2 \qquad \text{(F.3)}$$

where k_1 is the compressional wave number (B.1). Transforming (F.2) into $x - y$ coordinates gives

$$\phi = S_1 \, e^{-jk(x \cos \theta + y \sin \theta)} \, e^{-rz}. \qquad \text{(F.4)}$$

This is the appropriate scalar potential for a compressional wave, propagating at an angle θ with the $+x$ axis.

The displacements and stress components of a compressional wave are determined from (B.3) and (F.1) respectively, using the scalar potential (F.4). They are

$$u_x = - jk \cos \theta \, S_1 \, e^{-jk(x \cos \theta + y \sin \theta)} \, e^{-rz}$$

$$u_y = - jk \sin \theta \, S_1 \, e^{-jk(x \cos \theta + y \sin \theta)} \, e^{-rz}$$

$$u_z = - rS_1 \, e^{-jk(x \cos \theta + y \sin \theta)} \, e^{-rz}$$

and

$$\sigma_{xx} = - \mu(k_2^2 + 2r^2 - 2k^2 \sin^2\theta) S_1 \, e^{-jk(x \cos \theta + y \sin \theta)} \, e^{-rz}$$

$$\sigma_{yy} = - \mu(k_2^2 + 2r^2 - 2k^2 \cos^2\theta) S_1 \, e^{-jk(x \cos \theta + y \sin \theta)} \, e^{-rz}$$

$$\sigma_{zz} = \mu(2k^2 - k_2^2) S_1 \, e^{-jk(x \cos \theta + y \sin \theta)} \, e^{-rz}$$

$$\sigma_{yz} = 2\mu jkr \sin \theta \, S_1 \, e^{-jk(x \cos \theta + y \sin \theta)} \, e^{-rz}$$

$$\sigma_{xz} = 2\mu jkr \cos \theta \, S_1 \, e^{-jk(x \cos \theta + y \sin \theta)} \, e^{-rz}$$

$$\sigma_{xy} = - \mu k^2 \sin 2\theta \, S_1 \, e^{-jk(x \cos \theta + y \sin \theta)} \, e^{-rz} \qquad \text{(F.5)}$$

where k_2 is the shear wave number (B.2).

(b) Vertically-Polarized Shear Wave (i.e. Polarized $\perp$ Surface)

The displacement of a shear wave may be determined from a vector potential $\bar{\psi}$ [(B.9) and (B.10)]. For a vertically-polarized plane wave, propagating in the direction +v [Fig. F.1], there is no wave displacement along the normal direction w, and no dependence the coordinate w. Thus, only the component $\psi_w \neq 0$, and $(\partial/\partial w)\psi = 0$. Assuming decay in z, the appropriate vector potential is thus of the form

$$\bar{\psi} = \hat{w}\, S_2\, e^{-j\bar{k} \cdot \bar{v}}\, e^{-qz}. \qquad (F.6)$$

For (F.6) to be a solution of the wave equation (B.10) we require

$$k_2^2 = k^2 - q^2. \qquad (F.7)$$

Transforming (F.6) to x - y coordinates gives

$$\bar{\psi} = (-\hat{x} \sin\theta + \hat{y} \cos\theta) S_2\, e^{-jk(x \cos\theta + y \sin\theta)}\, e^{-qz} \qquad (F.8)$$

which is thus the vector potential of a vertically-polarized

shear wave, propagating at an angle θ with the $+x$ axis.

In terms of the vector potential, the stress components are[62]

$$\sigma_{xx} = -2\mu \frac{\partial^2 \psi_y}{\partial x \partial z}$$

$$\sigma_{yy} = 2\mu \frac{\partial^2 \psi_x}{\partial y \partial z}$$

$$\sigma_{zz} = 2\mu \left(\frac{\partial^2 \psi_y}{\partial x \partial z} - \frac{\partial^2 \psi_x}{\partial y \partial z} \right)$$

$$\sigma_{yz} = \mu \left(\frac{\partial^2 \psi_x}{\partial z^2} - \frac{\partial^2 \psi_x}{\partial y^2} + \frac{\partial^2 \psi_y}{\partial x \partial y} \right)$$

$$\sigma_{xz} = -\mu \left(\frac{\partial^2 \psi_y}{\partial z^2} - \frac{\partial^2 \psi_y}{\partial x^2} + \frac{\partial^2 \psi_x}{\partial x \partial y} \right)$$

$$\sigma_{xy} = \mu \left(\frac{\partial^2 \psi_x}{\partial x \partial z} - \frac{\partial^2 \psi_y}{\partial y \partial z} \right) . \qquad \text{(F.9)}$$

Introducing the vector potential (F.8) into (B.9) and (F.9), the displacements and stress components are determined to be

$$u_x = q \cos\theta \, S_2 \, e^{-jk(x \cos\theta + y \sin\theta)} \, e^{-qz}$$

$$u_y = q \sin\theta \, S_2 \, e^{-jk(x \cos\theta + y \sin\theta)} \, e^{-qz}$$

$$u_z = - jk \, S_2 \, e^{-jk(x \cos\theta + y \sin\theta)} \, e^{-qz}$$

and

$$\sigma_{xx} = - 2\mu jkq \cos^2\theta \, S_2 \, e^{-jk(x \cos\theta + y \sin\theta)} \, e^{-qz}$$

$$\sigma_{yy} = - 2\mu jkq \sin^2\theta \, S_2 \, e^{-jk(x \cos\theta + y \sin\theta)} \, e^{-qz}$$

$$\sigma_{zz} = 2\mu jkq \, S_2 \, e^{-jk(x \cos\theta + y \sin\theta)} \, e^{-qz}$$

$$\sigma_{yz} = - \mu(k^2 + q^2) \sin\theta \, S_2 \, e^{-jk(x \cos\theta + y \sin\theta)} \, e^{-qz}$$

$$\sigma_{xz} = - \mu(k^2 + q^2) \cos\theta \, S_2 \, e^{-jk(x \cos\theta + y \sin\theta)} \, e^{-qz}$$

$$\sigma_{xy} = - \mu jkq \sin 2\theta \, S_2 \, e^{-jk(x \cos\theta + y \sin\theta)} \, e^{-qz}$$

(F.10)

(c) Horizontally-Polarized Shear Wave (i.e. Polarized || Surface)

Again, this shear wave is derivable from a vector potential $\bar{\psi}$ [(B.9) and (B.10)]. A plane wave, propagating in the direction +v [Fig. F.1], has no displacement in the z direction and no dependence on the coordinate w (normal to the propagation direction). For this type of shear wave thus $\psi_w = 0$ and ψ_v, ψ_z are both finite. For waves decaying in z, the appropriate divergence-free vector potential is thus

$$\bar{\psi} = (q\,\hat{v} - jk\,\hat{z})\,S_3\,e^{-j\bar{k}\cdot\bar{v}}\,e^{-qz} \qquad (F.11)$$

where the decay constant q again satisfies (F.7). In x - y coordinates the vector potential (F.11) is

$$\bar{\psi} = (\hat{x}\,q\cos\theta + \hat{y}\,q\sin\theta - \hat{z}\,jk)\,e^{-jk(x\cos\theta + y\sin\theta)}\,e^{-qz} \qquad (F.12)$$

which is thus the vector potential of a horizontally-polarized shear wave, propagating at an angle θ to the x axis.

The stress components, of these waves, are related to the components of the vector potential by[62]

$$\sigma_{xx} = 2\mu\left(\frac{\partial^2\psi_z}{\partial x\partial y} - \frac{\partial^2\psi_y}{\partial x\partial z}\right)$$

$$\sigma_{yy} = 2\mu\left(\frac{\partial^2\psi_x}{\partial y\partial z} - \frac{\partial^2\psi_z}{\partial x\partial y}\right)$$

$$\sigma_{zz} = 2\mu\left(\frac{\partial^2\psi_y}{\partial x\partial z} - \frac{\partial^2\psi_x}{\partial y\partial z}\right)$$

$$\sigma_{yz} = \mu\left(\frac{\partial^2\psi_x}{\partial z^2} - \frac{\partial^2\psi_x}{\partial y^2} + \frac{\partial^2\psi_y}{\partial x\partial y} - \frac{\partial^2\psi_z}{\partial x\partial z}\right)$$

$$\sigma_{xz} = \mu\left(\frac{\partial^2\psi_y}{\partial x^2} - \frac{\partial^2\psi_y}{\partial z^2} + \frac{\partial^2\psi_z}{\partial y\partial z} - \frac{\partial^2\psi_x}{\partial x\partial y}\right)$$

$$\sigma_{xy} = \mu\left(\frac{\partial^2\psi_z}{\partial y^2} - \frac{\partial^2\psi_z}{\partial x^2} + \frac{\partial^2\psi_x}{\partial x\partial z} - \frac{\partial^2\psi_y}{\partial y\partial z}\right) . \qquad \text{(F.13)}$$

Using the vector potential (F.12), the displacements and stress components are determined from (B.9) and (F.13) to be

$$u_x = -(k^2 - q^2)\sin\theta\, S_3\, e^{-jk(x\cos\theta + y\sin\theta)}\, e^{-qz}$$

$$u_y = (k^2 - q^2)\cos\theta\, S_3\, e^{-jk(x\cos\theta + y\sin\theta)}\, e^{-qz}$$

$$u_z = 0$$

and

$$\sigma_{xx} = \mu jk(k^2 - q^2) \sin 2\theta \, S_3 \, e^{-jk(x \cos \theta + y \sin \theta)} \, e^{-qz}$$

$$\sigma_{yy} = - \mu jk(k^2 - q^2) \sin 2\theta \, S_3 \, e^{-jk(x \cos \theta + y \sin \theta)} \, e^{-qz}$$

$$\sigma_{zz} = 0$$

$$\sigma_{yz} = - \mu q(k^2 - q^2) \cos \theta \, S_3 \, e^{-jk(x \cos \theta + y \sin \theta)} \, e^{-qz}$$

$$\sigma_{xz} = \mu q(k^2 - q^2) \sin \theta \, S_3 \, e^{-jk(x \cos \theta + y \sin \theta)} \, e^{-qz}$$

$$\sigma_{xy} = - \mu jk(k^2 - q^2) \cos 2\theta \, S_3 \, e^{-jk(x \cos \theta + y \sin \theta)} \, e^{-qz}$$

(F.14)

(d) Rayleigh Wave

A Rayleigh wave is a combination of a compressional wave and a vertically-polarized shear wave. Together these waves satisfy the stress free boundary conditions

$$\sigma_{xz}^{r} = \sigma_{yz}^{r} = \sigma_{zz}^{r} = 0 \qquad \text{(F.15)}$$

at $z = 0$.

From (F.5), (F.10) and (F.15) the ratio of the wave amplitudes is again given by (B.19). In addition the decay constants of the waves [(B.16) and (B.17)] must satisfy the determinantal equation (B.18).

The displacements and stress components of a Rayleigh wave, at oblique incidence, may be determined from (F.5), (F.10) and (B.19). We find

$$u_x^r = - jS_1 \left(k_r \, e^{-r_r z} - \frac{k_r^2 + q_r^2}{2k_r} \, e^{-q_r z} \right) \cos\theta \; e^{-jk_r(x \cos\theta + y \sin\theta)}$$

$$u_y^r = - jS_1 \left(k_r \, e^{-r_r z} - \frac{k_r^2 + q_r^2}{2k_r} \, e^{-q_r z} \right) \sin\theta \; e^{-jk_r(x \cos\theta + y \sin\theta)}$$

$$u_z^r = - S_1 \left(r_r \, e^{-r_r z} - \frac{k_r^2 + q_r^2}{2q_r} \, e^{-q_r z} \right) e^{-jk_r(x \cos\theta + y \sin\theta)}$$

and

$$\sigma^r_{xx} = -\mu S_1[(k_r^2\cos 2\theta - q_r^2 + 2r_r^2)e^{-r_r z} - (k_r^2 + q_r^2)$$

$$\cos^2\theta\, e^{-q_r z}]\, e^{-jk_r(x\cos\theta + y\sin\theta)}$$

$$\sigma^r_{yy} = -\mu S_1[(-k_r^2\cos 2\theta - q_r^2 + 2r_r^2)e^{-r_r z} - (k_r^2 + q_r^2)$$

$$\sin^2\theta\, e^{-q_r z}]\, e^{-jk_r(x\cos\theta + y\sin\theta)}$$

$$\sigma^r_{zz} = \mu S_1(k_r^2 + q_r^2)(e^{-r_r z} - e^{-q_r z})\, e^{-jk_r(x\cos\theta + y\sin\theta)}$$

$$\sigma^r_{yz} = 2\mu j\, S_1\, k_r r_r \sin\theta(e^{-r_r z} - e^{-q_r z})\, e^{-jk_r(x\cos\theta + y\sin\theta)}$$

$$\sigma^r_{xz} = 2\mu j\, S_1\, k_r r_r \cos\theta(e^{-r_r z} - e^{-q_r z})\, e^{-jk_r(x\cos\theta + y\sin\theta)}$$

$$\sigma^r_{xy} = -\mu S_1 \sin 2\theta\left(k_r^2\, e^{-r_r z} - \frac{k_r^2 + q_r^2}{2}\, e^{-q_r z}\right)$$

$$e^{-jk_r(x\cos\theta + y\sin\theta)}. \qquad \text{(F.16)}$$

REFERENCES

[1] J. D. Maines and E. G. S. Paige, "Surface-acoustic wave components, devices and applications," Proc. IEE, 120, no. 10R, IEE Reviews, pp. 1078-1110, October 1973.

[2] E. A. Ash, "Fundamentals of signal processing devices," Acoustic Surface Waves, Edited by A. A. Oliner, Springer-Verlag, New York, pp. 97-185, 1978.

[3] R. C. Williamson and H. I. Smith, "The use of surface-elastic-wave reflection gratings in large time-bandwidth pulse-compression filters," IEEE Trans. Microwave Theory and Tech., MTT-21, pp. 195-205, April 1973.

[4] H. A. Haus and R. V. Schmidt, "Cascaded SAW gratings as bandpass filters," Electronics Lett., 13, no. 15, pp. 445-446, July 1977.

[5] W. R. Shreve, "Surface-wave resonators and their use in narrowband filters," 1976 Ultrasonics Symposium Proc., IEEE Cat. No. 76 CH-1120-5SU, pp. 706-713.

[6] D. T. Bell, Jr., and R. C. M. Li, "Surface-acoustic-wave-resonators," Proc. IEEE, 64, pp. 711-721, May 1976.

[7] W. R. Shreve and R. E. Stigall, "Surface acoustic wave devices for use in a high performance television tuner," 1978 Report under FCC Contract No. 0206-6TQ, Texas Instruments, Inc.

[8] H. Mathews, Editor, Surface-Wave Filters: Design, Construction, and Use, J. Wiley and Sons, New York, 1977.

[9] H. M. Gerard, Principles of Surface-Wave Filter Design, Edited by A. A. Oliner, Springer-Verlag, New York, pp. 61-96, 1978.

[10] D. C. Webb, "SAW filters simplify signal sorting," Microwave Systems News, pp. 75-84, September 1978.

[11] W. J. Tanski, "UHF SAW resonators and applications," Proc. 34th Ann. Freq. Control Symposium, pp. 278-285, May 1980.

[12] R. C. Williamson, "Wideband SAW Fourier-transform processor design and applications," Lincoln Labs., Lexington, MA, 1979.

[13] R. C. Williamson, V. S. Dolat and D. M. Boroson, "A satellite-borne SAW chirp-transform system for uplink demodulation of FSK communication signals," 1979 Ultrasonics Symposium Proc., IEEE Cat. No. 79 CH-1482-9SU.

[14] O. W. Otto and H. M. Gerard, "On Rayleigh wave reflection from grooves at oblique incidence and an empirical model for bulk wave scattering in RAC devices," 1977 Ultrasonics Symposium Proc., IEEE Cat. No. 77 CH-1264-1SU, pp. 596-601.

[15] J. M. Owens and C. V. Smith, Jr., "Magnetostatic wave devices: A status report," 1978 Ultrasonics Symposium Proc., IEEE Cat. No. 78 CH-1344-1SU, pp. 684-688.

[16] J. M. Owens and C. V. Smith, Jr., "Beyond SAW filters: Magnetostatics show promise," Microwave Systems News, pp. 45-48, June 1979.

[17] M. L. Dakss, L. Kuhn, P. F. Heidrich, and B. A. Scott, "Grating coupler for efficient excitation of optical guided waves in thin films," Appl. Phys. Lett., 16, no. 523, 1970.

[18] K. S. Pennington and L. Kuhn, "Bragg diffraction beam splitter for thin film optical guided waves," Optics Communications, 3, no. 5, July 1971.

[19] D. C. Flanders, H. Kogelnik, R. V. Schmidt, and C. V. Shank, "Grating filters for thin-film optical waveguides," Appl. Phys. Lett., 24, no. 4, February 1974.

[20] A. Katzir, A. C. Livanos, and A. Yariv, "Chirped-grating output couplers in dielectric waveguides," Appl. Phys. Lett., 30, no. 5, March 1977.

[21] A. C. Livanos, A. Katzir, A. Yariv, and C. S. Hong, "Chirped-grating demultiplexers in dielectric waveguides," Appl. Phys. Lett., 30, no. 10, May 1977.

[22] G. Hatakoshi and S. Tanaka, "Grating lenses for integrated optics," Optics Lett., 2, no. 6, June 1978.

[23] S. K. Yao and D. E. Thompson, "Chirp-grating lens for guided-wave optics," Appl. Phys. Lett., 33, no. 7, October 1978.

[24] M. Miller and M. Skalsky, "Chirped and curved grating coupler focusing both outgoing beam and guided wave," Optics Communications, 33, no. 1, April 1980.

[25] W. J. Tanski, "Developments in resonators on quartz," 1977 Ultrasonics Symposium Proc., IEEE Cat. No. 77 CH-1264-1SU, pp. 900-904.

[26] J. Melngailis and R. C. Williamson, "Interaction of surface waves and bulk waves in gratings: Phase shifts and sharp surface-wave/reflected bulk wave resonances,"

1978 Ultrasonics Symposium Proc., IEEE Cat. No. 78 CH-1344-1SU, pp. 623-629.

[27] R. C. M. Li and J. Melngailis, "Second-order effects in surface-wave devices due to stored energy at step discontinuities," 1973 Ultrasonics Symposium Proc., IEEE Cat. No. 73 CH-0807-8SU, pp. 503-505.

[28] R. C. M. Li and J. Melngailis, "The influence of stored energy at step discontinuities on the behavior of surface-wave gratings," IEEE Trans. on Sonics and Ultrasonics, SU-22, no. 3, pp. 189-198, May 1975.

[29] K. H. Yen, K. F. Lau and R. S. Kagiwada, "Second-harmonic SAW resonators," 1978 Ultrasonics Symposium Proc., IEEE Cat. No. 78 CH-1344-1SU, pp. 442-447.

[30] H. Shimizu and M. Takeuchi, "Theoretical studies of the energy storage and the second harmoic responses of SAW reflection gratings," 1979 Ultrasonics Symposium Proc., IEEE Cat. No. 79 CH-1482-9SU, pp. 1-6.

[31] P. V. Wright and H. A. Haus, "Theoretical analysis of second-order effects in surface-wave gratings," Proc. 34th Ann. Freq. Control Symposium, pp. 262-268, May 1980.

[32] H. A. Haus and P. V. Wright, "The analysis of grating structures by coupling-of-modes theory," 1980 Ultrasonics Symposium Proc., pp. 277-281.

[33] H. Kogelnik, "Coupled wave theory for thick hologram gratings," Bell System Technical Journal, 48, no. 9, pp. 2909-2947, November 1969.

[34] H. Kogelnik and C. V. Shank, "Coupled-wave theory of distributed feedback lasers," J. Appl. Phys., 43, no. 5, pp. 2327-2335, May 1972.

[35] W. S. Goruk, P. J. Vella, and G. I. Stegeman, "An exponential coupling theory for interdigital transducers," 1974 Ultrasonics Symposium Proc., IEEE Cat. No. 74 CH-0861-1SU, pp. 402-405.

[36] P. S. Cross, R. V. Schmidt, and H. A. Haus, "Acoustically cascaded SAW resonator-filters," 1976 Ultrasonics Symposium Proc., IEEE Cat. No. 76-CH-1120-5SU, p. 277.

[37] H. A. Haus and R. V. Schmidt, "Transmission response of cascaded gratings," IEEE Trans. on Sonics and Ultrasonics, SU-24, no. 2, pp. 94-101, March 1977.

[38] L. Solymar and M. P. Jordan, "Finite beams in large volume holograms," Microwaves, Optics and Acoustics, 1,

no. 3, pp. 89-92, April 1977.

[39] P. D. Bloch, E. G. S. Paige, and L. Solymar, "Reflection of surface acoustic waves from arrays of strips," 1978 Ultrasonics Symposium Proc., IEEE Cat. No. 78 CH-1344-1SU, pp. 639-642.

[40] P. St. J. Russell and L. Solymar, "The properties of holographic overlap gratings," Optica Acta, 26, no. 3, pp. 329-347, 1979.

[41] H. M. Gerard, O. W. Otto, and R. D. Weglein, "Wideband dispersive surface wave filters," Hughes Aircraft Company, ECOM Report 73-0110-F, December 1974.

[42] O. W. Otto, "Multiple reflection effects in acoustic surface wave reflective arrays," 1974 Ultrasonics Symposium Proc., IEEE Cat. No. 74-CH-0896-1SU, pp. 208-211.

[43] P. V. Wright and H. A. Haus, "A closed-form analysis of reflective-array gratings," 1980 Ultrasonics Symposium Proc., IEEE Cat. No. 80-CH-1602-2SU, pp. 282-287.

[44] B. A. Auld, Acoustic Fields and Waves in Solids, J. Wiley and Sons, New York, 1973, Vol. I, p. 59.

[45] A. Yariv, "Coupled-mode theory for guided-wave optics,"

IEEE J. Quantum Elect., QE-9, no. 9, pp. 919-933, Sept. 1973.

[46] R. C. M. Li, J. A. Alusow and R. C. Williamson, "Experimental exploration of the limits of achievable Q of grooved surface-wave resonators," 1975 Ultrasonics Symposium Proc., IEEE Cat. No. 75 CH-0994-4SU, pp. 279-283.

[47] R. C. M. Li, "Analysis of surface-wave reflection from a periodic array of grooves," 1972 Ultrasonics Symposium Proc., IEEE Cat. No. 72 CH-0708-8SU, pp. 263-266.

[48] B. A. Auld, Ibid., Volume II, p. 92.

[49] O. W. Otto, "Scattering of Rayleigh waves from topographic irregularities at oblique-incidence," J. Appl. Phys., 48, no. 12, pp. 5105-5110, December 1977.

[50] H. Kogelnik, "Filter response of nonuniform almost-periodic structures," Bell System Technical Journal, 55, no. 1, pp. 109-126, January 1976.

[51] M. Abramowitz and I. Stegun, Editors, Handbook of Mathematical Tables, National Bureau of Standards, Applied Mathematics Series, 55, December 1972, Section 19, pp. 686-720.

[52] M. Abramowitz and I. Stegun, Ibid, Section 13, pp. 503-535.

[53] F. B. Hildebrand, Advanced Calculus for Applications, Second Edition, Prentice-Hall, Inc., Englewood Cliffs, NJ, 1976, p. 396.

[54] N. P. Erugin, "Functionally-invariant solutions of a partial differential equation of second order in two independent variables," Uchenye Zapiski LGU, Mathematical Series, 16, no. 111, 1949, pp. 142-166.

[55] Z. Rubinstein, A Course in Ordinary and Partial Differential Equations, Academic Press, Inc., New York, 1969, pp. 319-323.

[56] R. C. Williamson, V. S. Dolat and H. I. Smith, "L-band reflective array compressor with a compression ratio of 5120," 1973 Ultrasonics Symposium Proc., IEEE Cat. No. 73 CH-0807-8SU, pp. 490-493.

[57] J. Melngailis, R. C. Williamson, J. Holtham, and R. C. Li, "Design of reflective-array surface wave devices," Wave Electronics, 2, pp. 177-198, 1976.

[58] I. A. Viktorov, Rayleigh and Lamb Waves, Plenum, New York, 1967, p. 1.

[59] I. A. Viktorov, Ibid, p. 2.

[60] B. A. Auld, Ibid, Volume I, p. 145.

[61] H. A. Haus, "Bulk scattering loss of SAW grating cascades," IEEE Trans. on Sonics and Ultrasonics, SU-24, no. 4, pp. 259-267, July 1977.

[62] B. A. Auld, Ibid, Volume I, pp. 66, 167.